12-2017

Evaluation of Shallow Hydraulic Fractures Characterized Using Geophysical Methods

Jessica L.S. Denison
Clemson University

EVALUATION OF SHALLOW HYDRAULIC FRACTURES CHARACTERIZED USING GEOPHYSICAL METHODS

A Thesis
Presented to
the Graduate School of
Clemson University

In Partial Fulfillment
Of the Requirements for the Degree
Masters of Science
Hydrogeology

---

by
Jessica L. S. Denison
December 2017

Accepted by:
Dr. Lawrence Murdoch, Committee Chair
Dr. Stephen Moysey
Dr. Ronald Falta

ABSTRACT

Hydraulic fractures are often used to stimulate fluid flow from wells in low permeability geologic units. This capability has been beneficial to the oil and gas industry as well as the remediation industry. The shape and extent of a hydraulic fracture and the distribution of granular proppant affects the performance of a hydraulic fracture during well stimulation. Several methods of tracking the location of hydraulic fractures have been developed (tiltmeter mapping, microseismic detection, and electric potential), but none have the ability to image the distribution of proppants. Electrical resistivity tomography (ERT) has been proposed as a new method to track the location of proppants containing electrical or magnetic contrast agents.

The objective of this study is to evaluate the ability of ERT to determine the location of proppant injected into hydraulic fractures at depths of a few meters. This shallow depth is intended to provide a proof of concept for applications where proppant is injected into much deeper reservoirs. To achieve this goal, hydraulic fractures were created, and fine grained coke breeze or steel shot were injected during the fracturing process to create a proppant layer with an electrical conductivity that contrasts with the enveloping formation. ERT, soil core, and excavation data were collected and compared in order to evaluate the ability of ERT to image the proppant. This contrast was intended to increase the ability of ERT to resolve the proppant layer. A field site in Powdersville, SC was chosen, and it was divided into six 9 meter by 9 meter cells. One fracture was created in each cell at a depth of 1.5 meters (5 feet). Two fractures contained a coke

breeze proppant. Two fractures contained a coke breeze and sand proppant mix. Two fractures contained steel shot proppant. Different amounts of proppant were injected into each cell. In Cells 1 through 4, about 2000 N of proppant were injected into the fractures, and in Cells 5 and Cell 6, about 5500 N of proppant were injected into the fractures. The slurry volumes injected into the cells varied from 0.33 m^3 to 0.83 m^3.

ERT data were measured prior to proppant injection and then again after injection. Then the difference in these two data sets was inverted to estimate the changes in electrical conductivity caused by proppant injection. The ERT inversions were then compared to results from soil core data and direct inspection in excavation. Uplift was measured with optical levels, and these results were interpreted to estimate the locations of the fractures. The created fractures had an average fracture uplift length of 7 meters at the surface of the earth based on field site measurements of the uplift. Approximately 130 soil cores were collected from the field site. The cores were analyzed to determine the presence and location of the fractures. The soil core data were compiled to create maps and cross sections that were compared to the ERT data. Trenches were dug in the vicinity of two cells, and the fractures were described where they were exposed on the trench walls.

The uplift, soil core, excavation, and ERT data show similar results. Comparisons with the soil core and trench mapping data show that the ERT inversions consistently match the direct observations. For example, in 83% of the soil cores that contained the fracture, the ERT data also indicated the fracture was present. In 96% of the cores where

the fracture was absent in the core, the ERT data also indicated that the fracture was absent. Comparisons with the soil core and trench cross sections demonstrate that the ERT results overestimate the fracture depth in approximately ¾ of the instances. However, the error is likely due to sampling since the p-value of 0.90 indicates that the ERT and soil core data are from the same population. The average and standard deviation of the error in the depths is -0.17±0.19 meters with the negative sign indicating that the ERT indicated depth was deeper than the soil core depth on average. The close match between the ERT data and the ground checked data all point to the ERT method as a potentially new, non-invasive tool that can be employed to determine fracture shape, extent, and depth. This new non-invasive method could benefit the oil industry by allowing them to determine the extent of the fractures they created without the high costs of invasive methods such as coring.

ACKNOWLEDGEMENTS

I would like to thank my advisor, Dr. Lawrence Murdoch, for his support and suggestions throughout the research and writing process. I would also like to thank my committee members: Drs. Stephen Moysey and Ronald Falta. I am forever grateful for the assistance of Douglas LaBrecque and Russell Brigham for sharing their knowledge about the ERT field methods. Thank you to all of the employees at FRx for assisting with the field work. Finally, I would like to thank my wonderful husband Joe for his love, support, and constructive criticism throughout this process. This research was supported by funding from the Advanced Energy Consortium: http://www.beg.utexas.edu/aec/ . Member companies include BP America Inc., Petrobras, Repsol, Schlumberger, Shell, Statoil, and Total.

TABLE OF CONTENTS

Page

LIST OF TABLES

Table Page

LIST OF FIGURES

Figure Page

CHAPTER 1: INTRODUCTION

Fractures are created naturally and as man-made structures. Some man-made fractures are formed by injecting fluid into a well, and this process is called hydraulic fracturing (Gidley et al., 1989). The use of hydraulic fracturing has increased in the oil and gas industry and with the application of the technology to the remediation industry. For hydraulic fractures to be useful, the shape and extent of the fracture needs to be determined. In the oil and gas industry, the fractures need to intersect the target reservoir for the fractures to increase production (Gidley et al., 1989). In the remediation industry, the fractures need to intersect the contaminated soil to effectively reduce the contamination (Chen and Murdoch, 1999; Davis Hoover et al., 1994; Murdoch et al., 1997; Murdoch and Chen, 1997). To determine the shape and extent of the fractures, invasive methods such as soil coring and excavation have been employed (Murdoch et al., 2006). Some methods of remotely monitoring fractures have been developed. The main two methods interpret tiltmeter and microseismic measurements. However, these methods detect deformation caused by the fracture and they are unable to determine the location of the proppant injected into a fracture. This is important because the location of the proppant is expected to strongly control the performance of the fracture. One possible solution is to use electrical resistivity tomography (ERT) to locate the fractures. The purpose of this work is to evaluate the ability of ERT to image fractures created in the shallow subsurface.

CHAPTER 2: BACKGROUND

Fractures are important to fluid flow in geologic materials because they can either increase or decrease the permeability. Mode I fractures have an opening displacement normal to the fracture surface (Pollard and Aydin, 1988). The displacement on Mode II fractures is a shear parallel to the fracture plane and perpendicular to the fracture propagation front (Pollard and Aydin, 1988). In Mode III fractures, the shearing motion is still parallel to the fracture plane but is parallel to the fracture propagation front (Pollard and Aydin, 1988). Joints are an example of a type of naturally occurring fracture with Mode I displacement (Pollard and Aydin, 1988). Faults are Mode II or Mode III fractures (Pollard and Aydin, 1988). Hydraulic fractures are typically Mode I, but they can also include Mode II and III types of displacements.

The opening displacement that occurs in Mode I fractures can create a feature with a permeability that is significantly greater than the surrounding formation. The permeability of Mode II and Mode III fractures can be greater than the enveloping rocks, but the shear associated with these types of fractures can cause permeability to be reduced. This occurs because shearing displacement crushes rock grains and can cause pores to collapse.

Fracture Form

Sub-horizontal fractures created at shallow depths have been studied in detail and similar features are present in the majority of them (Murdoch, 1995; Murdoch, 2002; Murdoch et al., 2006; Murdoch and Slack, 2002). One of the important aspects of fracture

form is fracture orientation, which is controlled by the stress state in the formation (Hubbert and Willis, 1972). There are three principal stresses in the subsurface. Mode I fractures, such as hydraulic fractures, will typically open in the plane that is perpendicular to the direction of the least principal compressive stress. From this idea, it follows that the orientation of fractures will depend on the stress states in the surrounding rock or soil. For example, in areas that are tectonically relaxed, such as those distinguished by normal faulting, the least principal compressive stress is near horizontal. As a result, Mode I fractures created in this type of tectonic setting will be vertical. In regions characterized by tectonic compression, the direction of least principal stress is near vertical. As a result, Mode I fractures that occur in this tectonic setting will develop in the horizontal direction (Hubbert and Willis, 1972). The least compressive stress in soils depends on the degree of consolidation. It is horizontal in normally consolidated soils and vertical where the soils are over-consolidated.

Since the stress state affects the fracture orientation, human interaction with the surface of the earth can change the fracture orientation. In a study by Murdoch (1995), it was determined that when equipment trucks were parked near the location where hydraulic fracturing was taking place, the fracture would propagate away from the area with the increased load. The ambient direction of least compressive stress was vertical in those soils, so the hydraulic fractures were generally flat-lying. However, the load from the vehicles locally increased the stress and this caused the fractures to propagate away from the vehicles.

Interaction with the ground surface can also affect the shape of a hydraulic fracture (Murdoch, 1995; Pollard and Holzhausen, 1979). Mechanical interactions between the fracture and the ground surface can result in the fracture sloping upward and move towards the surface of the earth. The factor is dependent on the fracture depth (d) and length (a). For a horizontal fracture, if $a/d<0.6$ then the upturn of the hydraulic fracture will be insignificant. As the ratio increases to $0.6< a/d<2.0$, there is an increased likelihood that the fracture will upturn toward the surface. When $a/d>2.0$, there is a rapid increase in the tendency of the fracture to upturn toward the surface of the earth. The reason for this phenomenon is that shear develops at the fracture tip because to the top surface of the horizontal fracture is located farther from the axial plane than the bottom surface. As a result, the depth of fracture initiation influences the rate at which a fracture will turn up towards the surface. If a horizontal fracture has a length much shorter than the depth of fracture initiation, the fracture will propagate in a horizontal direction. As the fracture length increases, it will begin to propagate up towards the ground surface as the fracture length approaches the fracture depth (Murdoch, 1995; Pollard and Holzhausen, 1979).

The forms of hydraulic fractures have been determined in studies involving sampling the fracture at points using cores, or excavating the vicinity of the fracture and mapping traces of the fracture on the walls of excavations. Several mineback studies have been completed to obtain this information (Murdoch, 1995; Murdoch et al., 2006). Mineback involves digging trenches in the area of a fracture or demolishing lithified rock to expose traces of the fractures (Murdoch, 1995; Murdoch et al., 2006; Northrop and

Warpinski, 1978; Teufel and Warpinski, 1983). In both instances, this allows fractures to be mapped and permits the study of fracture form in greater detail.

In an excavation study by Murdoch et al. (2006), shallow horizontal hydraulic fractures were created in saprolite material in South Carolina. The fractures were excavated, and the cross sections were mapped. The cross sections confirmed that the fractures are asymmetric bowl shapes that remained relatively flat near the injection well but curved upward as the fracture moved away from the borehole (Murdoch et al., 2006). The fractures had an elongate shape (Murdoch et al., 2006). Observation of the fracture aperture in the trenches confirmed that the aperture decreases as distance from the injection well increases (Murdoch et al., 2006).

The proppant thickness is variable throughout the fracture. In general, the proppant thickness decreases as distance from the injection well increases in some cases (Murdoch et al., 2006). When the proppant or sand thickness is plotted versus distance from the casing, a third order polynomial teardrop shape can be fitted to the data (Figure 1) (Murdoch et al., 2006; Murdoch and Slack, 2002). This data show that the thickest part of the fracture was displaced away from the injection well in the fractures described by Murdoch et al. 2006. The teardrop shape that fits the proppant thickness data for the fractures in the Murdoch et al 2006 study is similar to the polynomial that fits the data collected from igneous dikes. When the dike half thickness is plotted versus distance, the data are also best fit by a teardrop shaped polynomial (Figure 2) (Pollard and Muller, 1976).

In a study by Murdoch (1995), sub-horizontal fractures were created in fresh, undisturbed glacial drift deposits. Trenches were later dug in the area around the injection well, and the fractures were mapped based on the areas where the proppant was exposed on the trench walls (Murdoch, 1995). The distribution of proppant thickness was described, and in some areas a hydraulic fracture was identified based on the presence of dye staining on the fracture surface, even though sand filling was absent (Murdoch, 1995).

Three main zones characterizing form were identified in the fractures described by Murdoch (1995) (Figure 3). Zone 2 consists of a sub-horizontal fracture that extends several meters out from the injection well and is absent in some instances (Murdoch, 1995). The majority of the fracture is made of up zone 3 (Murdoch, 1995). This zone consists of a planar to trough shaped fracture with a low angle dip in the direction of the borehole (Murdoch, 1995). Zone 4 occurs about 0.5 meters from the surface of the Earth and consists of a steeply dipping section of the fracture (Murdoch, 1995). Zone 4 is the location of the fracture vent in the case that the fracture reaches the surface (Murdoch, 1995). The horizontal extent of these fractures is often much greater than the fracture depth, and 2 to 3 orders of magnitude greater than the aperture thickness (Murdoch, 2002). Zone 1 is only present under special circumstances (Murdoch, 1995). This zone is closest to the injection well, and the fracture is oriented sub-vertically parallel to the injection well (Murdoch, 1995). Zone 1 was only present in the early fractures observed by Murdoch 1995 because the notch was not deep enough to nucleate the fracture. This

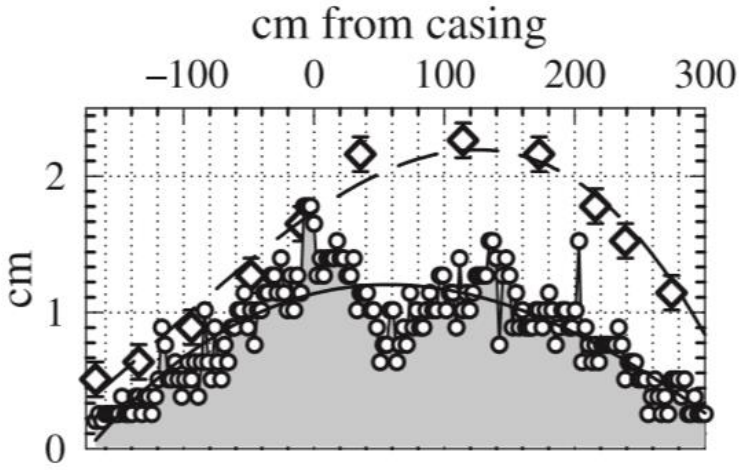

Figure 1: Cross section of proppant thickness versus distance from the casing. Circles represent proppant thickness and the diamonds represent uplift. Note that a third order polynomial in the shape of a teardrop fits both sets of data.
(Murdoch, L. C., Richardson, J. R., Tan, Q., Malin, S. C., and C. Fairbanks; Forms and sand transport in shallow hydraulic fractures in residual soil; Canadian Geotechnical Journal 43 (10), 1061-1073 © Canadian Science Publishing or its licensors) (With permission from the publisher)

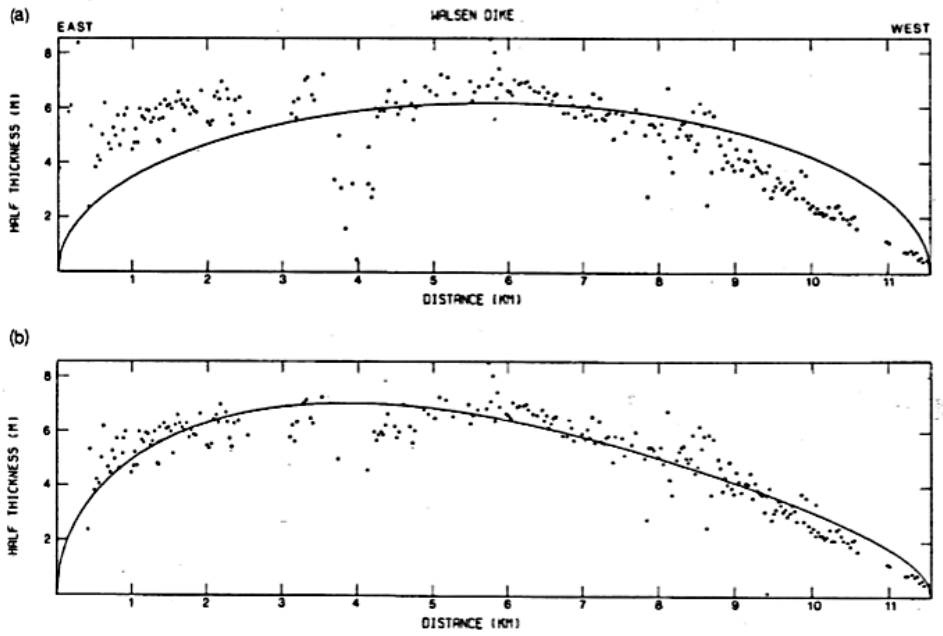

Figure 2: Data from the Walsen dike. The half thickness of the dike is plotted versus the distance from the east end of the dike. (a) Data fitted with an elliptical form. (b) Data fitted with a teardrop form. Note how the teardrop form is the better fit.
(Pollard, D. D. and O. H. Muller; The effects of gradients in regional stress and magma pressure on the form of sheet intrusions in cross section. Journal of Geophysical Research 81, 975-984) (With permission from the publisher)

zone will not be present when a deeper notch is created prior to fracture initiation (Murdoch, 2002; Murdoch et al., 2006; Murdoch and Slack, 2002).

Horizontal fractures grow radially as the proppant and fracturing fluid and pumped into the well (Murdoch, 2002). The leading edge of the fracture grows in the same manner in which echelon cracks link together. Echelon cracks link together as the bridges between cracks break apart as the cracks dilate (Nicholson and Pollard, 1985). This same process occurs at the leading edge of fractures. Echelon cracks form at the fracture's leading edge due to changing stress states. As the stress state changes in the sediment the fracture is forming in, it is easier for the fracture to develop an echelon pattern than to twist the whole fracture to be perpendicular to the direction of the lowest

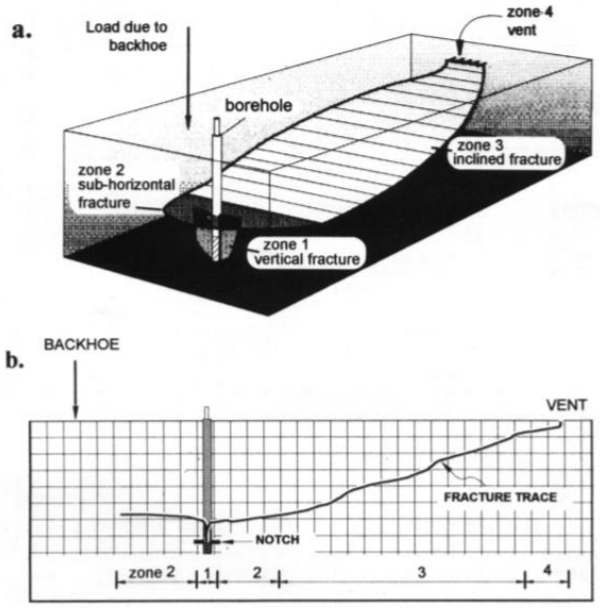

Figure 3: Cross section of a fracture that shows the four zones present in a typical shallow horizontal fraction a. Fracture in oblique view; b. Cross section of fracture along the major axis
(From Murdoch, L.C. Forms of hydraulic fractures created during a field test in overconsolidated glacial drift. Quarterly Journal of Engineering Geology and Hydrogeology, 28, 23-35) (with permission from the publisher)

stress. This occurs because it takes less work and less surface area for the fracture to adjust. While the fracture grows, tension occurs at the tip of the fracture and smaller echelon mode I fractures form. As the cracks dilate, the bridges between them break linking the cracks together. These linked echelon cracks then link to the leading edge of the main fracture (Nicholson and Pollard, 1985; Pollard et al., 1982). On the larger scale, this results in fractures growing via a series of lobes that branch out from the injection well (Murdoch et al., 2006). These lobes continue to grow and eventually coalesce to form the fracture (Murdoch et al., 2006).

A preferred direction of propagation develops in a sub-horizontal fracture creating an asymmetric form (Murdoch, 2002). This causes one axis of the fracture to be longer than the other (Murdoch, 2002). The preferential propagation direction and resulting asymmetric form can create a disparity between the location of the injection well and the point of maximum uplift (Murdoch, 2002).

The preferred propagation direction and ideal fracture form are affected by discontinuities in the subsurface such as stress contrasts, faults, joints, and bedding planes. The effects of these discontinuities are demonstrated by several mineback experiments were completed at the U.S. DOE Nevada Test Site. In these experiments, fractures were created about 1400 feet (425 meters) below the surface in rock and were observed by excavating tunnels into the rock. When fractures encounter joints in the subsurface, they are often offset. Two or more fractures also begin at the joint surface.

These fractures can either be short or long; they will often branch apart and merge back together (Warpinski and Teufel, 1987).

Some of the fractures observed during mineback encountered faults. When the fractures encountered the faults, they would often terminate. In some instances, the fracture would propagate across the fault surface for a short distance before it would end. When the fracture propagated across the fault plane, orientation would usually change. This is ascribed to the change in stress across the fault plane (Warpinski and Teufel, 1987).

The mineback experiments also observed fractures that encountered bedding planes. The fracture that was observed seemed to end at a parting plane, but on closer inspection, it propagated 1 to 2 inches across the plane (Warpinski and Teufel, 1987).

The effect of discontinuities on proppant transport was also observed in the mineback experiments. Discontinuities can cause fractures to divide into smaller multi-strand fractures instead of propagating as a single fracture. Fractures were observed where colored sand was used as the proppant. Black sand was pumped into the fracture first followed by red sand and then blue sand. Very little black sand was found in the fractures and red and black sand was found in the fracture section offset across a joint plane. It is interpreted that well screen out occurred, and therefore little fracture growth was feasible afterwards (Warpinski and Teufel, 1987).

Fractures can be created in rock by many processes, including hydraulic fracturing (Murdoch, 1995). Hydraulic fractures are created when the fluid pressure

inside an existing fracture or flaw exceeds a critical value. A hydraulic fracture grows when fluid is supplied to the fracture fast enough to maintain the pressure during propagation. Some natural processes can lead to fracturing (Nicholson and Pollard, 1985), but hydraulic fractures are often man-made. A common example is the hydraulic fractures created in the vicinity of wells and used to increase production from oil reservoirs, or to enhance environmental remediation. This process is carried out by first creating a well in the area chosen for the hydraulic fracture and ensuring that the end of the well casing is located within the target formation. The formation is accessed by either perforating the casing with an explosive charge or water jet, or in some cases the formation can be accessed below the bottom of open casing. In many cases, the formation is cut to create a notch where the hydraulic fracture nucleates. Once the notch is cut, fluids are pumped into the well. They flow into the notch and continue outward perpendicular to the well to form the man-made hydraulic fracture. While the fluids are being pumped into the well, sand or other solids known as *proppant* are mixed in with the fracturing fluids. These solids serve to hold open the newly created fractures once the fracturing fluids disperse through the surrounding material (Gidley et al., 1989; Murdoch, 1995, Murdoch and Slack, 2002).

One of the main uses of hydraulic fractures is in the oil and gas industry. Hydraulic fracturing has been employed in the petroleum industry since the 1940s as a method for stimulating oil and gas wells (Gidley et al., 1989). The vertical fractures created in these wells are held open by a propping agent that creates an area of higher permeability, which increases the oil and gas recovery in a well (Gidley et al., 1989).

This has led to previously lower yielding wells becoming economically producible (Gidley et al., 1989).

In recent years, fracturing technology has been expanded to apply to horizontal wells (Crosby et al., 1998; Soliman and Boonen, 1997). This technology involves drilling horizontal wells through low permeability formations and creating fractures in the horizontal wells to increase the hydrocarbon yield (Crosby et al., 1998). Two types of fractures can be created in these horizontal wells: longitudinal fractures and transverse fractures (Crosby et al., 1998). The longitudinal fractures propagate in the same plane as the horizontal well and as a result, they run parallel to the well (Crosby et al., 1998). The longitudinal fractures form in the well when the horizontal well is drilled parallel to the greater horizontal stress (Crosby et al., 1998). Transverse fractures form in the horizontal well when the well is drilled perpendicular to the greater horizontal stress (Crosby et al., 1998). As a result, transverse fractures propagate in a plane perpendicular to the horizontal well (Crosby et al., 1998). Transverse fractures offer benefits in increasing the productivity of oil and gas wells since they allow several fractures to be created along the horizontal well length (Crosby et al., 1998).

Another use of man-made hydraulic fractures is in environmental remediation processes. Induced hydraulic fractures can be applied to the technology of vapor extraction and increase the discharge particularly when applied to formations with low-permeability (Murdoch and Wilson, 1994). Man-made fractures can also be employed to aid in the recovery of LNAPLS by improving the discharge in the recovery wells. For this

to be accomplished, induced fractures are created within or a little below the contaminated area. The technology can also be applied to cleaning up DNAPL spills by increasing the permeability of formations. Great care must be taken if this is attempted. In the event that the induced fractures are vertically oriented, this could facilitate the DNAPL in sinking lower into the formation where it can no longer be recovered (Murdoch and Wilson, 1994). Bioremediation technology can also be paired with induced fractures to aid in remediation efforts (Davis Hoover et al., 1994; Murdoch and Wilson, 1994). The fractures can serve one of two purposes; they can increase the injection rate of oxygen containing fluid and nutrients, or the fractures can be filled with solid material containing ingredients needed for bioremediation (Murdoch and Wilson, 1994). Air injection techniques are also aided by induced fractures since the fractures increase the air injection rate. In a similar manner, fractures can be used in steam injection remediation techniques to heat formation with low-permeability (Murdoch and Wilson, 1994). Electrokinetic methods have benefited from the use of induced fractures (Murdoch and Chen, 1997; Chen and Murdoch, 1999; Murdoch and Wilson, 1994). In this technique, graphite is used as a proppant in the fractures and to make the fractures electrically conductive (Murdoch and Wilson, 1994). This results in the movement of water and contaminants by electrokinetics. In situ treatment zones are also benefited by the use of induced fractures. These treatment zones can be created by injecting biologically active or chemically active compound into the fractures. Man-made fractures can also aid in monitoring wells by increasing the sample recovery rate of the wells located in low permeability formations (Murdoch and Wilson, 1994).

In each of these examples, the shape and extent of the fracture impacts the success of the study. If the fracture does not extend far enough into the target zone, this could result in less oil or gas recovery or inability of remediation proppants to effectively treat the contaminated area. Therefore knowledge of fracture form (fracture shape, extent, dip angle) is vital to ensuring successful field applications.

Fracture Detection Methods

Tiltmeters

Several methods have been developed to detect hydraulic fractures, and tiltmeters are one of the most successful. Tiltmeters are geomechanical instruments used to measure tilt (Wright et al., 1999). Tilt is a measurement of surface deformation recorded in radians (Saleh and Blum, 2005). Many tiltmeters are biaxial in that they measure the tilt in two perpendicular directions. These data can be used to determine the magnitude and direction of the tilt vector (Saleh and Blum, 2005). Baseline tiltmeter data are recorded an hour to several days before experiments occur (Saleh and Blum, 2005). When fractures are created, deformation occurs as the rock or soil is parted to create the fracture aperture (Wright et al., 1999). As a result, the tilt signal can be measured during the creation of a fracture and be used to estimate the fracture form (Wright et al., 1999). This process is started by directly measuring the gradient of the displacement field produced through fracture deformation as a function of space and time (Wright et al., 1999). The data collected can then be inverted to estimate the fracture dimensions (Saleh and Blum, 2005; Wright et al., 1999). An estimation of fracture width can also be determined from the

surface deformation amplitude (Saleh and Blum 2005), particularly for sub-horizontal fractures that are long relative to their depth. A benefit of tiltmeters is that for certain fracture geometries, the deformation field is nearly unaffected by the properties of the surrounding formation (Wright et al., 1999). This is beneficial because the tiltmeter will give the same shaped tilt signal regardless of formation properties. Therefore, it is possible to infer the shape of the fracture based on the tilt signal (Wright et al., 1999).

Tiltmeters can be set up in several orientations including at the ground surface, at shallow depths, and at great depths downhole. Surface tiltmeter are used to collect data about vertical and horizontal fractures. Surface tiltmeters can be deployed by placing the tiltmeters on the ground surface surrounding the injection well (Saleh and Blum, 2005; Wright et al., 1998). Tiltmeters are calibrated before measurements begin (Wright et al., 1998).

Shallow tiltmeters are deployed by placing tiltmeters in an array of shallow holes surrounding the injection well (Wright et al., 1999). These holes are usually between 10 to 40 feet deep (Wright et al., 1999) for applications involving fractures that are much deeper. These instruments need to be level prior to taking measurements. For shallow tiltmeters, this is achieved by placing the tiltmeters in the holes and then tapping sand around the tiltmeter to level it (Wright, 1998).

Downhole tiltmeters are usually employed to collect data on deep vertical fractures. This is beneficial because it aligns a row of tiltmeters parallel to the long axis of the fracture (Wright et al., 1999). Downhole tiltmeter data are collected by lowering

wireline-conveyed tiltmeter arrays into a borehole offset from the injection well (Wright et al., 1999). The tiltmeters are positioned in the same depth interval that the vertical fracture encompasses (Wright et al., 1999). For vertical fractures detected by downhole tiltmeters, the tilt is zero in the zones above and below the fracture (Wright et al., 1999). In the area the fracture is located, the maximum tilt is located at the top of the fracture; there is zero tilt at the center of the fracture, and the bottom of the fracture has roughly the same tilt magnitude as the top of the fracture but in the opposite direction (Wright et al., 1999).

The benefit of using downhole tiltmeters to measure vertical fractures is that they are more sensitive to obtaining the fracture dimensions than surface tiltmeters (Wright et al., 1999). This is due to the tiltmeters aligning parallel with the long axis of the fracture (Wright et al., 1999). Downhole tiltmeters have some disadvantages such as sensitivity and attenuation. For example, even though they are more sensitive to fracture dimensions, they are not able to determine the perimeter of the fracture to a high degree of precision (Wright et al., 1999). As a result, the data only provide a rough estimate of the fracture extent (Wright et al., 1999). Another downside of this technology is that the characteristic tilt data pattern diffuses and attenuates as the distance from the source increases which limits the ability of the tiltmeters to obtain data on fractures far away from the instruments (Wright et al., 1999). Cost is also an issue when deploying downhole tiltmeters due to the expense of drilling wells and procuring the tiltmeter equipment (Beaumont et al., 1970)

When surface tiltmeters are employed to monitor vertical fractures, there are many benefits including the ability to determine fracture parameters, shape, and orientation. One benefit is that the surface tiltmeter data can be used to determine the fracture azimuth, dip, fracture volume, depth-to-fracture-center, and fracture offset caused by asymmetric growth (Wright et al., 1999). Another benefit is that the shape and orientation of the tilt field measured does not change as the fracture depth increases (Wright et al., 1999).

While surface tiltmeters are useful for measuring vertical fractures, there are also disadvantages to this method. One downside is that the induced tilt magnitude is attenuated as depth increases (Wright et al., 1999). This limits the practicality of surface tiltmeter mapping of vertical fractures to no more than 10,000 to 12,000 feet deep (Wright et al., 1999). Another disadvantage is that individual fracture extents cannot be determined if the fracture depth is much greater than the fracture extents (Wright et al., 1999). Surface tiltmeters also face depth limits and cannot be employed when the hydraulic fracture is created at a depth greater than 450 meters (Saleh and Blum, 2005). When tiltmeter data are collected far away from the fracture, the result is an infinite number of possible fracture dimensions that all have identical fracture volume (Lecampion et al., 2005). In addition, the fracture volume indicated by tiltmeter data is only an estimation (Lecampion et al., 2005). Tiltmeters also suffer from noise due to thermal changes and earth tides, and this noise must be filtered out (Beaumont et al., 1970; Wyatt and Berger, 1980).

Uplift

The uplift that occurs at the surface of the earth can also be used as a method to monitor shallow hydraulic fractures (Murdoch and Slack, 2002). To measure uplift, leveling equipment can be used to determine the change in elevation at the surface of the earth that occurs when fractures are created. It is interpreted that the elliptical uplift dome that occurs corresponds to the location of proppant in the subsurface. The uplift domes vary from symmetric to asymmetric (Murdoch and Slack, 2002). When uplift occurs, three distinct locations can be observed: the borehole location, the center of uplift, and the maximum uplift location (Figure 4). These locations occur along the same transect as the axis of maximum uplift. The maximum uplift and the borehole are usually on either side of the center of uplift (Murdoch and Slack, 2002).

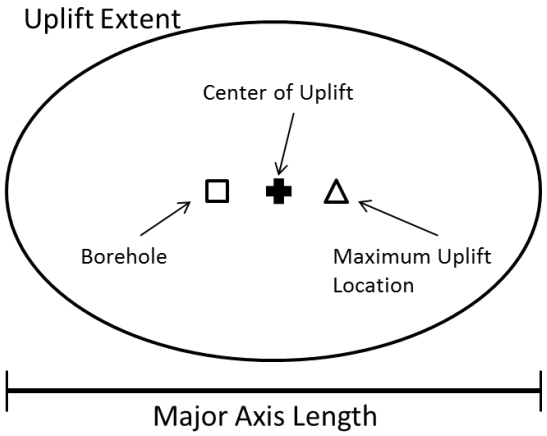

Figure 4: a) Image of the location of the borehole, center of uplift, and maximum uplift relative to each other. B) The location of the major axis.

Cracks often form at the surface of the earth when uplift occurs (Murdoch and Slack, 2002). The diameter of these cracks varies from a few mm to 1 cm. The surface cracks occur in the area around the top of the uplift dome. Cracks will not occur at the edges of the dome. The area around the maximum uplift location will correspond to the location with the largest number of cracks. The surface cracks in this location will also have the greatest apertures. The cracks will have the largest apertures directly after injection as occurred. As time passes, the apertures will decrease as the uplift recedes (Murdoch and Slack, 2002).

The volume of uplift that occurs is interpreted to correspond to the volume of slurry that was injected into the ground to create the fractures (Murdoch and Slack, 2002). When the volumes are compared, the calculated uplift volume can be about equal to the slurry volume or a little less than the injected volume. An exception is when a fracture vents at the surface of the earth. In this case, the uplift volume will be significantly less than the slurry volume (Murdoch and Slack, 2002).

Microseismic

Another monitoring method is measuring the microseismic activity or the microearthquakes that occur during hydraulic fracturing (Mahrer, 1993). The data are collected by placing geophones near the well where the hydraulic fracture is being created (Busetti et al., 2014). These geophones detect P- and S-wave arrival times for each microseismic event, and that data can be inverted to determine the six-component seismic moment tensor (Busetti et al., 2014). The information in this tensor can be

resolved to determine several source parameters (Busetti et al., 2014). The data can also be used to create a point cloud that shows the loci of the microseismic events (Busetti et al., 2014; Mahrer, 1993). It is interpreted that the area with the microseismic activity is the area that is affected by the hydraulic fracture.

Despite the wide-spread use of the microseismic method, there is a major drawback. Induced hydraulic fractures can activate pre-existing fracture and faults (Busetti et al., 2014; Huang et al., 2015). As a result, the microseismic data could either be indicating the location of the new induced hydraulic fracture or the locations of the pre-existing fracture and faults (Busetti et al., 2014; Huang et al., 2015). The issues with the activation of pre-existing faults and fractures in turn leads to problems interpreting the data. If the models used in the inversions do not account for the pre-existing discontinuities, this can lead to incorrect evaluation of the hydraulic fracture location (Verdon and Kendall, 2011).

Electric Potential Method

Some other hydraulic fracture detection methods have been employed on a more limited basis. One example is the electric potential method. Electrically conductive fracturing fluid is used to create an anomaly. The injection well and a remotely placed well are used for current injection. Between the two wells, potential probes are hammered into the ground around the injection well. Cables are connected to a set of probes which return potential data to the instrumentation. The measurements are taken using a positive current flow through the two wells and measuring the resulting potentials. Then the

process is repeated by reversing polarity and using a negative current flow. The surface potential is the difference between the two values. Based on these data, the direction and symmetry of the hydraulic fracture can be determined.

Keck and Schuster (1978) completed a study using this method. The fracture was created in a 24.4-meter-deep injection well that was cased to 12.2 meters. The electrical conductivity of the fracturing fluid was increased by adding 3% KCl. The electric potential results for the study completed by Keck and Schuster were compared with tiltmeter and down-hole camera data collected for the same study, and the results from the three different methods agree (Keck and Schuster, 1978).

A similar study was carried out by Wang et al., 1991. In this study, hydraulic fractures were created in glacial till with an electrically conductive fluid containing 3% KCl. One fracture was created at a depth of 3.87 meters and the others were created at a depth of 1.83 meters. The injection well casing served as the current electrode. A return electrode was positioned over 200 meters east of the injection well, and another electrode was positioned over 200 meters west of the injection well to serve as the reference electrode. The electric potential was measured throughout out the area using the mise-á-la-masse method. The data were then analyzed to convert the measurements to apparent resistivity. Attempts were made to fit the data using the DC alpha center method. Analysis of this method determined that the DC alpha center models were able to determine the fracture direction, but it was not able to determine the fracture length. It

was concluded that more work must be put forth to create a more accurate model for the background resistivity before this method can be accurately modeled (Wang et al., 1991).

These studies indicate that the method is promising for imaging the hydraulic fractures. Unfortunately, few studies have been completed with this method (Keck and Schuster, 1978; Wang et al., 1991), and more testing will have to be completed before it can be verified as an accurate technique.

New Fracture Imaging Method: Electrical Resistivity Tomography

A new method used for fracture imaging is electrical resistivity tomography (ERT). This method involves taking several current and voltage readings across boreholes and using that information to create resistivity images of the subsurface (Daily et al., 1990). The completed image can be compared with existing geologic information (Daily et al., 1990). To complete ERT tests, electrodes are placed in boreholes in contact with the formation (Daily et al., 1990). Depending on the objectives, surface electrodes might also be included (Stubben and LaBrecque, 1998). Once the electrodes are in place, a known current is applied between two electrodes, and the voltage difference between other pairs of electrodes is recorded (Daily et al., 1990). This method is repeated until all electrode pairs have served as the current electrodes (Daily et al., 1990). The apparent resistivity can be determined based on the ratio of the voltage measured at a pair of electrodes to the known current at the current terminals (Daily et al., 1990). An inversion process is then used to create images of the subsurface electrical resistivity or electrical conductivity (Daily et al., 1990; Stubben and LaBrecque, 1998). This process can be

repeated several times at the same site to allow monitoring of the subsurface over time (Stubben and LaBrecque, 1998).

The ERT method has been employed in several lab and field tests. Stubben and LaBrecque (1998) completed a field test where electrically conductive water was injected into the formation and monitored with surface and vertical electrode arrays over time. The ERT method was successful in tracking the location of the water within the aquifer (Stubben and LaBrecque, 1998). In a field test completed by Oldenborger et al. (2007), ERT was employed to track the location of conductive water containing KBr in the subsurface over several days (Oldenborger et al., 2007). The data collected with this method was also used to estimate the solute mass in the aquifer and the withdrawn solute mass (Oldenborger et al., 2007). Once again, the ERT method was successful in tracing the path of the conductive water in the aquifer over time (Oldenborger et al., 2007).

The ERT method was tested in a lab setting to determine its ability to locate wet and dry fractures. In a laboratory test by LaBrecque et al. (2004), limestone blocks were placed in a grid pattern, and electrodes were placed around the edges of the grid. Dry fractures were simulated by placing vinyl between two of the blocks (LaBrecque et al., 2004). The vinyl created a less conductive area relative to the surrounding limestone blocks (LaBrecque et al., 2004). A dipole-dipole electrode array was then used to collect data (LaBrecque et al., 2004). The data were inverted, and the maps were used to determine where the fractures were located (LaBrecque et al., 2004). These fracture locations on the maps were then compared with the actual fracture location to determine

if the ERT method could accurately determine the fracture location (LaBrecque et al., 2004). This same process was then completed with wet fractures that were created by adding water between the blocks (LaBrecque et al., 2004). The water created a more conductive area relative to the surrounding blocks (LaBrecque et al., 2004). The results demonstrated that the ERT method was able to accurately determine the locations of fracture (LaBrecque et al., 2004). The most accurate locations were where the simulated fracture was near the center of the block (LaBrecque et al., 2004). Accuracy decreased when the simulated fracture was near the edge of the block (LaBrecque et al., 2004). While this study demonstrates that ERT is able to find simulated fractures in a lab setting, a field scale test of the principle has not been executed. Therefore, it is unknown whether ERT would be able to detect and map the fractures at a larger scale.

The ERT method responds to the electrical properties of the material in the fracture, whereas tiltmeters and microseismic methods respond to deformation caused by the fracture. This suggests that electrically conductive proppant could be imaged by ERT. The deformation measured by tiltmeters and microseismics can be affected by processes that are independent of the location of proppant, so in general, interpretations of those data cannot reliably locate proppant. This is important because the location of proppant controls the performance of a hydraulic fracture, so ERT has the potential to provide data on fracture performance that is superior to interpretations of tiltmeter and microseismic data. However, this feasibility of using ERT to image hydraulic fractures is unknown. This is because the technique has never been evaluated using electrically conductive proppant.

CHAPTER 3: OBJECTIVES

The long-term objective of this line of research is to assess the feasibility of imaging hydraulic fractures at depths of thousands of feet using geophysical methods. To reach this goal, several interim steps will occur. The research presented here focuses on a pilot-scale field test with the following objectives: 1. characterize geophysical signals from hydraulic fractures created in natural materials. 2. Interpret the geophysical signals using inverse methods to predict hydraulic fracture form. 3. Evaluate the prediction of fracture form by comparing results to field observations of hydraulic fractures.

CHAPTER 4: APPROACH

Hydraulic fractures were created at a depth of 1.5 meters using electrically conductive proppant, and the vicinity of the fractures was monitored using geophysical and geomechanical methods. Soil cores obtained at approximately 112 locations at the site, and they were analyzed to determine the extent and depth of the fracture. The soil core data were also used to create cross sections and maps. Vicinities of two of the fractures were excavated, and the fractures on the walls of the excavations were mapped and described. ERT surveys were completed prior to fracture injection and then again after injection. The geophysical data were inverted using numerical methods and the resulting interpretations were then compared to the mapped fractures.

This project was a collaborative effort by the author and personnel with FRx Inc. and Multi-Phase Technologies, LLC. Bill Slack, Doug Knight and a group of investigators with FRx Inc. collected the tiltmeter and uplift data. I then used the data to create contour maps showing the vertical displacement that resulted from fracture creation. The soil cores were collected by the author and FRx Inc. I then inspected the cores to complete soil descriptions, determine whether or not the fracture is present in the core, and determine the depth of the fracture. The fracture excavations were carried out by FRx Inc., and the survey data were taken by the author and FRx Inc. Cross sections based on the survey data were created by me. The ERT data were completed by Multi-Phase Technologies, LLC with assistance by the author. The maps and cross sections of

the ERT data were created by Multi-Phase Technologies, LLC. All data comparison was carried out by the author.

CHAPTER 5: SITE CHARACTERISTICS

Location

The field work took place in the upstate of South Carolina in Powdersville near Greenville (Figure 5). The field site location was adjacent to River Road and located at the latitude and longitude coordinates 34°46'45.39" N 82°28'26.44" W. The field site had and area of approximately 1,285 m^2.

Land Use

The field site was cleared previously. Therefore very little vegetation is present at the site, and loose soil makes up the majority of the area.

Experimental Cells

The site area was divided up into six 9 meter by 9 meter cells with the intent to create one fracture in each cell (Figure 6). These cells were labeled one through six.

Geology

The soil series at the field site is the Hiwassee series (Soil Survey Staff). More than one hundred soil cores were collected at the site. A subset of the soil cores were cut open and three soil units were described. Based on the soil core analysis, the three soil horizons recognized at the site were a soil unit, a soil/saprolite upper transition unit, and a saprolite.

a)

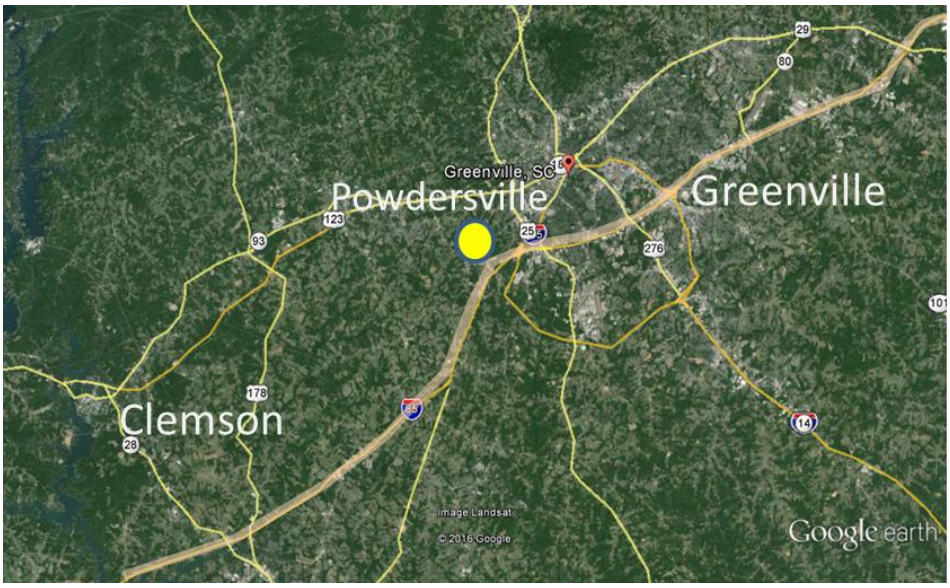

b)

Figure 5: a) Map of the field site location in relation to Interstate 85 (thicker orange outline) and surrounding cities. b) The pin point is the location of the field site adjacent to River Road.

Figure 6: Map view of locations of the six test cells used in this study. Outlines of the cells are in red. Injection wells are marked with a green cross. Blue dashed lines are wire coils surrounding Cells 5 and 6.

Soil Unit

The upper soil horizon was present in approximately 36 of the cores. In 29 of the soil cores, the color of soil unit was 2.5 YR 4/6 (red) according to the Munsell color system. In the other cores, the soil was also red but had a different hue, value, or chroma (e.g. 2.5 YR 4/8, 2.5 YR 5/8, 10 R 4/8, 10 R 5/8). In one soil core, the upper soil unit was 5 YR 5/8 (yellowish red). In a few of the soil cores, reddish yellow (7.5 YR 6/8) mottles were present in this soil horizon. The structure of the soil is remarkably consistent. The majority of the soil has a weak to medium subangular blocky structure. Only nine of the cores showed a different structure. In these cores, the top part of the soil unit had a moderate blocky structure. The soil is also moderately plastic. The mineralogy of the unit consists of red clay particles and mica flakes. In some instances, very small feldspars grains are present. In nine of the soil cores, dark layers (probably manganese oxide) were present. These dark layers were approximately 1 mm thick and were subhorizontal.

The United States Department of Agriculture soil classification system was employed to determine the type of soil present in this soil unit. Based on this classification system, the ribbon test was used to determine the soil type. It was possible to create a ribbon about 2.5 cm long before the ribbon broke. When the soil was rubbed with the forefinger, it varied from slightly gritty to smooth. This led to this soil horizon being classified as silty clay loam to clay loam and is labeled with an L on all of the following soil maps.

This soil unit can be further broken down into two sub-units: L3 and L4. The only significant difference between these two sub-units is L4 has a weak subangular blocky structure, and L3 has moderate subangular blocky structure.

Upper Transition Unit

Below the soil unit is a soil/saprolite upper transition unit. This zone contains quartz, feldspars, and micas such as biotite. The soil color in this soil horizon is inconsistent. It ranges from strong brown (7.5 YR 5/6) to brown (7.5 YR 4/4, 7.5 YR 5/4) to yellowish brown (10 YR 5/4, 10 YR 5/6) to light yellowish brown (10 YR 6/4), to light reddish brown (5 YR 6/4), to yellowish red (5 YR 4/6, 5 YR 5/6, 5 YR 5/8) to reddish yellow (5 YR 6/8, 5 YR 7/6,7.5 YR 6/6) to light red (2.5 YR 6/6, 10 R 6/8) to red (2.5 YR 5/8, 10 R 5/8). The most common colors were yellowish red, reddish yellow, and red. The only consistent characteristic that can be said about the color of the soil unit was that it was generally a darker color near the bottom of the core and became a lighter color as you moved up the core. The lack of texture of this layer is remarkably consistent. In 88%

of the cores, virtually no structure is present. The exceptions are two cores that have a weak blocky structure and one core where layers of saprolite material were present in the upper transition zone. Regardless of whether or not texture is present in this layer, the soil is in the unit always had a friable consistency. Like the L soil unit, thin (approximately 1 mm thick) subhorizontal dark layers (probably manganese oxide) are present locally. The contact between the L soil horizon and the soil unit is a gradational contact.

The United States Department of Agriculture soil classification system was employed to determine the type of soil present in the upper transition unit. Based on this classification system, the ribbon test was used to determine the soil type. The ribbon created by the soil was less than 2.5 cm long before the ribbon broke. When the soil was rubbed with the forefinger, it varied from gritty to smooth to neither gritty or smoothness predominating. This led to this soil horizon being classified as loam to sandy loam and is labeled with a T on all of the following soil maps.

Based on the characteristics of this layer, it was labeled as a upper transition zone since it is too highly weathered to be characterized as saprolite but not weathered enough to be considered part of the soil horizon.

Saprolite Unit

The deepest layer observed was the saprolite. Quartz, feldspars, and micas are present. The feldspars were still clearly visible when the soil was viewed with a hand lens. The majority of the saprolite was very pale brown (10 YR 8/2, 10 YR 8/3, 10 YR 8/4), white (10 YR 8/1), or yellowish brown (10 YR 5/6). The colors light gray (10 YR

7/2), brown (7.5 YR 5/4), or brownish yellow (10 YR 6/6) were present in three of the cores.

The saprolite had a phaneritic texture. No defined structure or fabric was present in 78% of the soil cores were the saprolite was present. The remaining three cores showed some evidence of fabric. One core (F6-4/275) had a layered fabric present. Another core (F6-4/169) had a layered structure where the felsic material was alternating with layers of red and yellowish brown material. Soil core C4-2/250 had a layered appearance due to the veins of large feldspar grains. The soil is in the saprolite unit always had a friable consistency. The saprolite material appears to be a weathered felsic rock such as granite or gneiss.

There were two types of contacts between the saprolite and the upper soil layers: the saprolite/upper transition contact and the saprolite/loam contact. In eight of the cores where the saprolite unit was present, the contact was between the loam soil unit and the saprolite. In the other six soil cores where the saprolite unit was present, the contact was between the upper transition unit and the saprolite. Both types of contacts were gradational except for soil core F6-4/169 which had a sharp contact between the loam soil unit and the saprolite unit. The soil cores collected at the site were not deep enough to determine the lower contact of the saprolite unit.

Soil Core Maps

The information from the soil cores was used to create a geologic map of the field site (Figure 7). The origin of the coordinates is the injection well of Cell 2. The crosses

indicate the locations where a soil core was collected. Each point is labeled with the unit that was exposed at the ground surface. The geologic map shows that the majority of the site is underlain by the L soil unit. The L4 subunit is the main subunit present with small isolated areas of L3 present. The upper transition unit is exposed at the surface in the northeast and southeast corners of the map. It is interpreted that the upper transition unit is present at the surface because the surface was excavated by the owner prior to the beginning of this research project. This is also the reason that the remaining L3 surfaces are isolated from each other.

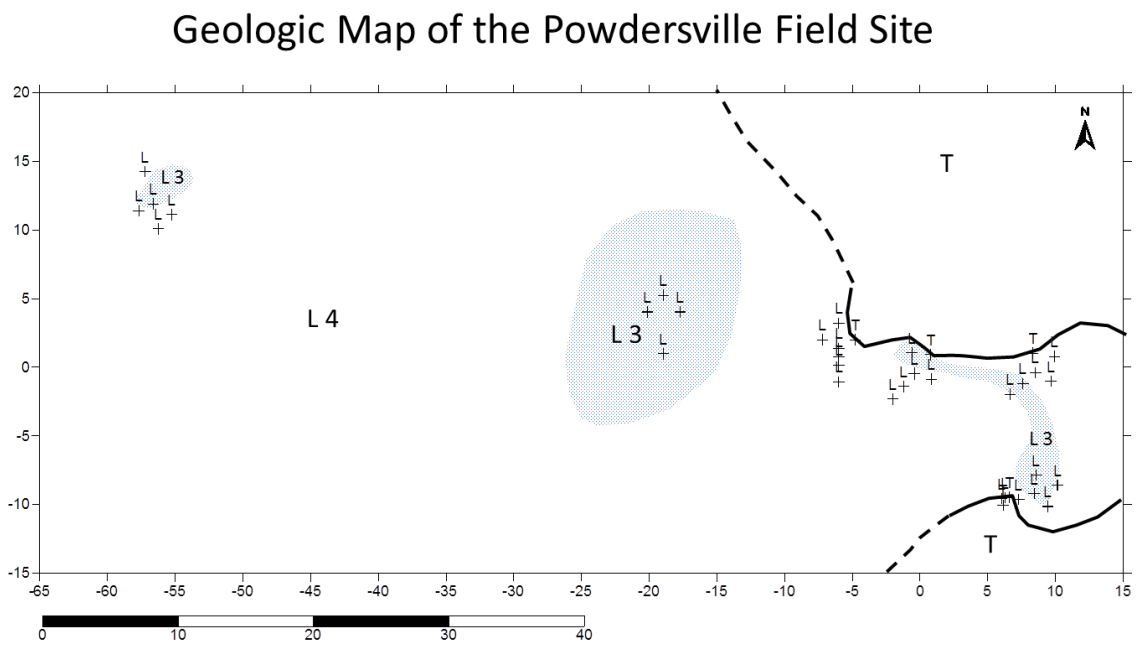

Figure 7: Geologic map of the Powdersville field site based on soil core data. The origin point (0,0) is the injection well of Cell 2. The crosses represent soil core locations. The data points are labeled with the unit that was located at the surface. L stands for Loam soil unit. T stands for the upper transition unit. The areas where L3 is present are shaded light blue. Solid lines represent boundaries that have a high degree of certainty due to a high data population in that location. The dashed lines indicate low certainty of the soil boundaries due to sparse data in those areas.

The soil core data were then employed to create soil unit maps of the surfaces of the upper transition unit and the saprolite unit. The contour map for the upper transition unit is shown in Figure 8. Once again, the origin point (0,0) is the injection well of Cell 2. The crosses represent soil core locations where the upper transition unit was present. The data points are labeled with the elevation above sea level of the upper transition unit. Solid contour lines have a high degree of certainty, and dashed contour lines have a low certainty due to sparse data in those areas. Red shaded areas show where the upper transition unit is now exposed at the surface of the earth. In the areas where the upper

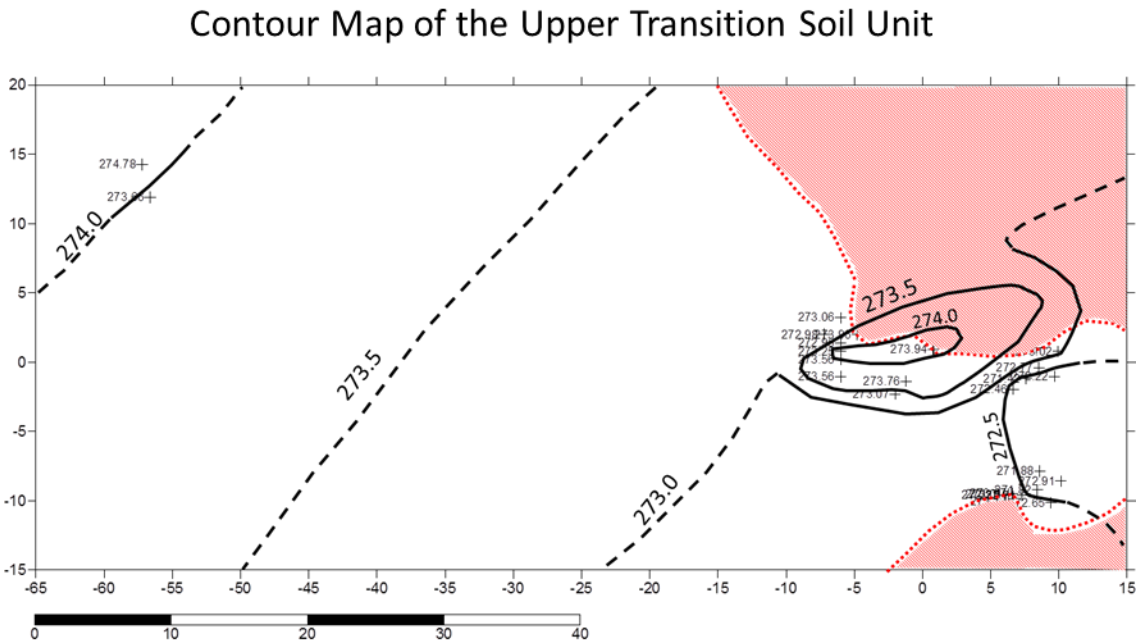

Figure 8: Contour map of the upper surface of the upper transition unit. The origin point (0,0) is the injection well of Cell 2. The crosses represent soil core locations where the upper transition unit was present. The data points are labeled with the elevation above sea level of the upper surface of the upper transition unit. Solid lines represent contours that have a high degree of certainty due to a high data population in that location. The dashed lines indicate low certainty of the contour lines due to sparse data in those areas. Red shaded areas show where the upper transition unit is now exposed at the surface of the earth. All values are in meters.

transition unit is now exposed to the surface of the earth, the unit has been weathered and eroded. As a result, it is not possible to determine the contours for the unaltered surface of the unit in these areas. The contours drawn in these red areas are highly suspect. The contour line for 273.5 meters is located in an area where no data were collected. Therefore, the strike of this contour line was drawn to mirror the approximate strike of the surface of the earth.

The contour map for the saprolite material is shown in Figure 9. As in the previous maps, the Cell 2 injection well is located at the origin. The soil core locations where saprolite was present are marked with crosses and labeled with the elevation in

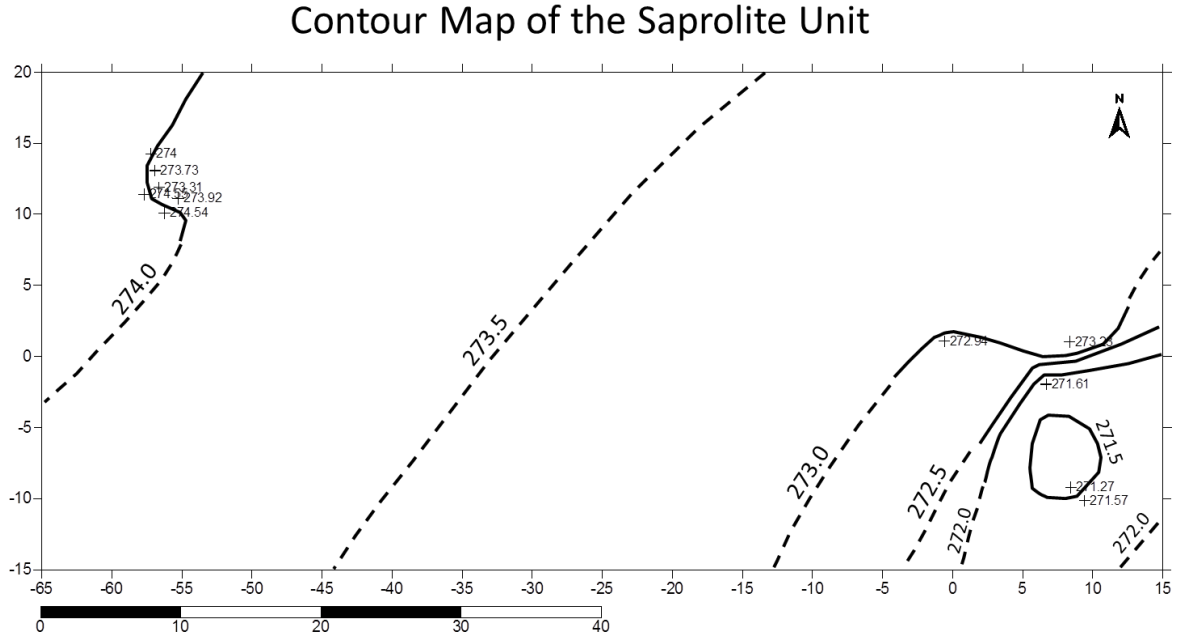

Figure 9: Contour map of the upper surface of the saprolite material. The origin point (0,0) is the injection well of Cell 2. The crosses represent soil core locations where the saprolite material was present. The data points are labeled with the elevation above sea level of the upper surface of the saprolite material. Solid lines represent contours that have a high degree of certainty due to a high data population in that location. The dashed lines indicate low certainty of the contour lines due to sparse data in those areas. All values are in meters.

meters. The solid contour lines represent areas with a high degree of certainty, and the dashed contour lines show where there is low degree of certainty. The contour lines for the surface of the saprolite unit follow the same approximate strike and dip direction as the earth's surface. Once again, the contour line for 273.5 meters is located in an area where no data were collected. Therefore, the strike of this contour line was drawn to mirror the approximate strike of the surface of the earth.

Field Site Hydraulic Conductivity

The hydraulic conductivity was measured at the site in three different locations using a Guelph permeameter. The first location was in Cell 2. The test was carried out 5 feet from the injection well of Cell 2 along an azimuth of 147°. A hand auger was used to create a hole 2 feet deep on the bench surrounding the trenches. This bench was 2 feet below the surface of the earth. Therefore, the depth that the Guelph permeameter was actually sampling was 4 feet below the ground surface. The soil removed from by the hand auger indicated that the soil unit that was being sampled was the upper transition unit. Two different tests were carried out. The first test set the water level in the well to 5 cm. The second test set the water level in the well to 10 cm. A combined reservoir was used for both tests. The water in the reservoir was recorded every 2 minutes. The data from these tests was entered in to a Guelph permeameter data sheet on Excel that calculated the hydraulic conductivity of the soil. Based on this data sheet, the hydraulic conductivity in the upper transition unit at this location is 7.33×10^{-4} cm/sec.

A similar test was carried out in the upper transition unit in Cell 4. This test was located 5 feet from the Cell 4 injection well along an azimuth of 154°. The hand auger was used to create a 1 foot deep hole on the bench surrounding the injection well. The bench was 2 feet below the surface of the earth. This indicates that the Guelph permeameter was determining the hydraulic conductivity of the soil 3 feet below ground surface. The soil removed by the hand auger indicated that the soil tested was the upper transition unit. As with the previous test, the combined reservoirs were used and the water level in the reservoir was recorded every 2 minutes. Two different tests were carried out. The first test set the water level in the well to 5 cm. The second test set the water level in the well to 10 cm. When the information from these tests was entered into an Excel Guelph permeameter data sheet, the hydraulic conductivity was determined to be $2.73x10^{-3}$ cm/sec.

A third Guelph permeameter test was completed outside the boundaries of the test cells. However, the location was notated in relation to Cell 2. The test took place 24 feet from the Cell 2 injection well and along an azimuth of 215°. The hand auger was used to create a hole 1 foot below the surface of the earth. Based on the soil removed by the hand auger, the soil unit the Guelph permeameter was located in was the upper soil unit. The combined reservoir was used for both tests that were carried out. The water level in the well for the first test was 5 cm, and the water level in the well for the second test was 10 cm. The water level in the reservoir was recorded every 2 minutes. When the data from this test was inserted into an Excel Guelph permeameter data sheet, the hydraulic conductivity was determined to be $1.26x10^{-3}$ cm/sec. However, this K value is suspect

because a number of problems occurred during the Guelph permeameter test at this location. During the test when the water level in the reservoir was 5 cm, the test had to be run several times. The water was draining out the reservoir so quickly that the water level could only be recorded at time 0 minutes and time 2 minutes.

The hydraulic conductivity values measured at the site are the same magnitude or greater than the average hydraulic conductivity of sand. This indicates that the hydraulic conductivity at the site is high and has the potential for a large amount of leakoff.

CHAPTER 6: METHODS

Fracture Creation

Fractures were created using three different proppants using methods developed by the company FRx. These fractures were then analyzed to determine their characteristics.

Fracture Creation

Methods developed by FRx were employed to create fractures at the Powdersville site. The site was divided up into six 9 meter by 9 meter cells. The cells were numbered 1 through 6. The first step in this process was to install a metal casing to a depth of 5 feet (1.5 meters) in the center of each cell. A notch was then cut at a 90° to the casing at the bottom of the borehole using a pressure washer. This notch serves to nucleate the fracture at the predetermined depth. The slurry injected into the well consisted of guar gum mixed with a cross linker and a breaker. The purpose of the breaker is to break down the crosslinked guar gum after fracture formation. This allows the slurry fluid to flow out through the formation and leave only the proppant in the fracture. The proppants for the fractures were mixed in the hopper on the truck. The proppant and the slurry were then mixed together using a screw auger. This fluid/proppant mix was pumped into the well using a centrifugal pump. The fluid flowed into the notch and expanded from this point to create a fracture. The proppant weight and slurry volume for each cell is listed in Table 1. During the fracturing process, the pressure was monitored. A sudden pressure decrease

Cell	Proppant	Proppant Thickness (mm)	Proppant Weight (N)	Slurry Volume (m^3)	Fracture Uplift Length (m)
1	Coke Breeze	14	2006	0.33	7.8
2	30% Coke Breeze and 70% Sand	20	2006	0.38	6.1
3	30% Coke Breeze and 70% Sand	15	1779	0.50	N/A
4	Coke Breeze	15	1708	0.83	7.1
5	Steel Shot	20	5560	0.45	7.4
6	Steel Shot	18	5560	0.83	6.8

Table 1 Details of Fracture Injection Volumes and Resulting Uplift: Table listing the proppant used in each cell, the average proppant thickness, the proppant weight injected into each fracture, the slurry volume injected into each fracture, and the length of the uplift caused by fracture created in each cell.

occurs at the beginning of fracturing, and the pressure continues to decrease as the fracturing progresses (Murdoch, 1995).

Proppant

Three different types of proppant were employed when creating the fractures: pure coke breeze, a coke breeze sand mix, and pure steel shot. A single proppant was

assigned to each of the cells. This information is summarized in Table 1. These three different proppants were chosen based on their geophysical contrast properties. The coke breeze proppant is composed of carbon and causes a resistivity contrast. The coke breeze was obtained from the company Loresco. According to the company website, the coke breeze is listed as product SC-2, and it is an electrically conductive earth contact backfill (SC-2 Super Conducting Earth Contact Backfill). The material is dust-free and increases electron flow between the anode and the coke breeze material (SC-2 Super Conducting Earth Contact Backfill). The maximum diameter of the coke breeze was 1 mm (SC-2 Super Conducting Earth Contact Backfill). The material easily mixes with water to form a mud like substance (SC-2 Super Conducting Earth Contact Backfill).

The coke breeze sand mix was a combination of 30% coke breeze and 70 % well-sorted quartz sand. The grain size of the sand was 20 mesh to 40 mesh (Multi-Phase Technologies, 2016). This proppant was made by mixing together the two materials by hand in the 25 $ft.^3$ hopper of the fracturing rig. When pouring the materials into the hopper, the sand and coke breeze were added in an alternating order. This resulted in a rough and imperfect mix of the materials. The sand and coke breeze was then mixed dry with a screw auger before being mixed with the slurry material with another screw auger. This proppant also results in a resistivity contrast between the proppant and the surrounding soil.

The steel shot proppant is composed of recycled steel shot and has a magnetic and resistivity contrast. The steel shot was obtained from GMA Industries. The steel shot is made up of recycled material that is washed and cleaned (Steel Shot and Steel Grit).

Geomechanical Methods

Two types of geomechanical data were collected: tiltmeters data and uplift data. This data were analyzed to determine the shape and extent of the fracture.

Tiltmeter and Uplift Data

Tiltmeter data were collected during fracture formation. A mixture of the high-gain and mid-range Model 701-2 Platform Tiltmeters by Jewell Instruments, LLC were employed at the field site. The tiltmeters are 150 mm x 150 mm x 100 mm (700 Series High-Precision Tiltmeters). They are made of painted and anodized aluminum and have adjustable legs that allow the unit to be leveled (700 Series High-Precision Tiltmeters). Each unit has two perpendicular tilt sensors that are parallel to the base plate sides. Each tiltmeter is also equipped with a temperature sensor (700 Series High-Precision Tiltmeters). The tiltmeters have two low-pass filter settings and two switchable gains (700 Series High-Precision Tiltmeters). The high-gain tiltmeters have a resolution of 0.1 μradian, and the mid-range tiltmeters have a resolution of 1 μradian (700 Series High-Precision Tiltmeters). Paving stones were set up in concentric pentagons around the injection well. The tiltmeters were set on top of the paving stones and leveled using a bubble level.

A Northwest Instrument 2'' Reflectorless Total Station Model NTS02 was employed to survey the tiltmeters before, during, and after fracture creation. The total station has an Electronic Distance Measure (EDM) Laser to collect reflector-less measurements and has a 2" angular accuracy (Engineer Supply, LLC). The unit has a magnification of 30x or 1°20' field of view and a resolving power of 4.0" (Engineer Supply, LLC). The minimum sight distance for the total station is 1.2 meters or 3.94 feet (Engineer Supply, LLC).

The fifteen tiltmeters were set up and surveyed before fracturing occurs. The tiltmeters remained in this same location during fracture creation. During the fracturing process, the creation of the fracture resulted in uplift of the Earth's surface. The tiltmeters were then surveyed again after the fracture had been created. Because of the uplift caused by the injection, there was a change in location along the Z axis. The Z axis measurement recorded before fracture injection can be subtracted from the Z axis measurement recorded after fracture injection to determine the change in the Z axis value. This change in Z is the amount of uplift that occurred during the fracture creation. Sketches of the cracks formed at the Earth's surface during fracture creation were also recorded.

Analysis

The tiltmeter and uplift data were analyzed and inverted by FRx Inc. The uplift data were recorded in Surfer®, and uplift contour plots were created for each cell using the default kriging method. The fracture length was estimated by measuring the diameter of the uplift on the contour plots (Table 1). After the contour maps were created, the

fracture surface cracks were sketched on top of the maps. These uplift contour plots were overlain on the respective ERT data maps to determine if both sets of results indicate the same location and extent of the fracture.

To compare the uplift maps from each cell, several measurements were made based on the 3 mm uplift contour on each plot. These measurements included the major axis length, the minor axis length, the distance from the center of uplift to the borehole, and the distance from the center of uplift to the maximum uplift (Murdoch and Slack, 2002). The center of uplift is the point at which the major axis and minor axis cross.

These measurements were then used to calculate the borehole eccentricity and the displacement eccentricity (Murdoch and Slack, 2002). The equations for these calculations are shown below.

$$Borehole\ Eccentricity = \frac{Distance\ from\ the\ Center\ of\ Uplift\ to\ the\ Borehole}{Major\ Axis\ Length} \quad (1)$$

$$Displacement\ Eccentricity = \frac{Distance\ from\ the\ Center\ of\ Uplift\ to\ the\ Maximum\ Uplift}{Major\ Axis\ Length} \quad (2)$$

The ratio of major axis length to the initiation depth and the ratio of the major axis length to the minor axis length were also calculated.

Geophysical Methods

Three geophysical methods were employed at the site: electrical resistivity tomography (ERT), magnetometric resistivity (MMR), and ground penetrating radar (GPR). The MMR was collected as part of the larger project. The GPR data was collected

by our collaborators as part of the larger project to analyze geophysical methods that are able to detect fractures in the subsurface. An assessment of ERT will be the focus of this work.

Electrical Resistivity Tomography

Electrical resistivity tomography uses electrodes hammered into the ground to measure the voltage between different pairs of electrodes. A current is applied between two electrodes and the voltage difference is measured between the remaining sets of electrodes (Daily et al., 1990). This process is repeated until all the electrode pairs have served as the current electrodes (Daily et al., 1990).The current and the measured voltage are then used to determine the resistivity of the subsurface. The ERT tests consisted of creating a two dimensional array of electrodes instead of the conventional design of electrodes in a single line (LaBrecque et al. 2004). This method allows a two dimensional or three dimensional image of the resistivity of the area to be developed using inversion methods (LaBrecque et al. 2004).

To complete the geophysical surveys at this site, a 9 m by 9 m grid was created around the injection well. The injection well served as the origin point within the grid. The grid extended 4.5 meters to the north, south, east, and west of the origin. The electrodes were placed 1 meter apart with the injection well at the center. A set of 12 cables were employed to connect these surface electrodes to the ERT DAS-1 system to record the electrical resistivity tomography data. Saltwater was poured on the electrodes to decrease the contact resistance between the Earth and the electrodes. Four vertical

electrode cables were included near the corners of the cell. The surface cables were employed to connect the vertical electrodes cables to the ERT DAS-1 system. A dipole-dipole electrode geometry was used to collect and analyze the data. Two sets of geophysical measurements were completed. An ERT survey was completed for each of the cells prior to fracture creation. A survey was also completed at each cell between 24 and 48 hours after the fractures were created.

Electrical Resistivity Tomography Analysis

Analysis of this data was completed in the ERTLab 3-D Inversion Software (personal communication). The electrical resistivity data were converted into electrical conductivity data using the MMPT3D inversion algorithm (LaBrecque et al, 2003). This inversion algorithm employs a modified version of Occams inversion to determine the smoothest possible solution (LaBrecque and Yang, 2001; LaBrecque et al, 2003). This algorithm is a difference inversion (LaBrecque and Yang, 2001). To complete this process, the background data are first inverted using Occams inversion process (LaBrecque and Yang, 2001). The data collected after the proppant was injected are then subtracted from the background data and are inverted using the modified algorithm to create maps and cross sections of the change in electrical conductivity at the site (Stubben and LaBrecque, 1998; LaBrecque and Yang, 2001).

Magnetometric Resistivity

Magnetometric resistivity data were collected by measuring the magnetic field induced by running an electric current through the electrodes. The magnetic field was

employed to estimate the electrical resistivity and the induced polarization (Multi-Phase Technologies, 2016).

Magnetometric Resistivity Analysis

The MMR results were analyzed by converting the magnetic field measurements to electrical resistivity and then to electrical conductivity. The MMR results were inverted simultaneously with the ERT results to determine the location and extent of the fracture (Multi-Phase Technologies, 2016). The same inversion algorithm used to process the ERT data was employed to process the MMR data (personal communication).

Soil Coring

Soil cores were collected and analyzed to measure the location of injected proppant and to determine the soil composition. The soil cores were obtained after fracture creation.

Field methods

An AMS 9100 ATM Powerprobe attached to an all-terrain vehicle was used to collect the soil cores. The cores were obtained by hammering two clear cylindrical butyrate sample tubes into the soil, and then recovering the sample tubes containing the cores. The soil cores were about seven feet long and two inches in diameter. The ends of the tubes were sealed with plastic caps in the field and transported to the lab. An initial set of seven soil cores was collected from each of the six test cells. Each core contained soil from the surface to a depth of 2.1 meters (7 feet). A coordinate system with the

injection well at the origin was established in each cell. The soil cores were located and named based on the azimuth to the soil core and the distance from the injection well to the core location. For each cell, a soil core was taken 1.2 meters or 4 feet from the well in 4 directions that are 90° from each other. One of the azimuths chosen was the direction of maximum fracture extent based on the surface cracks during fracturing, uplift data and tiltmeter data. Soil cores were also collected at distances of 0.6 meter (2 feet), 1.8 meters (6 feet), and 3 meters (10 feet) from the well along the direction of maximum fracture extent.

The first round of soil cores was opened in the lab. A tape measure was employed to measure either the distance from the top or the distance from the bottom of the core to the fracture location. If the distance to the fracture was measured from the top of the core, the depth to fracture was recorded as the measured value. If the distance to the fracture was measured from the bottom of the core, the measured value was subtracted from the depth of the hole to determine the depth to the fracture.

Based on the results of the first round of soil cores and the initial results of the ERT data, locations for a second round of cores were chosen to further confirm the fracture location. The second round of cores was analyzed in the field to enable immediate adjustment to the coring plans. This helped ensure that only cores containing or just beyond the fracture extent were collected and prevent time being spent analyzing cores farther out from the fracture.

Measurement of the depth of the hole created when collecting the core was obtained by dropping a tape measure down the hole and recoding the depth below surface. Fracture depth was also confirmed in the cells with steel shot proppant by dropping a magnet down the soil core hole and measuring the depth. To complete this field check, a strong magnet was tied to the end of a string and slowly lowered down the borehole. Once the magnet attached to the fracture, the string and magnet were withdrawn from the borehole, and the length of the string was measured with a measuring tape to determine the depth to the fracture.

Analysis

The soil core location, azimuth of the core relative to the injection well, and depth from the surface of the earth to the fracture was recorded in Excel (Appendix A). Cross sections were created using the soil core data. The location of the injection well was included on these cross sections as a fixed location marker. The soil core location data were also sent to Multi-Phase Technologies, LLC so they could plot the soil core locations on ERT maps they created.

Excavation and Mapping

Trenches were dug in Cells 2 and 4 to characterize the shape of the fracture in detail and compare it to the ERT data. The trenches were dug with a backhoe with a 0.6 m wide bucket during two separate field sessions. These trenches were benched by removing the top two feet of soil surrounding the trenches. During July 2015, a single trench was dug in each of the chosen cells (Figure 10). These trenches were designated

Cell 2 Trench 1 and Cell 4 Trench 1. The trenches were straight, dug past the location of the injection well, and parallel to the long axis of the fracture. The long axis of the fracture was chosen based on the ERT data and uplift maps. In Cell 2, the azimuth of Trench 1 was 137°/227°. In Cell 4, the azimuth of Trench 1 was 64°/244°. One wall of the trench was located within a few tenths of a meter from the cell injection well. Therefore, this exposure served as a rough radial cross section of the fracture. The opposite wall of the trench was a parallel cross section that was offset from the radial cross section by about 0.6 meters. In October 2015, two more trenches transverse to Trench 1 were dug in Cell 2. One of these trenches (Trench 2) was located 1.5 meters southwest of the injection well and had an azimuth of 122°/302°. Trench 3 in Cell 2 was dug at the northeast end of Trench 1 and also had an azimuth of 122°/302°. Cell 2 Trench 3 was dug at the northeast end of Trench 1 in an effort to expose the tip of the fracture. As a result, the fracture was only present on south wall of the trench. Efforts to find the tip of the fracture across the entire trench also caused the west face of the south wall to be located 0.76 meters closer to the injection well than the east face (see trench maps in Figure 21).

In the area surrounding the trenches, 0.5 to 1.0 meters of soil was removed in order to create benches that decrease the depth of each trench face (Figure 10). This was done as a safety measure. The trenches dug 0.5 to 1.0 meters below the depth of the fracture to facilitate mapping (Figures 11 through 13).

The soil was smeared on the walls of the trenches during excavation, and this either obscured or distorted the appearance of the fractures. To remove the effects of the smearing, the walls of the trenches were cleaned with a knife. This created an approximately planar exposure surface that could be mapped. Over time, the loose proppant in the fractures would fall out of the fractures causing the fractures to recede

Figure 10: Excavation of Cell 2. a.) Backhoe used to dig trenches b.) Trench 1 exposing hydraulic fracture in Cell 2 c.) Surveying Trench 1 in Cell 2 d.) panorama of field site during excavation

a)

b)

Figure 11: Trench 1 showing hydraulic fracture in Cell 2. a) East wall of Trench 1. Injection casing is on the upper left side. Yellow band is a measuring tape above the fracture. Small white squares above the fracture are 1 cm x 1 cm scales for close pictures. b) Trace of the fracture on the west wall of Cell 2.

a)

b)

Figure 12: Mapping Cell 2 Trench 1. a) East side of Trench 1. b) West side of Trench 1.

a)

b)

Figure 13: Mapping hydraulic fracture in Trench 1. a) Fracture trace exposed on east wall of Trench 1 in Cell 2. White squares are 1 cm x 1 cm scales spaced one foot apart along the fracture. Horizontal datum defined by measuring tape starting at southern tip of fracture. b) West wall of Cell 2 Trench 1.

over time. To alleviate this problem, the fractures were scraped multiple times during the mapping process.

At the beginning of the mapping phase of the project, a horizontal scale was established by attaching a measuring tape to the wall of the trench. This reference measuring tape extended from the tip of the fracture at one end of the trench to tip of the fracture at the opposite end of the trench. In Cell 2 Trench 1, the zero foot mark of the tape was always placed at the south end of the trench. In Cell 2 Trench 2, Cell 2 Trench 3, and Cell 4 Trench 1, the zero foot mark was always placed at the east end of the trench. Markers were placed on the walls of the trench every foot or 0.3 meters along a tape. The reflective markers were 1.0 cm x 1.0 cm squares with internal gradations of 2 mm. A small piece of reflective tape was placed in the center of these squares to make them reflective. The markers were placed 2.5 cm above the fracture, and survey data of the fracture was then taken with an optical transit station. The transit station was then used to record the location of the fracture within the trench. This process was repeated for each wall of the trenches where the fracture was present. These data were analyzed to create cross sections of the fractures. The distribution of proppant was observed in the cells with the coke breeze and sand proppant to determine if the components separated.

The cross sections for each of the trenches were compared with the fracture cross sections generated by the ERT data. The borehole locations were also compared. In general, the cross-sections and borehole data were used to develop quantitative estimates of the error associated with predictions made by the geophysical methods.

Photographs were taken of the walls of the trenches that were combined into panorama scenes by stitching together multiple pictures. The majority of the photographs were taken with a Panasonic Lumix 10 Megapixal camera. Some of the photos were taken with the camera held by hand and supported by the photographer's hip, and the rest were taken with a tripod. The photographs were made at three different scales. For the largest scale photos, the camera employed a wide angle lens and was held about 0.4 meters from the trench wall. This field of view included both the fracture and the reference tape measure positioned above the fracture. The field of view of each photo was chosen to ensure that it overlapped with each of the surrounding photos. A second set of photographs were taken at approximately half the distance of the large scale photos. These small scale pictures showed more detail, but the reference tape was out of the field of view of most of the pictures. This resulted in a large-scale photo being used to determine the location of each of the small-scale photos. Some photographs were taken even closer to the wall to provide an even greater degree of detail.

To create the panorama photographs, the large-scale photos were stitched together using software. The stitching process recognizes overlapping areas in the photographs and merges them to create a single image. The software packages are designed to stitch together photographs that were taken from the same location. However, the photograph location changed for each of the pictures taken in the trenches. To determine the best method of stitching together these photos taken at different locations, several different stitching software packages were employed and compared. A package in Adobe Photoshop created an acceptable panorama of the Cell 2 Trench 1 East Wall, but it was

not capable of stitching together the photographs from Cell 2 Trench 1 West Wall or the photos from Cell 4. To create panoramas of these walls, the program AutoStitch was employed (http://matthewalunbrown.com/autostitch/autostitch.html). When photographs are stitched together, the original pictures are distorted in order to combine them all together to create a panorama with seamless transition between the photos. Since the measuring tape was present in all of the photographs, it was used to determine the scale and the degree of distortion that occurred during the stitching process. For example, the measuring tape appeared curved in some of the panoramas even though it was relatively straight at the field site. In Adobe Photoshop, some of the distortion was eliminated manually. Panoramas with a significant amount of distortion were eliminated. The remaining panoramas were compared with the cross sections created from the excavation data. The close match between the panoramas and excavation cross sections indicated that the degree of distortion in the panoramas was minor. The panoramas created in Adobe Photoshop were imported into Adobe Illustrator and were exported as high resolution *.jpeg files. The panoramas were used to evaluate details related to how the fracture relates to the wall rock, as well as the distribution and thickness of proppant in the fracture.

CHAPTER 7: RESULTS

In this chapter, results from the geomechanical, geophysical, soil core and excavation data will be examined.

Geomechanical Data

The contour uplift plots are shown in Figure 14. Based on these plots the general shape of the fracture can be observed. In Cell 1 (Figure 14.a), the uplift shows a generally rounded shape that is centered in the middle of the cell. The maximum uplift is 18.9 mm and is located at the same location as the injection well. Based on the three mm contour line, the length of the major axis is 7.8 m. The orange lines represent the surface cracks that occurred during the fracturing process. In Cell 1, there were few cracks at the surface. Three of the cracks were centered on the injection well while one of the cracks extended due west.

The uplift contour plot for Cell 2 (Figure 14.b) shows a fracture with a generally circular shape once again. However, the geometric center of this fracture is offset from the injection well and extends towards the southwest. The major axis length is 6.97 m. The maximum uplift is 25.4 mm and is also offset to the southwest. The surface cracks show a similar pattern. There are a cluster of 4 cracks that emanate from the injection well. Another series of cracks are present in the southwest section of the cell, and these cracks appear to be stemming from the location of maximum uplift.

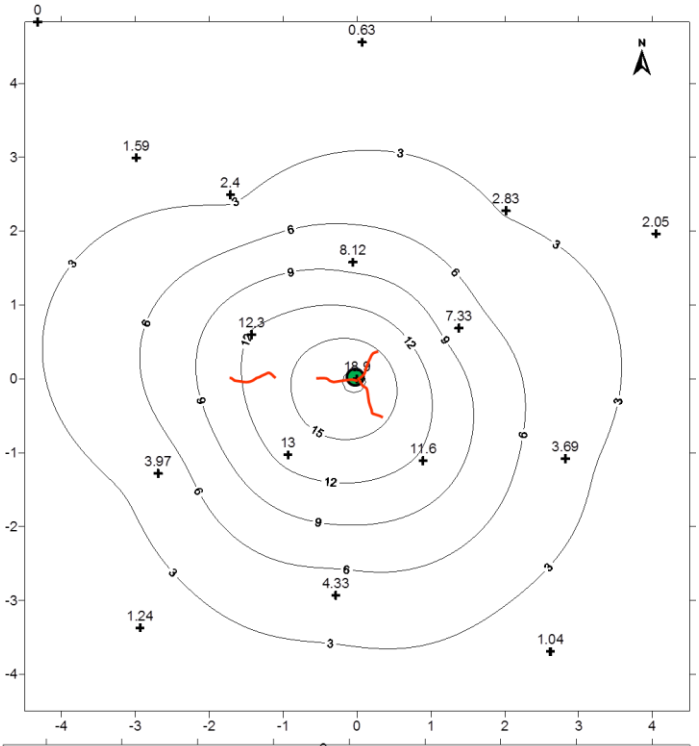
0
0.63
N
1.59
2.4
2.83
2.05
8.12
12.3
7.33
13
11.6
3.97
3.69
4.33
1.24
1.04

a)

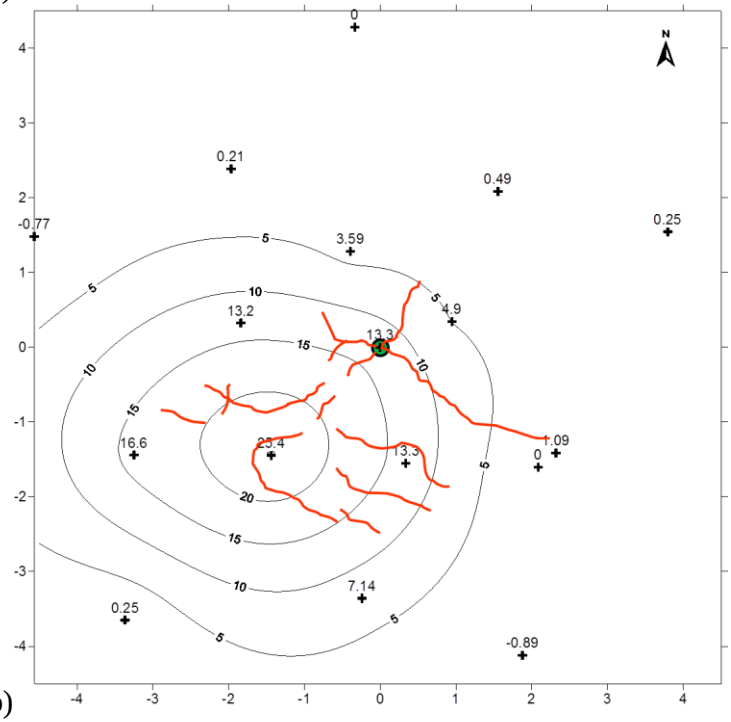
0
N
0.21
0.49
-0.77
3.59
0.25
13.2
4.9
16.6
23.4
13.3
1.09
0
7.14
0.25
-0.89

b)

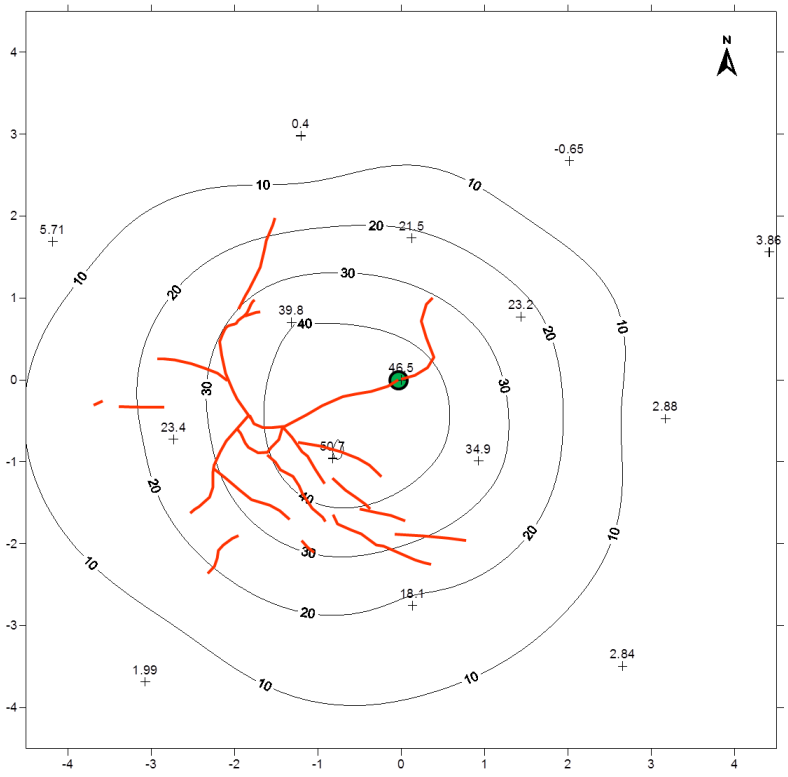
N
0.4
-0.65
5.71
21.5
3.86
39.8
23.2
46.5
2.88
23.4
50.7
34.9
18.1
2.84
1.99

c)

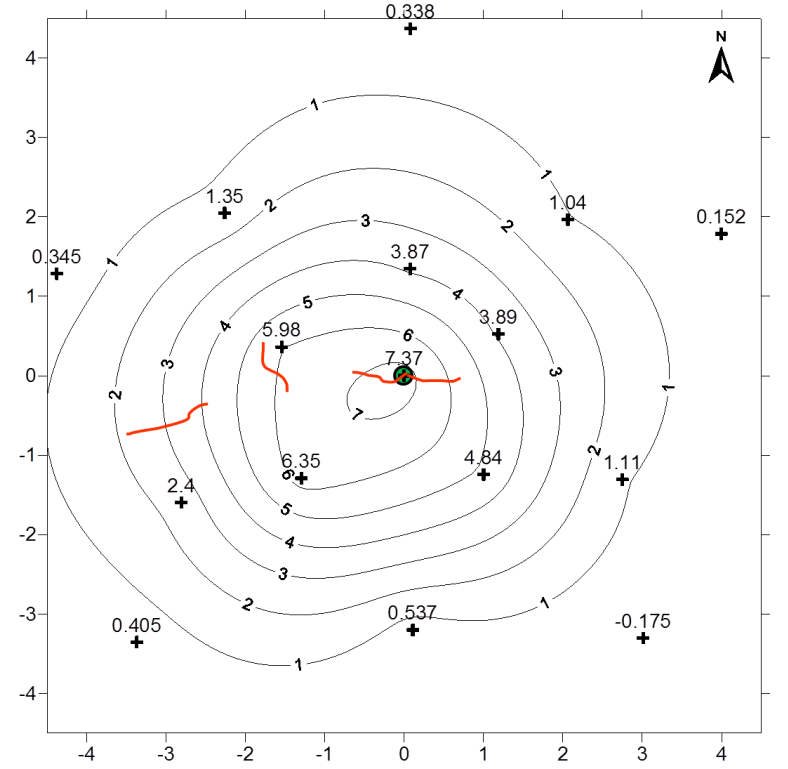
N
0.338
1.35
1.04
0.152
0.345
3.87
3.89
5.98
7.37
6.35
4.84
1.11
2.4
0.537
0.405
-0.175

d)

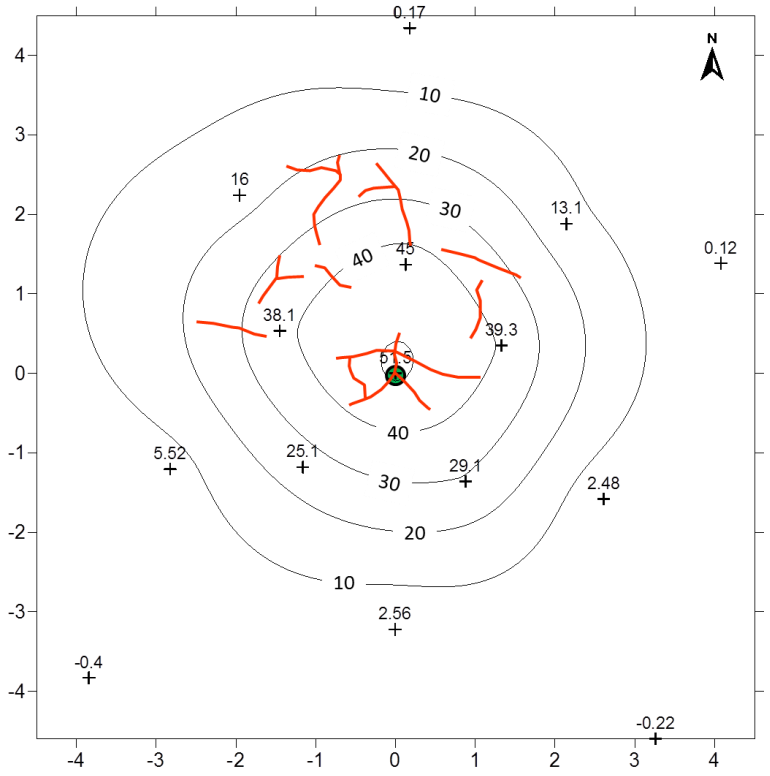

e)

Figure 14: Contour maps of uplift in mm. The injection well is the origin of the coordinates and is marked with a green circle. Locations of uplift measurements are shown with a "+" symbol. The observed uplift is in mm. The map scale is in meters. The orange lines are surface cracks that were present at the end of injection. a) Cell 1 b) Cell 2 c) Cell 4 d) Cell 5 e) Cell 6

The contour plot of Cell 4 (Figure 14.c) also indicates that the general shape of the fracture is circular, and the major axis length is 9.4 m. This fracture extends slightly towards the southwest. The maximum uplift is 50.7 mm, and the location is offset towards the southwest. There are only two cracks that emanate from the injection well in Cell 4. The remaining cracks are located in the southwest and northwest quadrants of the cell. The cracks in the southwest quadrant have an overall northwest to southeast

orientation. Those in the northwest quadrant have an overall northeast to southwest orientation.

The uplift contour plot for Cell 5 (Figure 14.d) displays a circular shape indicating that the underlying fracture also has a circular shape. The major axis length based on the 3 mm contour is 4.8 m. The uplift is mainly centered on the injection well with the contour lines indicating a slight shift towards the southwest. The maximum uplift is 7.4 mm and is centered on the injection well. Few surface cracks formed during the fracturing process. Two of the cracks originate at the injection well. The other two cracks are located to the west of the injection well. However, the presence of the two cracks to the west is suspect since it is possible that these were actually mud cracks present at the surface of the earth before fracturing.

The uplift contour map of Cell 6 (Figure 14.e) displays an uplift pattern that is relatively circular with a slight offset to the north. The major axis length of Cell 6 is 8.7 m. The maximum uplift is 51.5 mm and is centered on the injection well. Several surface cracks formed during the fracturing process. Three of these cracks emanate from the injection well. The remaining cracks are located north of the injection well and have varying orientations.

When statistics of the uplift data were calculated, several parameters were observed (Table 1). Cell 4 had the greatest major axis length at 9.4 meters, and Cell 5 had the smallest major axis length at 4.8 meters. The average major axis length was 7.5 meters. The same cells had the maximum and minimum minor axis lengths respectively.

	Cell 1	Cell 2	Cell 4	Cell 5	Cell 6	Average	Maximum	Minimum
Major Axis Length (m)	7.80	6.97	9.41	4.80	8.68	7.53	9.41	4.80
Minor Axis Length (m)	6.84	6.17	7.94	4.74	7.45	6.63	7.94	4.74
Maximum Uplift (mm)	18.90	25.40	50.70	7.37	51.50	30.77	51.50	7.37
Distance from Center of Uplift to Borehole (m)	0.18	2.29	1.03	0.66	0.57	0.95	**Table 2 Fracture Statistics Determined from Uplift Contour Maps**: Statistics taken from uplift contour maps. All measurements were taken based on the 3 mm contour line.	
Distance from Center of Uplift to Max Uplift (m)	0.18	0.23	0.29	0.66	0.57	0.39		
Borehole Eccentricity	0.02	0.33	0.11	0.14	0.07	0.13		
Displacement Eccentricity	0.02	0.03	0.03	0.14	0.07	0.06		
Ratio of Major Axis Length to Initiation Depth	5.20	4.65	6.27	3.20	5.79	5.02		
Ratio of Major Axis Length to Minor Axis Length	1.14	1.13	1.19	1.01	1.17	1.13		

The minor axis length of Cell 4 was 7.94 meters; the minor axis length in Cell 5 was 4.74 meters. The data from all of the cells gave an average minor axis length of 6.6 meters.

The maximum uplift varied across the cells. The highest uplift was 51.5 mm in Cell 6, but Cell 5 only had a maximum uplift of 7.37 mm. The cells could be grouped into three different groups based on the maximum uplift. Cell 4 and Cell 6 both had maximum uplifts close to 50 mm. Cells 1 and 2 both had maximum uplifts near 22 mm. Cell 5 was an outlier with an uplift of only 7.4 mm. It is possible that leak off contributed to the smaller maximum uplift in Cell 5. This is a potential explanation since a greater slurry volume and proppant weight was injected into Cell 5 than in to Cells 1 and 2, but Cells 1 and 2 still had a greater maximum uplift than Cell 5 (Table 1).

The distance from the center of uplift to the borehole also varied. The maximum distance was 2.29 meters (Cell 2), and the minimum distance was 0.18 meters (Cell 1). This gave an average distance of 0.95 meters.

The distance from the center of uplift to the maximum uplift was less variable. The maximum distance for this value was 0.66 meters (Cell 5), and the minimum distance was 0.18 meters (Cell 1). The average distance calculated from all the values was 0.39 meters. This indicates that the center of uplift and the maximum uplift were very close together for the fractures that were created in Powdersville.

The borehole eccentricity values also had very little variability with a maximum value of 0.33 (Cell 2) and a minimum value of 0.02 (Cell 1). The data from all of the cells gave an average value of 0.13. The displacement eccentricity values also showed little variability. The lowest value was 0.02 (Cell 1) and the greatest value was 0.14 (Cell 5). An average value for displacement eccentricity was 0.06. The low values for the borehole eccentricity and displacement eccentricity indicate that the fractures created at the site are roughly circular.

Another statistic that was calculated was the ratio of major axis length to initiation depth. These values ranged from 3.2 (Cell 5) to 6.3 (Cell 4) with an average value of 5.0. These values indicate that the created fractures have a greater horizontal extent relative to the depth of initiation.

The ratio of the major axis length to the minor axis length was also calculated. These values ranged from 1.01 (Cell 5) to 1.19 (Cell 4), and the average value was 1.13.

All of the values were close to 1. This indicates that the major axis and minor axis were close to the same length further implying that the fractures have a circular shape.

The borehole eccentricity and the ratio of the major axis length to the minor axis are similar between the Powdersville data set and the data present in Murdoch and Slack, 2002 (Table 3). The borehole eccentricity for the Powdersville data set was 0.13, and the value from the Murdoch and Slack, 2002 paper was 0.14. The ratio of the major axis length to the minor axis length was 1.13 for the Powdersville data and was 1.2 for the data from the Murdoch and Slack, 2002 paper.

Many of the other statistic comparisons showed some discrepancies. The average major axis length at the Powdersville field site was about 1 meter less than the average major axis reported by Murdoch and Slack, 2002. The maximum uplift from the Powdersville site was also significantly higher. Murdoch and Slack determined that the average maximum uplift was 19 mm while the average maximum uplift at the

	Average from Powdersville Data	Average from Murdoch and Slack, 2002
Major Axis Length (m)	7.53 ± 1.78	8.5
Maximum Uplift (mm)	30.8 ± 19.6	18.8
Borehole Eccentricity	0.13 ± 0.12	0.14
Displacement Eccentricity	0.06 ± 0.05	0.14
Ratio of Major Axis Length to Initiation Depth	5.02 ± 1.19	3
Ratio of Major Axis Length to Minor Axis Length	1.13 ± 0.07	1.2

Table 3 Comparison of Uplift Statistics with Previous Literature: Comparison of uplift statistics from the Powdersville site and the uplift statistics presented in Murdoch and Slack, 2002.

Powdersville site was 31 mm. The standard deviations of the Powdersville data were also calculated, and the averages from the Murdoch and Slack, 2002 paper fell within the standard deviations of the Powdersville data for all categories except for displacement eccentricity and ratio of major axis length to initiation depth.

The displacement eccentricity for the Powdersville field data was 0.06; the displacement eccentricity for the data from Murdoch and Slack, 2002 was 0.14. The lower displacement eccentricity of the Powdersville data indicates that the fractures created at this field site have a more circular shape than those analyzed by Murdoch and Slack. This can be confirmed by observing the locations of the borehole, center of uplift, and maximum uplift location on the contour maps (Figure 14). The distance between the borehole, center of uplift, and maximum uplift is expected to increase as the fracture grows and becomes more asymmetric. The fractures created for this study had a more circular shape, and several of the locations (borehole, center of uplift, maximum uplift) overlapped. For example, the maximum uplift occurs at the borehole in Cells 5 and 6. In Cell 1, the maximum uplift and the center of uplift are in the same location. These overlaps and the general outline of the uplift contours confirm that the fractures have a more circular shape than those described in Murdoch and Slack, 2002.

The ratio of the major axis length to the depth of initiation was also different between the two data sets. Murdoch and Slack determined that the average ratio was 3.4. The Powdersville data gave a value of 5. This high value indicates that the fractures created in Powdersville have a greater extent in the horizontal plane than those created by

Murdoch and Slack, 2002. This discrepancy could also be caused by the differences in the initiation depths. The fracture created by Murdoch and Slack, 2002 were created at depths from 1 meter to 12 meters.

The overall similarity in the uplift statistics indicates that the fractures created at the Powdersville site are similar to the shallow hydraulic fractures created in previous studies. Thus, they are useful for determining whether the ERT method is capable of determining shallow fracture form and extent.

Geophysical Data

Inversions of the geophysical data were completed in ERTLab 3-D Inversion Software. The grid blocks for Cell 4 were 0.125 m and the grid blocks for the other cells were 0.25 m. This software was used to create a 3D field of changes in electrical conductivity that best explains the changes in the voltage between ERT surveys before and after the fractures were created. The 3D field was then displayed in 2D map view at different depths and vertical cross sections (Figures 15 through 19). Due to the higher conductivity of the proppant relative to the surrounding soil, it is interpreted that these areas of high conductivity are the location of the fracture.

The map view image of the ERT data for Cell 1 shows a high electrical conductivity area southwest of the borehole (Figure 15). This high conductivity area has a northwest to southeast orientation. The greenish blue areas in the northeast quadrant are interpreted to be relics of the inversion process. The cross section view of the ERT data

also indicates the fracture location is southwest of the borehole, and the cross section demonstrates that the fracture remained below the surface of the earth.

The ERT map view image for Cell 2 also shows a high electrical conductivity area southwest of the borehole (Figure 16). The shape of the high conductivity area in this image is more oval shaped than the area in Cell 1. The cross section view of the ERT data also indicates that the fracture is predominately located southwest of the borehole. The cross section for this cell also showed that the fracture did not reach the surface of the earth.

The map view image for the ERT data for Cell 4 displays a high electrical conductivity area that is primarily centered on the borehole with a slight elongation to the southwest (Figure 17). The cross section of Cell 4 ERT data also indicates this location. In Cell 4, the cross section shows a fracture that is curving towards the surface of the earth southwest of the borehole. According to the ERT cross section, the fracture in Cell 4 either vented at the surface of the earth or was right below the surface.

The map view image of the ERT data from Cell 5 show a high electrical conductivity area around the borehole and with significant off set to the southwest (Figure 18). The shape of this high conductivity area was roughly circular. The cross section of the ERT data is not taken through the center of the fracture and instead shows the fracture along a north/south line running through the borehole. This cross section displays a thick fracture that is primarily centered on the borehole at this location.

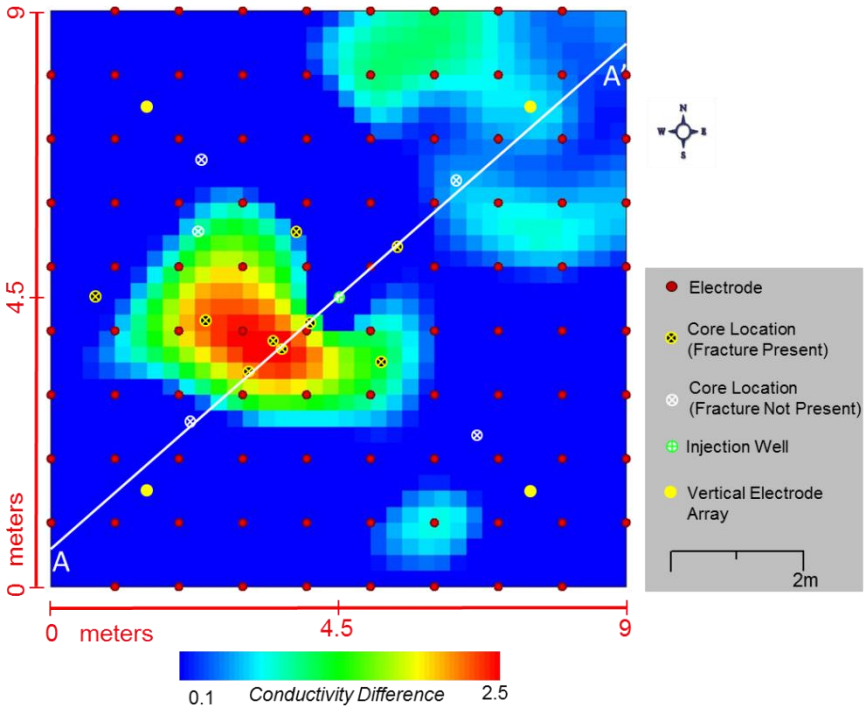

a)

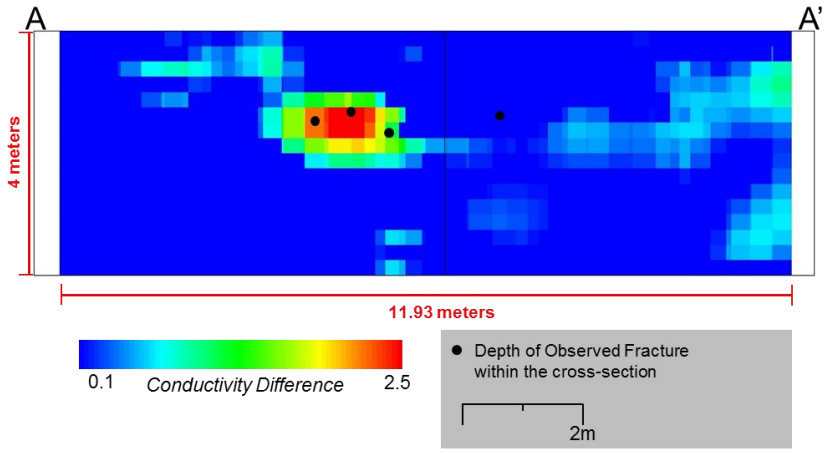

b)

Figure 15: Cell 1 ERT data. Red colored areas represent the greatest conductivity. Blue colored areas represent the lowest conductivity a) Map of electrical conductivity (color, in millisiemens log scale) at 1.6 m depth. b) Cross section on 50° azimuth of electrical conductivity (color, in millisiemens log scale).

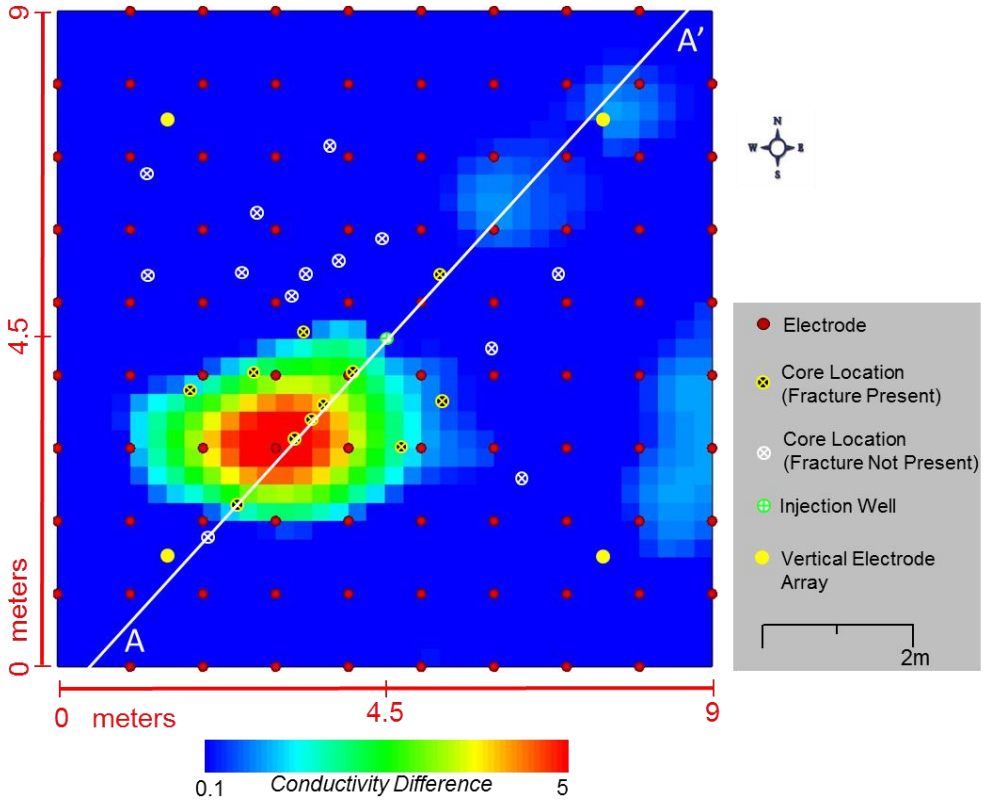

a)

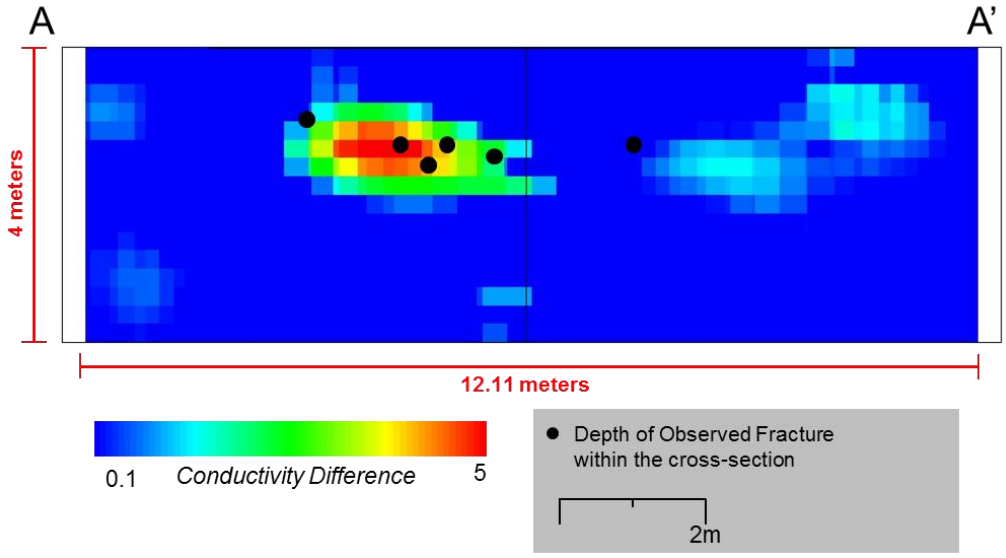

b)

Figure 16: Cell 2 ERT data. Red colored areas represent the greatest conductivity. Blue colored areas represent the lowest conductivity a) Map of electrical conductivity (color in millisiemens log scale) at 1.4 m depth. b) Cross section on 47° azimuth of electrical conductivity (color, in millisiemens log scale).

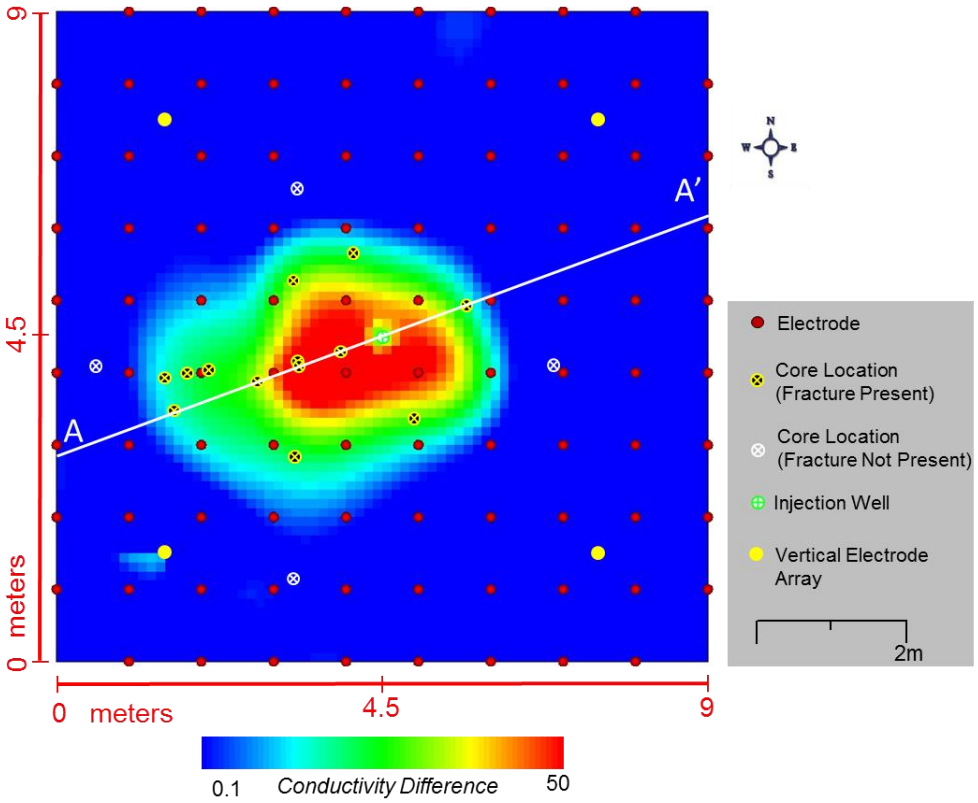

a)

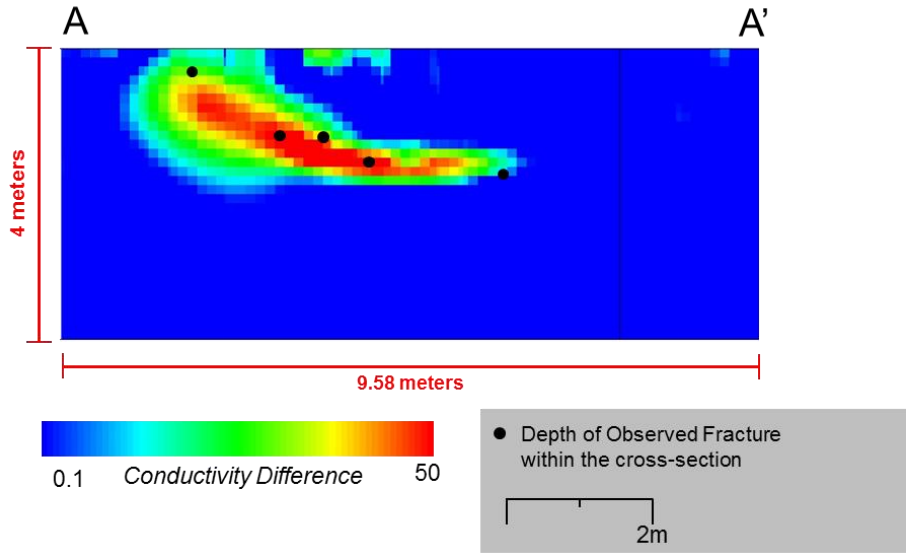

b)

Figure 17: Cell 4 ERT data. Red colored areas represent the greatest conductivity. Blue colored areas represent the lowest conductivity a) Map of the electrical conductivity (color, in millisiemens log scale) at 1.6 m depth. b) Cross section of electrical conductivity on 64° azimuth (color, in millisiemens log scale).

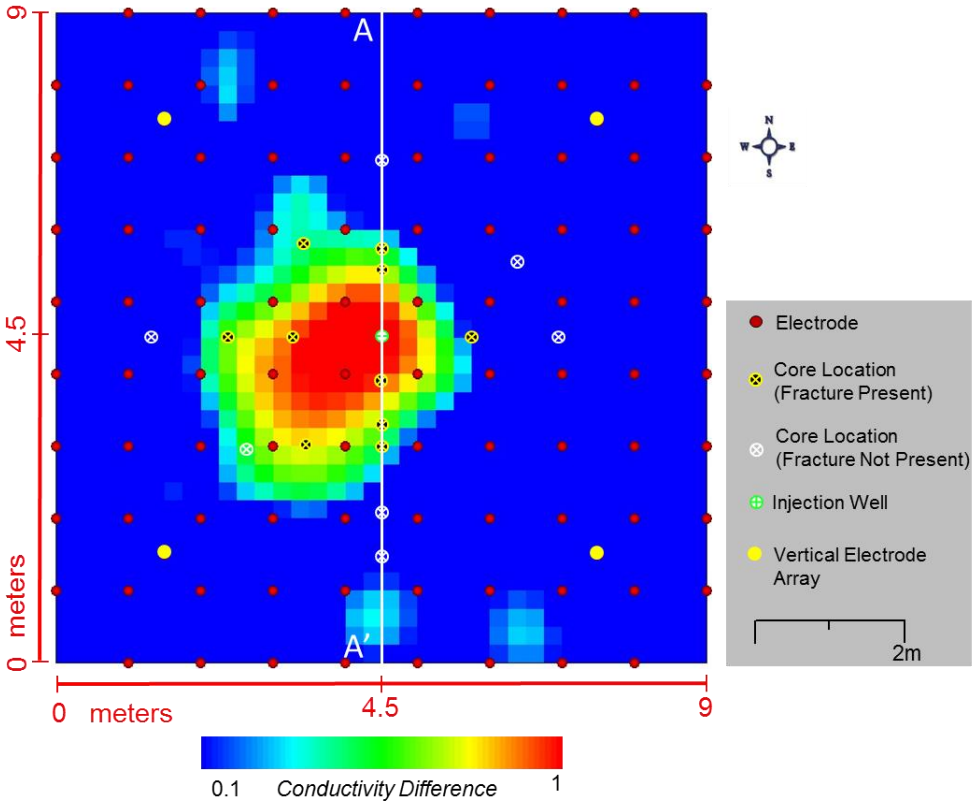

a)

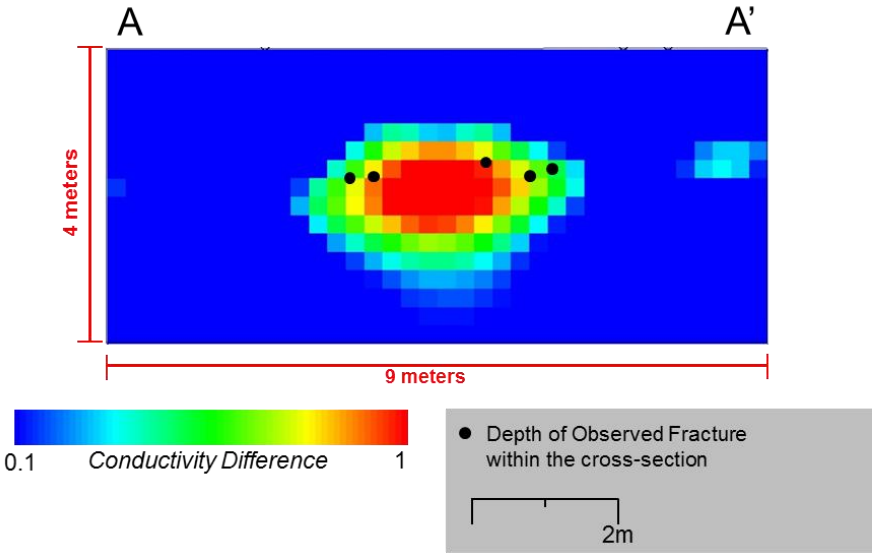

b)

Figure 18: Cell 5 ERT data. Red colored areas represent the greatest conductivity. Blue colored areas represent the lowest conductivity a) Map of electrical conductivity (color, in millisiemens log scale) at 1.6 m depth. b) Cross section on N/S azimuth of electrical conductivity (color, in millisiemens log scale).

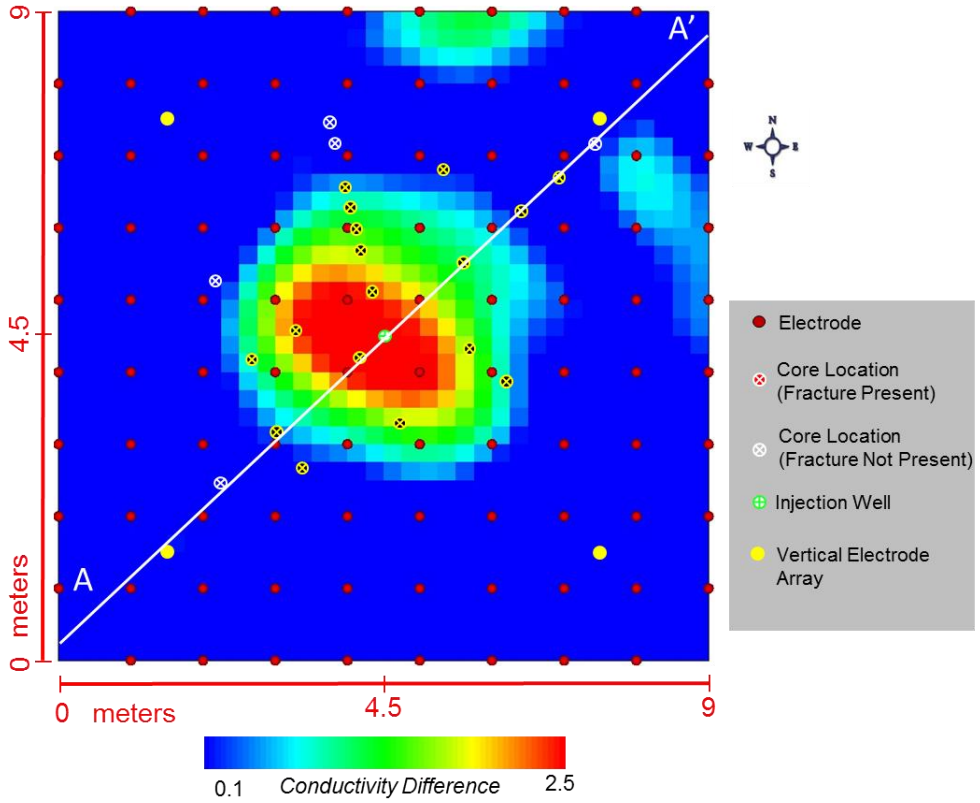

a)

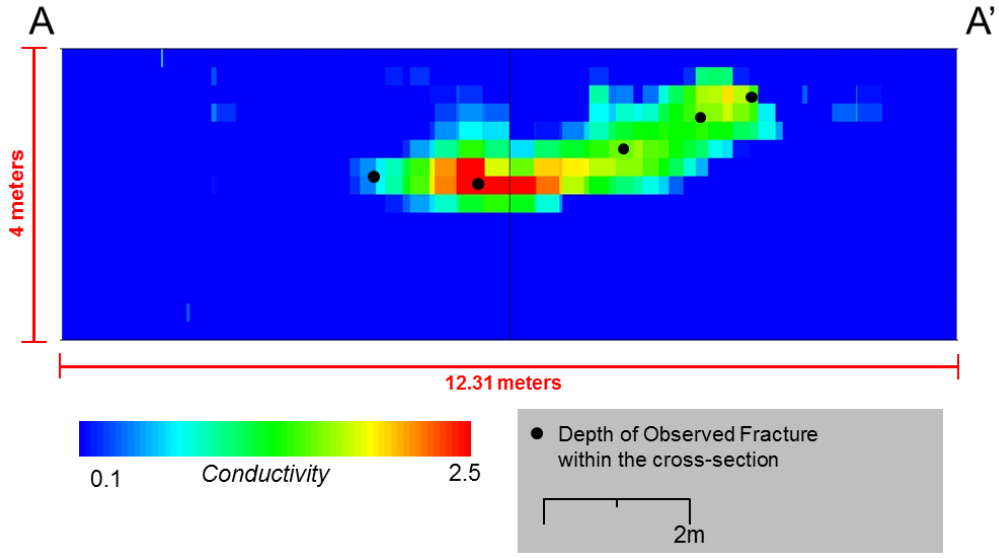

b)

Figure 19: Cell 6 ERT data. Red colored areas represent the greatest conductivity. Blue colored areas represent the lowest conductivity a) Map of electrical conductivity (color, in millisiemens log scale) at 1.76 m depth. b) Cross section on 48° azimuth of electrical conductivity (color, in millisiemens log scale).

The Cell 6 ERT data in map view displays a circular high electrical conductivity area centered on the borehole (Figure 19). Within this circular feature, the area of highest conductivity shows a northwest to southeast orientation. The cross section of the ERT data displays a high conductivity area that is curving towards the surface of the earth northeast of the borehole and came close to venting at the surface of the earth.

Soil Core Data

Cross sections of the soil core data were created in an effort to describe the shape of the fractures. The soil core descriptions were used to include contacts between the L soil unit and the upper transition zone soil unit on the cross sections.

The soil core cross section from Cell 1 shows a fracture is climbing towards the surface of the earth both northeast and southwest of the injection well (Figure 20.a). The lower bound for the maximum length of the fracture is 3.0 meters. The fracture has a gentle slope of about 10° northeast of the injection. Southwest of the injection well, the fracture has a steeper slope of about 50°. The L/T soil unit boundary included on the cross section demonstrates that the boundary decreases in depth until it levels off northeast of the injection well. The majority of the fracture is located in the upper transition unit. However, once the fracture enters the L horizon on the southwest end of the cross section, the fracture begins to descend and move away from the surface of the earth. It is possible that the there is a depth discrepancy for the soil core depth located 1.2 meters southwest of the injection well. The depth of the fracture was estimated in this core since it was sent to the University of North Carolina and was not cut open prior to

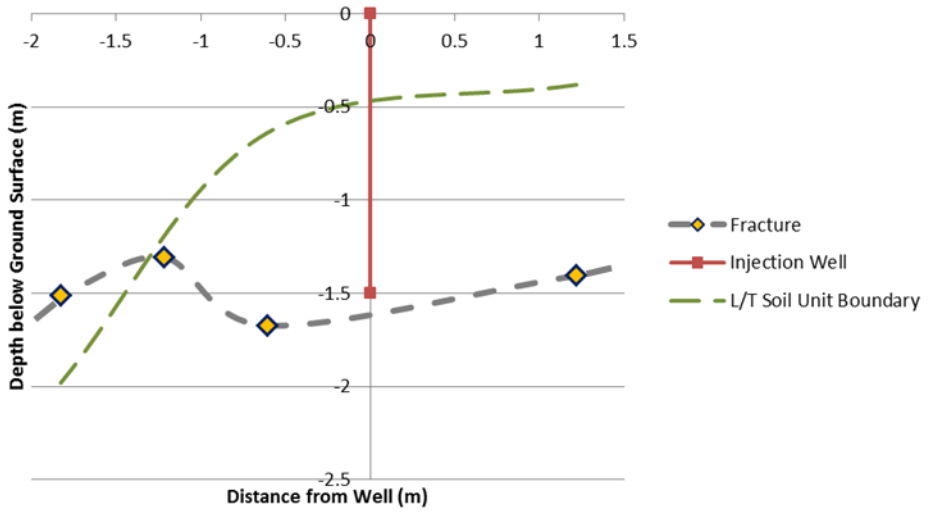
Depth below Ground Surface (m)
Distance from Well (m)
Fracture
Injection Well
L/T Soil Unit Boundary

a)

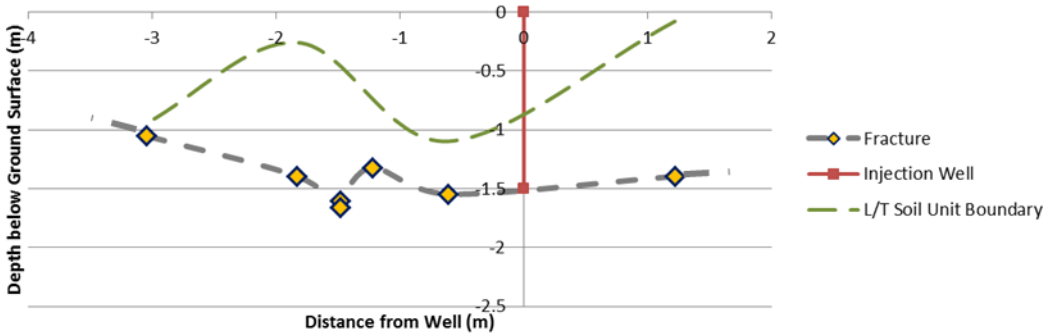
Depth below Ground Surface (m)
Distance from Well (m)
Fracture
Injection Well
L/T Soil Unit Boundary

b)

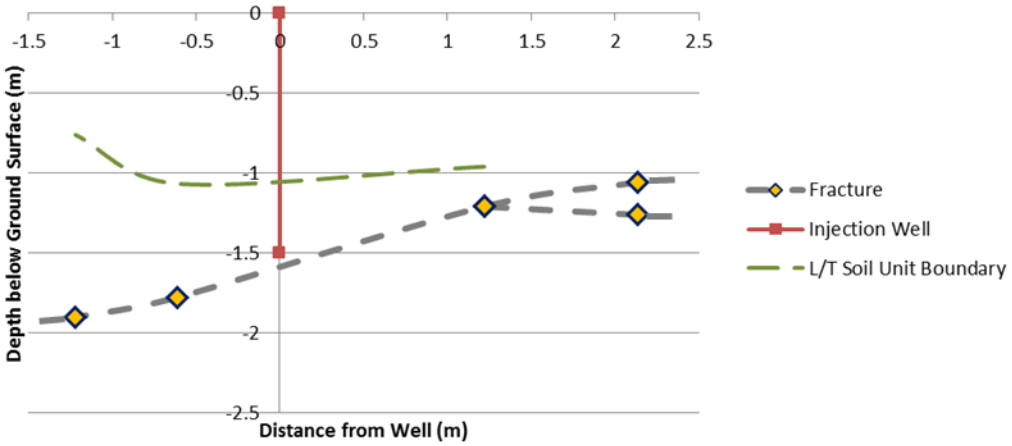
Depth below Ground Surface (m)
Distance from Well (m)
Fracture
Injection Well
L/T Soil Unit Boundary

c)

d)

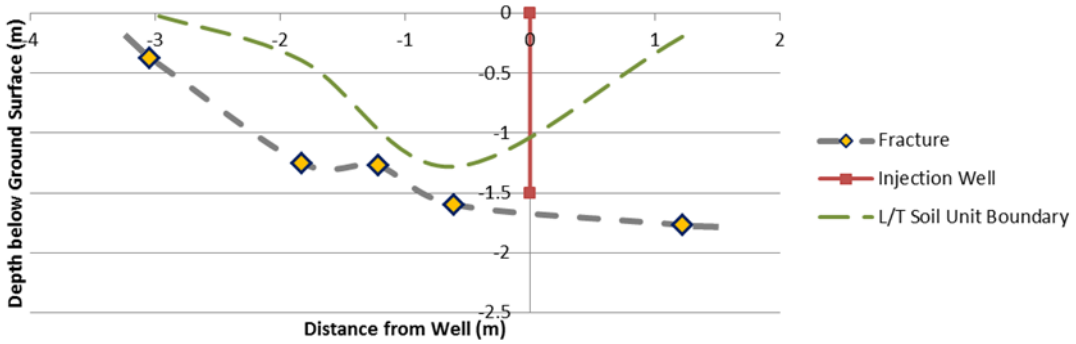

e)

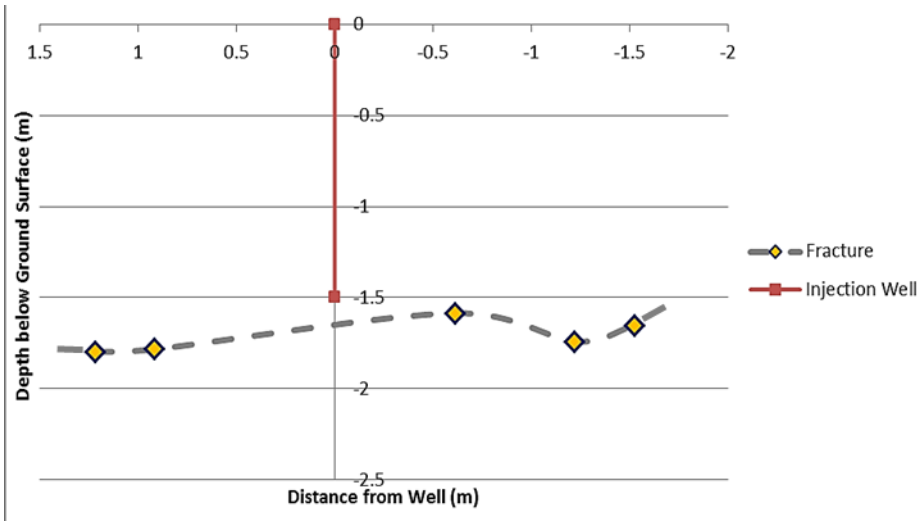

f)

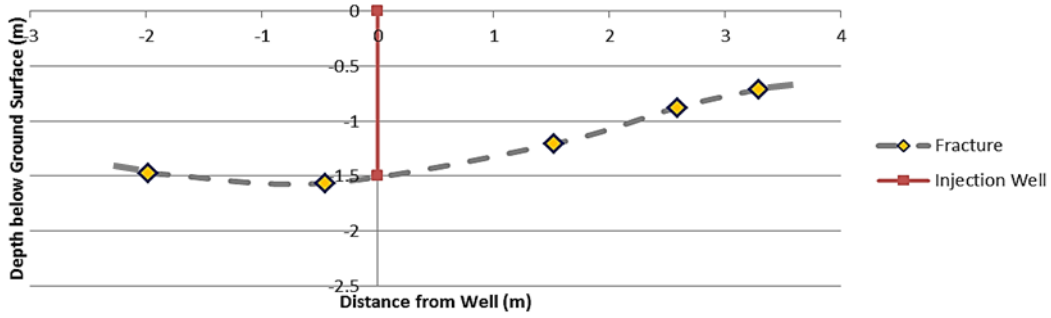

Figure 20: Cross sections of the hydraulic fractures based on soil core data a) Cell 1 along azimuth 50°/230° b) Cell 2 along azimuth 41°/221° c) Cell 3A along azimuth 0°/180° d) Cell 4 along azimuth 70°/250° e) Cell 5 along azimuth 0°/180° f) Cell 6 magnet fracture depths along azimuth 48°/288°

shipping. The thickness of the proppant was measured in the soil cores. The greatest thickness observed is 14 mm and the thinnest thickness is 3 mm. The average thickness of the proppant is 7 mm.

The soil core cross section for Cell 2 displays a fracture that is flat lying in the vicinity of the injection well (Figure 20.b). The lower bound for the maximum length of the fracture is 4.3 m. The end of the fracture that is northeast of the injection well has an upward slope of 4.5°. The end of the fracture southwest of the injection well shows a gentle upward slope of 10° that is climbing toward the surface of the earth. The exception to this trend is an area of undulation 1.5 meters southwest of the injection well. There could be some depth discrepancy in the soil core depth 1.2 meters southwest of the injection well since the core was not cut open for analysis before being sent to the University of North Carolina, and the depth was estimated. The L/T soil unit boundary displays an undulating trend. Based on the data collected, the fracture does not cross the boundary and remains in the upper transition unit. The thickness of the proppant was measured in the soil cores. The minimum proppant thickness observed is 3 mm. The greatest thickness is 20 mm. The average thickness is 9 mm.

The soil core data from Cell 3A show a cross section of the fracture parallel to the north/south azimuth (Figure 20.c). The lower bound of the maximum length is 3.4 m. To the north of the injection well, the fracture climbs toward the surface of the earth and eventually splits into two fractures. To the south of the injection well, the fracture increases in depth as it moves away from the surface of the earth. The slope of the

fracture is 16°. The L/T soil unit boundary is located on the cross section. When viewing the cross section from south to north, the boundary increases in depth with a steep slope before slightly decreasing in depth with a gentle slope. The majority of the fracture is located in the upper transition zone. However, the data for the boundary of the L/T soil unit ends 1.2 meters north of the injection well. It is interpreted based on the geologic map that the soil unit farther north of the injection well is part of the upper transition zone. When the thickness of the proppant was recorded, it was determined that the maximum proppant thickness is 15 mm and the minimum proppant thickness is 3 mm. The average proppant thickness in Cell 3A is 7 mm.

The fracture displayed in the soil core cross section of Cell 4 has a length of 4.3 m. This is the lower bound of the maximum length (Figure 20.d). As the fracture progresses from the injection well to the southwest of the injection well, the fracture climbs toward the surface of the earth at an angle of 14°. There is a slight decrease in depth about 1.2 meters southwest of the injection well. This core was not cut open for analysis before being sent to the University of North Carolina and the depth was estimated. After this slight decrease in depth, the fracture continues to climb towards the surface of the earth at 33.5° angle. Northeast of the injection well, the fracture increases in depth at an angle of 5°. The L/T soil unit boundary is shown on this cross section. Southwest of the injection well, the boundary is increasing in depth. When it approaches the injection well, it begins to move towards the surface of the earth again and decrease in depth. The entire fracture is located in the upper transition zone. When the thickness of the proppant was recorded, it was determined that the greatest proppant thickness is 20

mm, and the minimum proppant thickness is 2 mm. The average proppant thickness is 7 mm.

The soil core cross section for Cell 5 displays the fracture parallel to the north/south azimuth (Figure 20.e). The lower boundary of the maximum extent of the fracture is 2.7 m. The fracture increases in depth at an angle of 7° to the north of the injection well. To the south of the injection well, the fracture initially decreases in depth. When the fracture is 1.2 meters south of the injection well, it once again increase in depth for a short distance before resuming the trend of climbing towards the surface of the earth. Once again, the discrepancy in at the location 1.2 meters south of the injection well could be due to a discrepancy in the fracture depth in this core. The fracture depth in this core approximation was made because the core was not opened before it was shipped to the University of North Carolina. The L/T soil unit boundary was not plotted on the cross section due to lack of data regarding the boundary in this location. When the proppant thickness data were analyzed, it was determined that the maximum proppant thickness is 20 mm and the minimum proppant thickness is 3 mm. The average proppant thickness in Cell 5 is 10 mm.

The soil core cross section from Cell 6 displays a fracture with a length of 5.3 m. This is the lower boundary of the maximum thickness. The fracture has a gentle slope northeast and southwest of the injection well (Figure 20.f). The slope northeast of the injection well is 11° to 15°. The slope of the fracture southwest of the injection well is 3°. The fracture decrease in depth both to the northeast and southwest of the injection well.

This gives the fracture a shallow saucer shape. Once again, the L/T soil unit boundary was not plotted on the cross section due to lack of data regarding the boundary in this location. Analysis of the proppant thicknesses determined that the maximum proppant thickness is 20 mm and the minimum proppant thickness is 2 mm. The average proppant thickness in Cell 6 is 9 mm.

The soil core data and cross sections display some overarching trends. The fractures are roughly flat lying with one side of the fracture extending farther past the injection well than the opposite side. This gives the fracture a saucer like shape. The average lower bound for the maximum length of the fractures is 3.8 m. The steepest measured dip is 50° and the gentlest dip is 3°. However, the majority of the fracture dips ranged from 10° to 20°. The proppant thickness ranges from 2 mm to 20 mm, and the average proppant thickness is 8 mm.

The fractures typically were created in the upper transition zone. The majority of the fractures remained in the upper transition unit and did not penetrate the silty clay loam to clay loam that lay above the upper transition unit. It is plausible that the strength and horizontal compressive stress in the clay loam are greater than in the underlying upper transition unit, although these strengths and stress of the units were not measured. These factors could have caused the clay loam unit to obstruct the upward propagation of the fractures.

Excavation Data

The excavation data were first analyzed by creating trench maps. The location of the trenches was plotted on top of the uplift maps for Cell 2 and Cell 4. Each trench and the walls of each trench were assigned names (Figures 21 and 22). The extent of the fracture was drawn on the maps based on the extent of the fracture in the trenches.

Cell 2 Excavation Descriptions

The elevation of the fracture was measured every foot along each trench and the results were plotted to show the fracture traces in cross section (Figures 23 and 24, Appendix B). The cross section of the Cell 2 Trench 1 NW wall has a maximum length of 4.3 meters (Figure 23.a). As the distance along the reference measuring tape increases, the fracture increases in depth at an angle of 6.5°. At the northeast end of the trench, the fracture splits into two segments. South of the six ft. mark and north of the eleven ft. mark on the reference scale the fracture gradually curved upward in a series of steps (Figure 25). These steps have also been observed in other fracture studies such as Murdoch et al. (2006). The aperture of the fracture was measured each 0.5 ft. along the trench face. The minimum thickness that was measured was at the southwest end of the trench where the fracture was only the size of a hairline crack. The greatest thickness was 17 mm. The average proppant thickness along this trench is 9 mm.

The cross section for the Cell 2 Trench 1 SE wall has a maximum length of 4.6 meters, and the injection well was located at the eleven ft. mark (3.4 meter) on the reference measuring tape (Figure 23.b). On this trench wall exposure, 1.2 meters of the

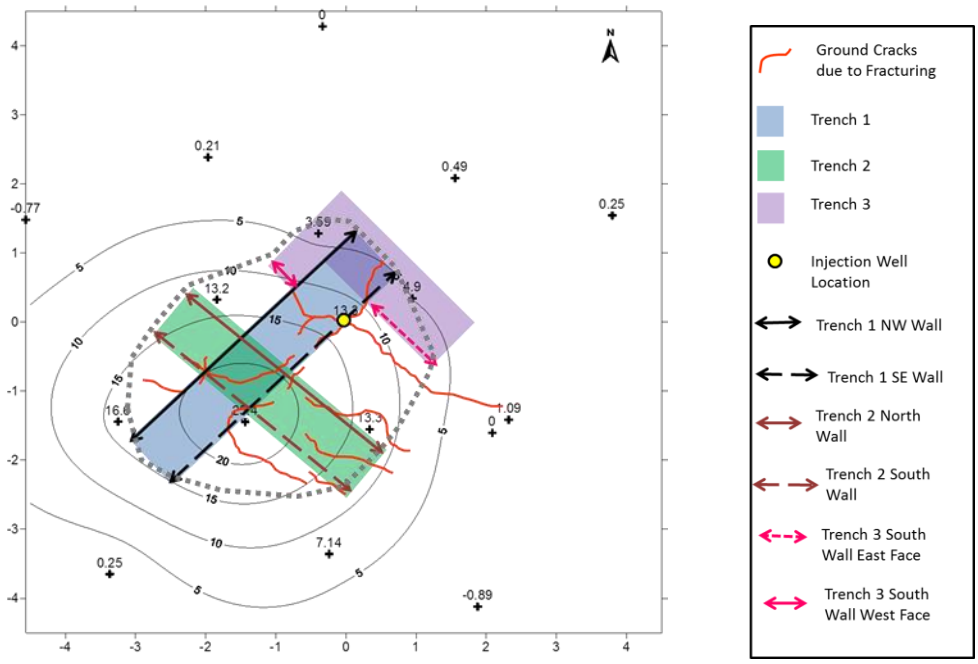

Figure 21: Contour map of uplift in mm in Cell 2. The orange lines are surface cracks at the end of injection. The yellow circle is the location of the injection well. Trench 1 is shaded blue; Trench 2 is shaded green; Trench 3 is shaded purple. The trench walls are show by the arrows listed on the key. The gray dotted line shows the estimated extent of the fracture.

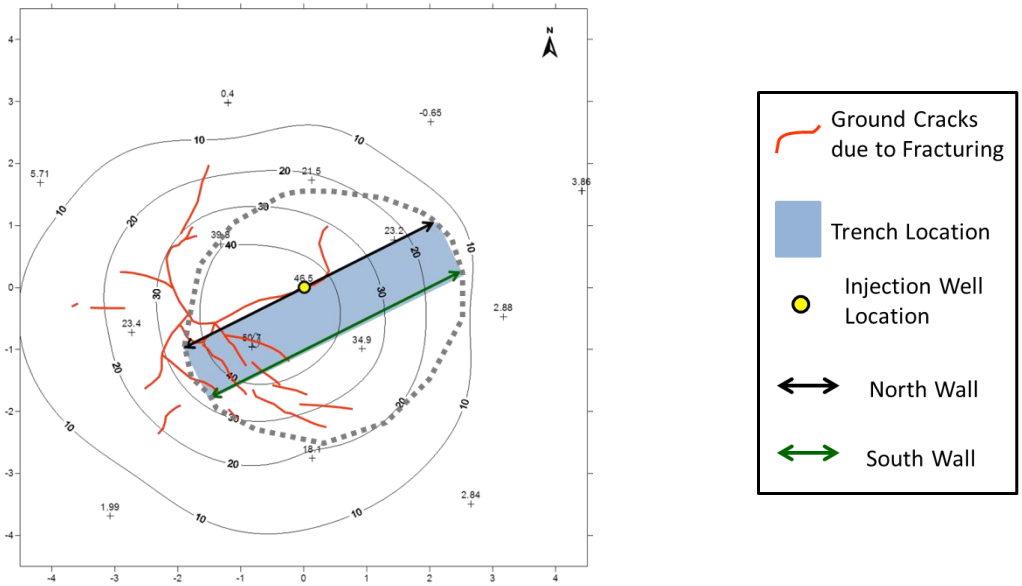

Figure 22: Contour map of uplift in mm in Cell 4. The orange lines are surface cracks at the end of injection. The yellow circle is the location of the injection well. Trench 1 is shaded blue; The trench walls are show by the arrows listed on the key. The gray dotted line shows the estimated extent of the fracture.

a)

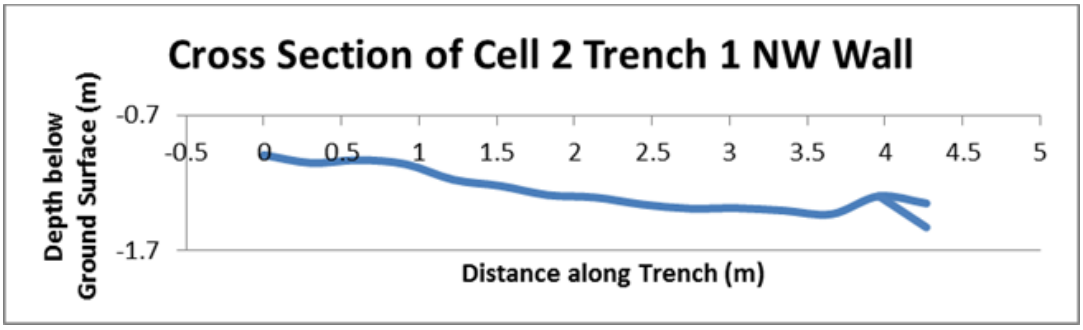
Cross Section of Cell 2 Trench 1 NW Wall
Depth below Ground Surface (m)
-0.7
-1.7
-0.5
0
0.5
1
1.5
2
2.5
3
3.5
4
4.5
5
Distance along Trench (m)

b)

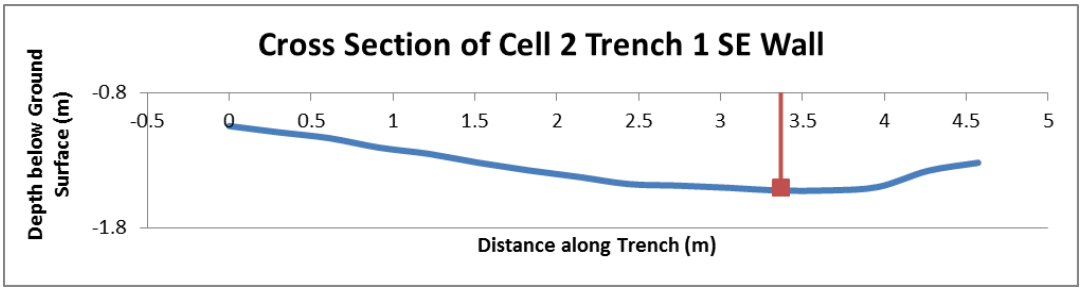
Cross Section of Cell 2 Trench 1 SE Wall
Depth below Ground Surface (m)
-0.8
-1.8
-0.5
0
0.5
1
1.5
2
2.5
3
3.5
4
4.5
5
Distance along Trench (m)

c)

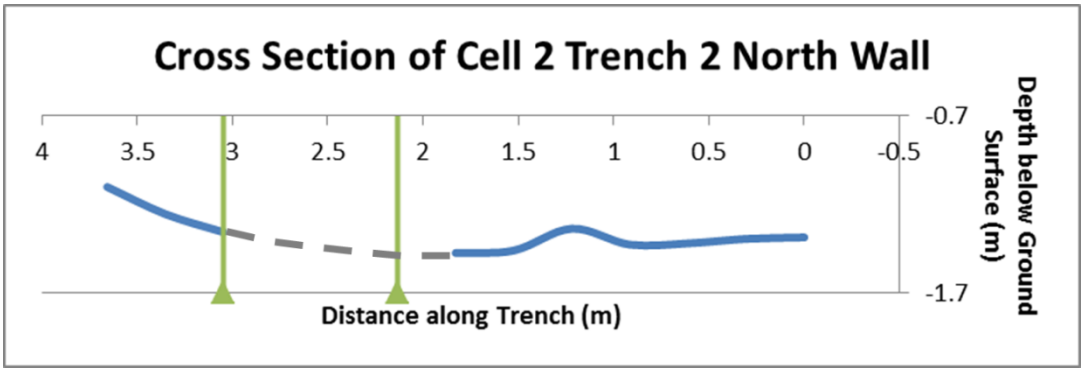
Cross Section of Cell 2 Trench 2 North Wall
4
3.5
3
2.5
2
1.5
1
0.5
0
-0.5
-0.7
-1.7
Depth below Ground Surface (m)
Distance along Trench (m)

d)

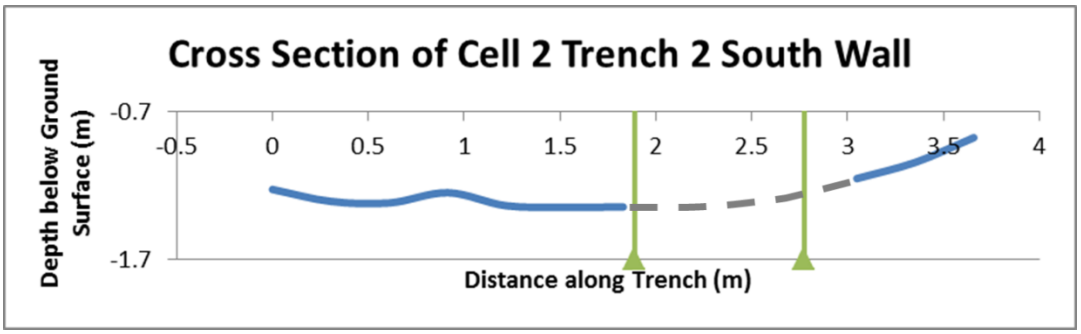
Cross Section of Cell 2 Trench 2 South Wall
Depth below Ground Surface (m)
-0.7
-1.7
-0.5
0
0.5
1
1.5
2
2.5
3
3.5
4
Distance along Trench (m)

e)

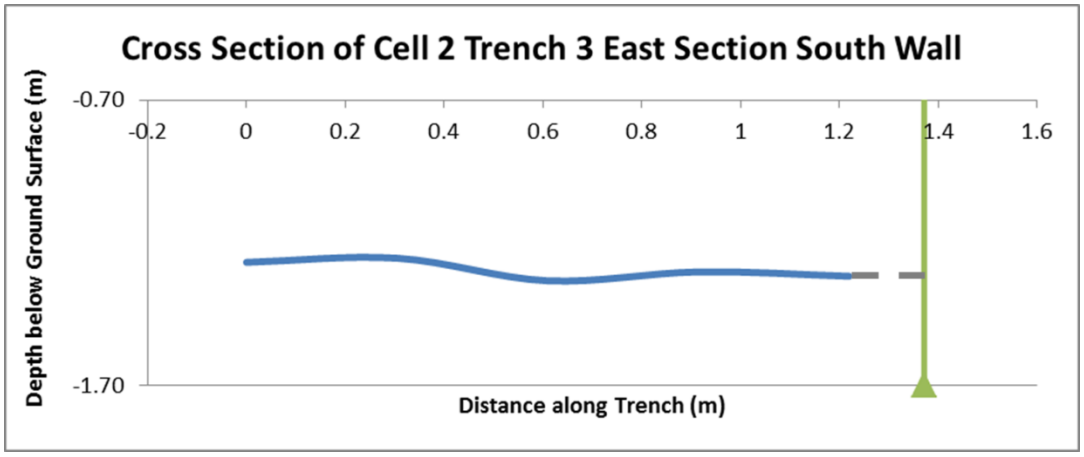

f)

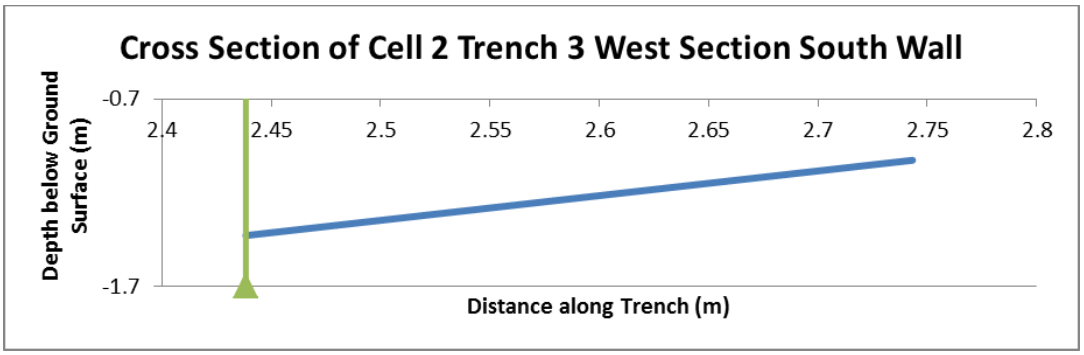

Figure 23: Cross sections of the sand coke breeze fracture in Cell 2 based on survey excavation data a) Trench 1 NW Wall b) Cell 2 Trench 1 SE Wall c) Cell 2 Trench 2 N Wall d) Cell 2 Trench 2 S Wall e) Cell 2 Trench 3 SE Wall f) Cell 2 Trench 3 SW Wall. The gray dashed lines show where the outline of the fracture is inferred.

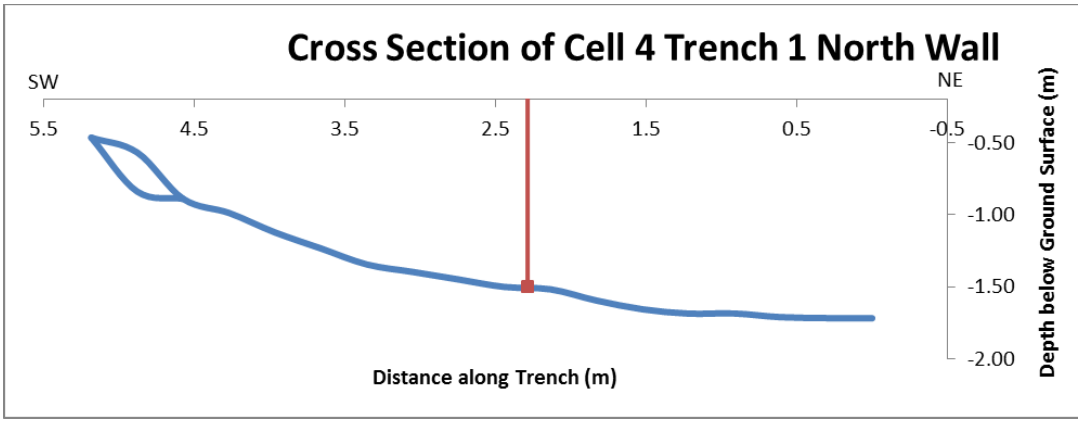

Figure 24: Cross section of the pure coke breeze fracture in Cell 4 Trench 1 N Wall based on survey excavation data.

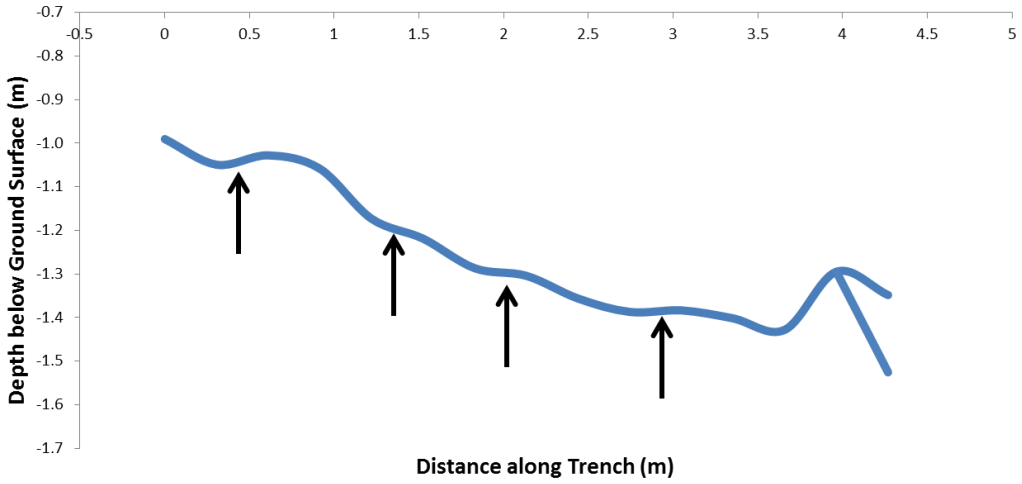

Figure 25: Cross section of Cell 2 Trench 1 NW Wall with vertical exaggeration. The vertical exaggeration enables the steps to be seen along the cross section The black arrows notate the places where each fracture step levels off.

fracture extended to the north of the injection well, and 3.4 m extended to the south of the injection well. Near the injection well, the fracture was relatively flat lying. To the northeast of the injection well, the fracture is roughly flat lying at first, but then it begins to decrease in depth at an angle of 14.5°. To the southwest of the injection well, the facture propagates up towards the surface of the earth at an angle of 5.5°. The proppant thickness was measured along the trench face. The minimum proppant thickness was 1 mm. The maximum proppant thickness was 52.0 mm. This large aperture was located in the notch around the injection well. The average proppant thickness was 9 mm.

The cross section of Cell 2 Trench 2 North wall shows a fracture with a maximum length of 3.7 meters (Figure 23.c). The blank space located between the green parallel lines represents where Trench 2 intersected Trench 1. West of the Trench 1 intersection, the fracture propagates upward at an angle of 4° while it propagates upward at an angle of

20° on the east side of the intersection. The minimum proppant thickness is 3 mm, and the maximum proppant thickness is 65 mm. The average proppant thickness along this trench wall is 14 mm.

The cross section of Cell 2 Trench 2 South wall displays a fracture that has a maximum length of 3.7 meters (Figure 23.d). To the west of the Trench 1 intersection, the fracture propagates towards the surface of the earth at an angle of 20°. East of the Trench 1 intersection the fracture is roughly flat lying before it propagates upward at an angle of 12° for 0.5 m before ending. The minimum proppant thickness along the trench face is 1 mm, and the maximum is 22 mm. The average proppant thickness is 11 mm.

The cross section of Cell 2 Trench 3 East Section of the South Wall only shows the data collected on the section of the south wall that is east of the Trench 1 intersection (Figure 21). The fracture in this section is 1.2 meters long and is roughly flat lying (Figure 23.e). The minimum proppant thickness in this section of the trench is 1 mm, and the maximum is 15 mm. The average proppant thickness is 4 mm.

The cross section of the Cell 2 Trench 3 West Section of the South Wall shows the data collected on the south wall west of the Trench 1 intersection (Figure 21). The fracture in this section is 0.3 meters in length (Figure 23.f). Only two data points could be collected in the section. As a result, the propagation angle of 7° is suspect. Four data points were collected to analyze the proppant thickness. Based on these points, the minimum proppant thickness in this section is 2 mm and the maximum is 15 mm. The average proppant thickness is 10 mm.

Based on the observations of the cross sections of Cell 2, the fracture is roughly flat lying and creates a saucer shape. The average dip is in the range of 0° to 10°, but it is as high as 20° in two locations. The range of proppant thickness is 1 mm to 65 mm. The average proppant thickness is 10 mm.

Cell 2: Sand and Coke Breeze Distribution

After the excavation, observations of the fracture were made such as the extent of the sand and coke breeze proppant present in the fracture at several locations along the measuring tape and the shape of the fracture. In the majority of the fracture in Cell 2, the sand and the coke breeze proppant was a homogeneous mixture. However, the coke breeze was present in higher concentrations locally.

A high concentration of coke breeze occurred at the boundary between the fracture and the upper and lower trench wall (Figure 26). This layer of high coke breeze concentration was greatest near the injection well at the eleven ft. mark on the measuring tape. In this location, the high coke breeze layer ranged from 0.5 to 3 mm in thickness (Figure 26). As the distance from the injection well increased, the thickness of the coke breeze layer on the upper and lower trench wall decreased, and it became difficult to identify in cross section. However, the coke breeze layer could be easily seen when the facture surface was inspected from above or below (Figures 27 through 30). This was possible by removing the overburden above the fracture, and then describing the proppant from top to the bottom. One of these areas was in Trench 1 at the eight ft. mark on the measuring tape (Figure 27). The top section of the proppant contained an almost pure

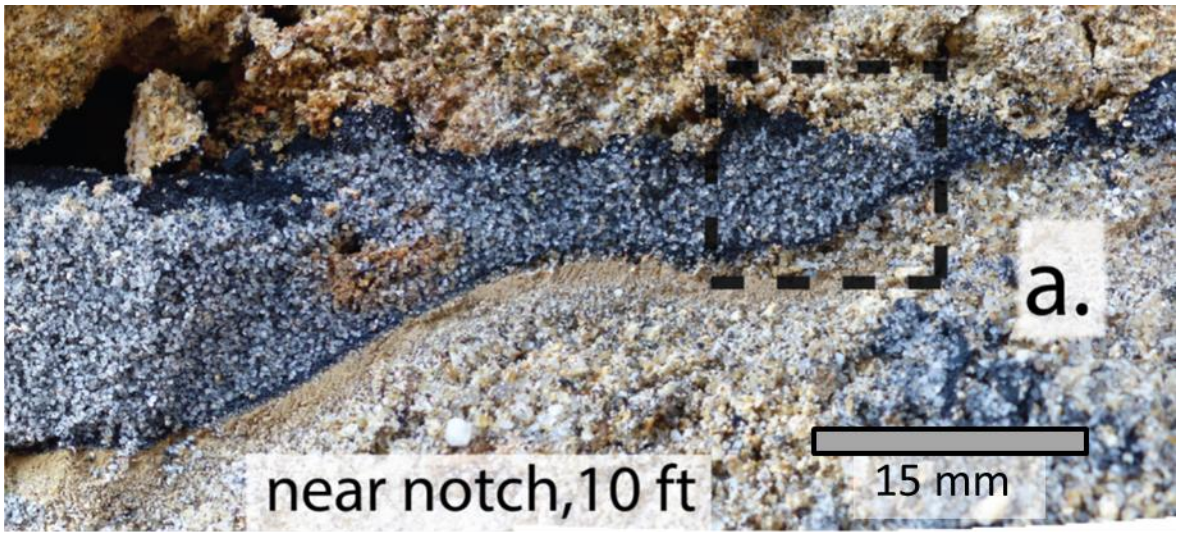

b)

Figure 26: Close up pictures of the fracture in Cell 2 Trench 1. The pictures are taken near the notch at the injection well. a) Close up photo of fracture at the ten ft. mark. b) Close up of the area outlined by the black box in figure a. Note the white sand grains and black coke breeze grains.

coke breeze layer that was 1 to 3 mm thick (Figure 27b). Below this was a section of proppant about 1 cm thick composed of sand with minor amounts of coke breeze. This made up the middle of proppant (Figure 28). The top and middle sections of proppant were then carefully removed from the fracture surface to reveal the bottom section of proppant. This bottom section was composed of a layer of coke breeze with sand absent (Figure 29). The coke breeze layers observed at the eight feet mark were present throughout the fracture. For example, the fracture was excavated at the one foot mark, and thin coke breeze layers were present on the top and bottom fracture surfaces (Figure 30). There were sections composed of the wall rock, and the proppant was absent. These fragments of wall rock only made up less than 10% of the fractures.

In the middle section of the proppant, internal discontinuous layers of concentrated coke breeze several mm thick were present in some localities. These layers are separated by sand grains from the pure coke breeze layers on the top and bottom of the fracture. They also contained a small fraction of sand and were distributed throughout the fractures while the pure coke breeze layers on the top and bottom of the fractures were continuous.

The internal coke breeze layers from the one to five ft. section of the fracture were mapped on photographs taken of the trench walls (Figure 31). The internal coke breeze layers were noted on the photographs where the resolution was high enough to display the coke breeze grains. The internal coke breeze zones were present in the fracture from three to five feet. They had lengths ranging from a 1 centimeters to 12 centimeters. In the

a)

b)

Figure 27: Images of the excavation of the upper surface of the fracture in Cell 2 Trench 1 SE Wall at the eight ft. mark. a) Excavation of the upper surface of the fracture. b) Sample of the upper surface of the fracture. Pure coke breeze present as a layer at the interface between the fracture and the wall rock.

a) 

b) 

Figure 28: Cell 2 Trench 1 SE Wall at the eight ft. mark. a) Image of the middle proppant layer. b) Close up photo of the middle layer of proppant. This layer is a mixture of sand and coke breeze. Both images were taken at the same location as the image in Figure 27 except that additional proppant has been removed to reveal the middle proppant layer.

a)

b)

Figure 29: Cell 2 Trench 1 SE Wall at the eight ft. mark. a) Image of the bottom of the proppant. b) Close up photo of the bottom of the proppant layer. The proppant is nearly pure coke breeze. Both images were taken at the same location as the image in Figure 28 except that additional proppant has been removed to reveal the bottom proppant layer.

Figure 30: Cell 1 Trench 1 SE Wall at the one foot mark. Top) The fracture. Middle) Nearly pure coke breeze layer present on the top of the proppant layer next to the fracture wall. Bottom) Nearly pure coke breeze on the bottom surface.

tip of the fracture from zero feet to three feet, the proppant was uniform and no internal high coke breeze areas were present (Figure 31).

Cell 4 Excavation Descriptions

The excavation in Cell 4 revealed a hydraulic fracture about 5.2 meters long and filled with black, fine-grained coke breeze (Figures 24 and 35). The north and center sections of the fracture are fairly flat lying. As shown in the cross section, the fracture propagates downward at an angle of 12° before leveling off to a flat lying fracture on the northeast side of the injection well. The south section of the fracture curves upward (Figures 24 and 35). This end of the fracture initially propagates upward at an angle of 9°, but then propagates at a steeper angle of 19° (Figures 24 and 35).

The coke breeze proppant thickness along the trench was recorded and ranged from several millimeters to between 1 and 2 centimeters. The minimum proppant thickness in the trench is 3 mm and the maximum is 34 mm. The average proppant thickness is 12 mm. The majority of the proppant fell in a range of 0.5 to 1 cm thick. In some locations, the proppant thickness was relatively uniform (e.g. three, four, six, and eight ft. in Figure 35). In other locations such as the five, nine, and ten ft. locations, the proppant thickness was variable (See insets of Figure 35).

The contact between the wall rock and the proppant was non-regular even in the areas with uniform proppant thickness. At some locations, the contact shifted by several mm, and it seemed that the contact broadened as the proppant filled in the pore space present in the wall rock. In some of the locations, wall rock and proppant were mixed

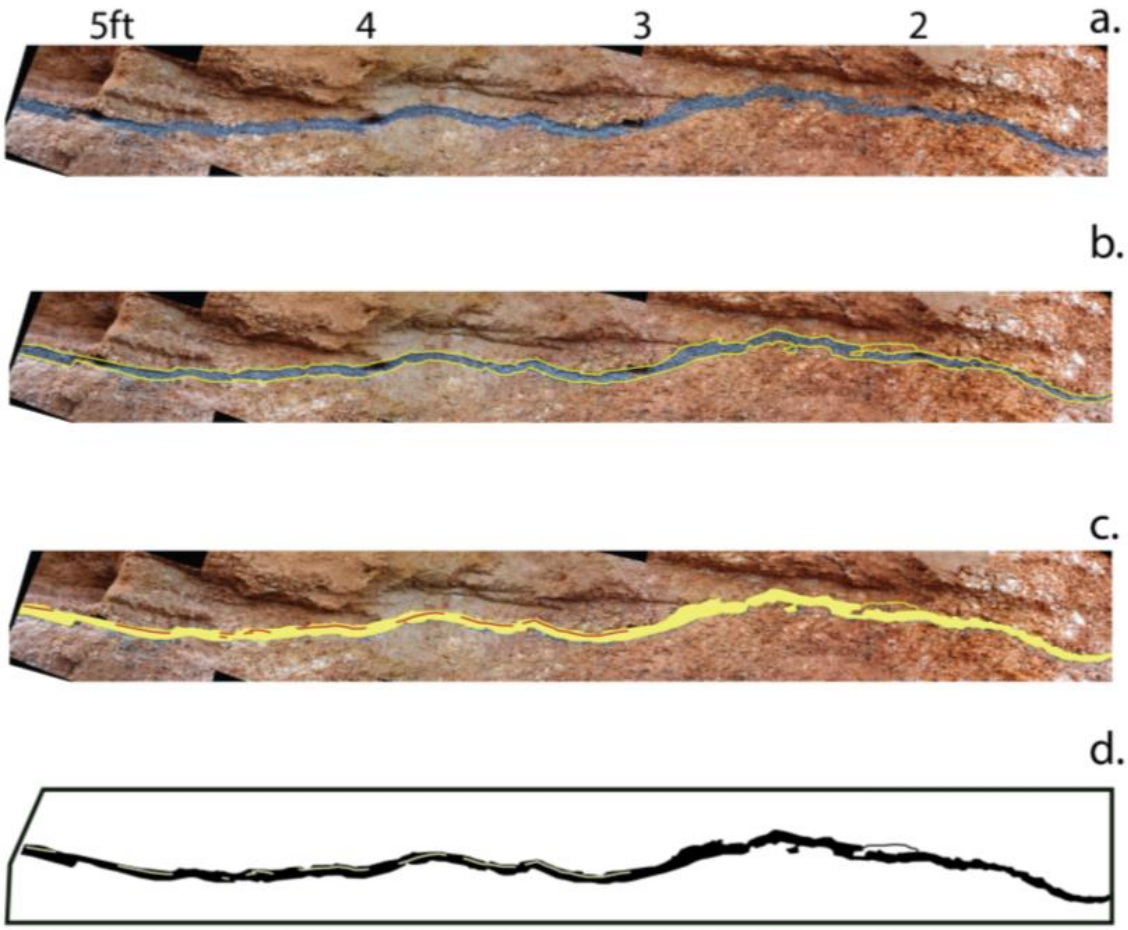

Figure 31: Cell 2 Trench 1 SE Wall. a) The fracture on the SE wall from one to five ft. b) The contact between the proppant and the wall rock is marked with a yellow line. c) The proppant is filled in with yellow color. The locations where there is internal coke breeze layers are present are marked in orange. d) The trace of the fracture. This is the same image shown in Figure 31c except that the background is removed and the color was changed to emphasize the fracture form.

together at the contact (Figure 32). This was likely due to the proppant filling in the empty pore space in the wall rock. In other localities along the fracture, the contact between the proppant in the fracture and the wall rock was a sharp boundary, and no wall rock was mixed in with the coke breeze.

The proppant material created a nearly continuous layer across the trench wall. There were four locations (1.2 ft., 6.2 ft., 7.7 ft., and 13 ft.) where the proppant layer was offset and wall rock material filled the area between the fracture segments (Figure 35:Thirteen ft. Inset). There were other locations where the fracture was again offset between segments, but a bridge of proppant connected the offset sections.

Photo Mosaic Panoramas, Variograms, and Proppant Thickness Analysis

As part of the excavation proceedings in Cell 2 and Cell 4, close up photographs were taken of the fractures in the trenches. These images were located to ensure that each

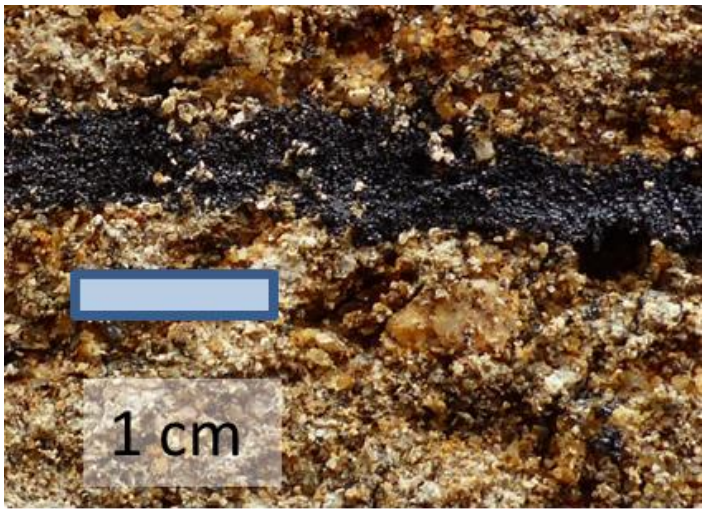

Figure 32: Close up picture of the wall rock mixed in with the coke breeze proppant at the wall rock interface.

picture overlapped the two pictures on each side. These photographs were then combined in Adobe Photoshop to create photo mosaic panoramas of the trench walls. These panoramas were created for the Cell 2 Trench 1 NW Wall, the Cell 2 Trench 1 SE Wall, and the Cell 4 Trench 1 South Wall. These panoramas are displayed in Figures 33 through 35.

The panoramas were used to measure the thickness of the proppant along the fracture. The thickness of the proppant was measured every 5 cm along the fracture. The tape measure scale on the pictures was used to convert the number of millimeters measured on the panorama to the corresponding number of real world millimeters.

The variance was then calculated with increasing lag until the lag interval was equal to the total length of the fracture. This data were then plotted to create a variogram to represent the variance of the proppant thickness as a function of the lag length (Figures 36 – 38). Two horizontal scales are included on the variogram plots: the lag and the lag divided by the total length of the fracture.

The variance of the proppant thickness increases as the lag distance increases. The variance then increases and reaches a maximum variance. The variance of the proppant thickness has the shape of a semi-variogram when the lag is less than 1.5 m in Figures 36 and 38 and 2 m in Figure 37. In the variogram for Cell 2 Trench 1 NW Wall, the variance increases until it attains a sill of 30 mm^2 at a lag of 1.5 m. The variance then increase until a maximum variance of 70 mm^2 is reached at a lag of 2.2 m.

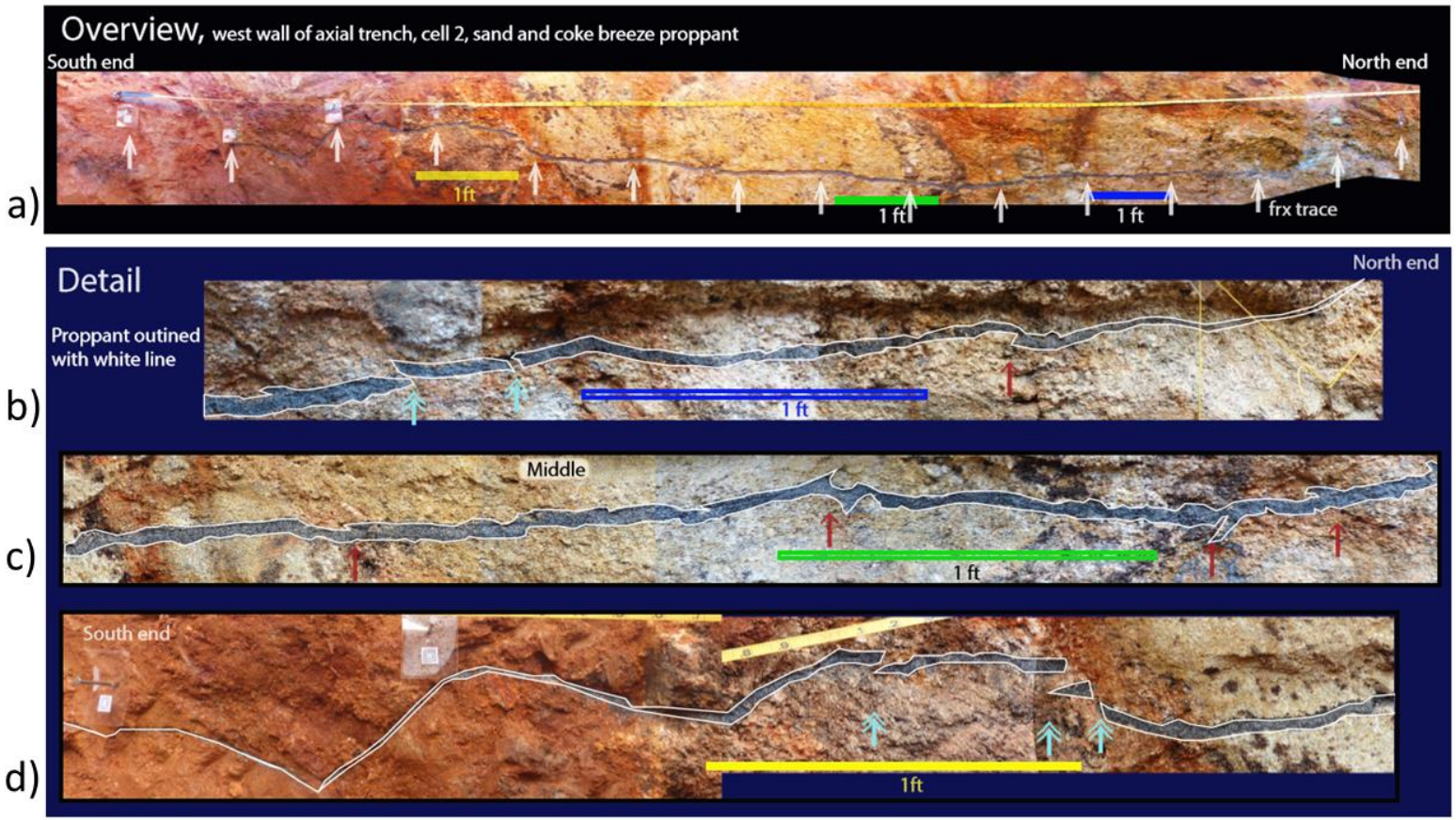

Figure 33: Photo mosaic panorama created of Cell 2 Trench 1 NW Wall. a) Picture shows the panorama of the entire trench. The black material is the location of the fracture filled with the sand/coke breeze proppant. The white arrows mark the location of each foot marking on the measuring tape. Several scale bars were included due to the distortion that occurred when the photos were combined. b) Panorama of the north end of the trench. c) Panorama of the middle section of the fracture. d) Panorama of the south end of the trench. b-d) The blue arrows indicate where the proppant layers where offset and rock material filled in-between the proppant. The red arrows indicate where the proppant layers where offset and proppant formed a bridge between the offset layers. The L soil horizon and the upper transition zone are present in these panoramas.

Figure 34: Photo mosaic panorama created of Cell 2 Trench 1 SE Wall. The fracture is the dark black band that traverses the panorama. The reference tape measure is located at the top of the picture, and the numbers mark each foot along the tape. The injection well and the notch are located at the eleven ft. mark.

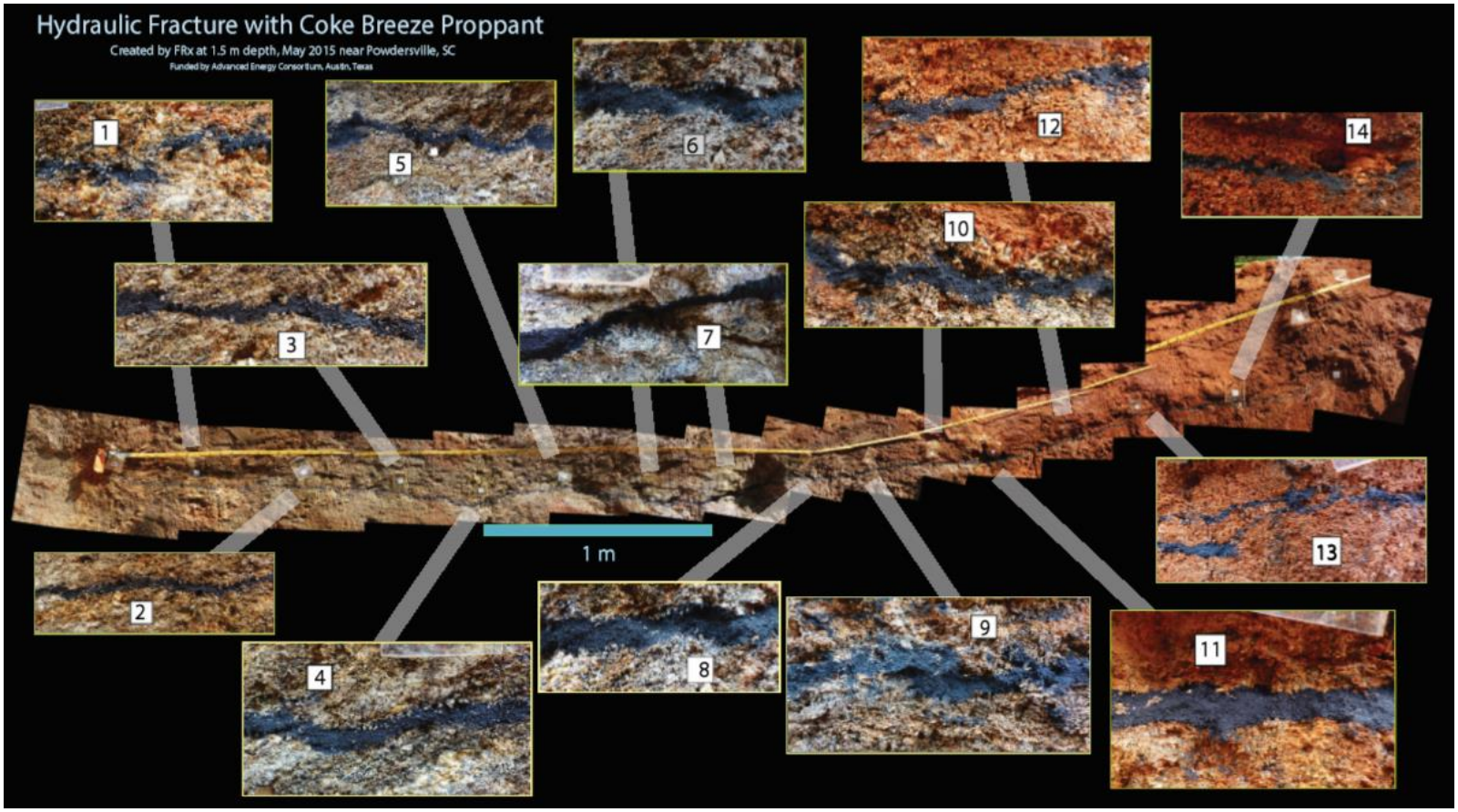

Figure 35: Photo mosaic panorama created of Cell 4 Trench 1 South Wall. The black line represents the location of the fracture filled with coke breeze proppant. The reference measuring tape is located near the top of the panorama. The insets show close up views of the fracture at each foot mark along the reference measuring tape. The number in each inset box is the foot mark on the reference tape at the location of the inset.

In the variogram of Cell 2 Trench 1 SE Wall, the variance increase as the lag increase until it levels off at a sill of 42 mm^2 at a lag of 2 m. The variance then increases to a maximum variance of 87 mm^2 at a lag of 3.3 m.

The variogram of Cell 4 Trench 1 South Wall shows a similar pattern to the variogram for Cell 2 Trench 1 NW Wall. The variance increases as the lag increase until it reaches a sill of 40 mm^2 at a lag of 1.3 m. The variance then increases to a maximum variance of 60 mm^2 at a lag of 1.7 m.

The variance of the proppant thickness seems to be determined by the shape of the fracture. The shape of the fracture was demonstrated by plotting the proppant thickness along the trench wall versus the distance along the trench for Cell 2 Trench 1 SE Wall (Figure 39). The maximum proppant thickness of 52 mm was removed from the plot since it was determined to be an outlier. The minimum thicknesses are located at the ends of the fracture. A line was then fit by hand to the data. This line gives an asymmetric teardrop shape. The greater proppant thicknesses are located on the southwest side of the injection well, and the thinner sections of proppant are located to the northeast of the injection well. This teardrop shape and asymmetry is expected based on the work of Murdoch et al., 2006 and Murdoch and Slack, 2002. As a result of this fracture form, the maximum variance occurs where the lag is about half the length of the proppant. The maximum thickness of the proppant in a fracture is offset from the half length of the proppant. This tear drop form accounts for why the location of the maximum variance is offset from the mid-point of total proppant length.

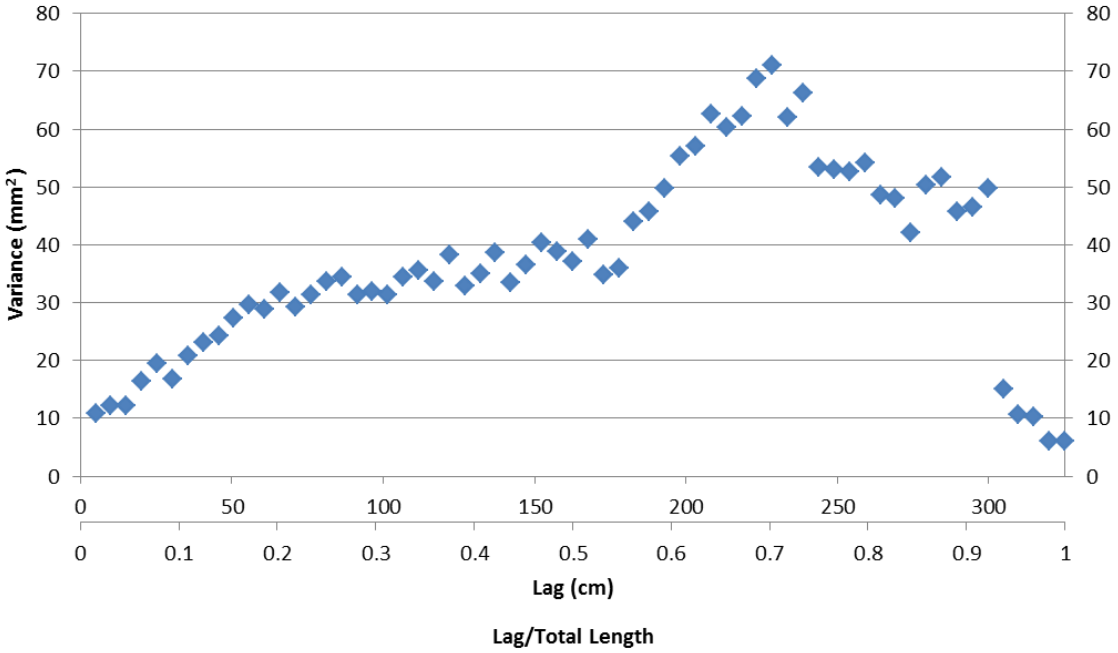

Figure 36: Variogram of the proppant thickness along the Cell 2 Trench 1 NW Wall.

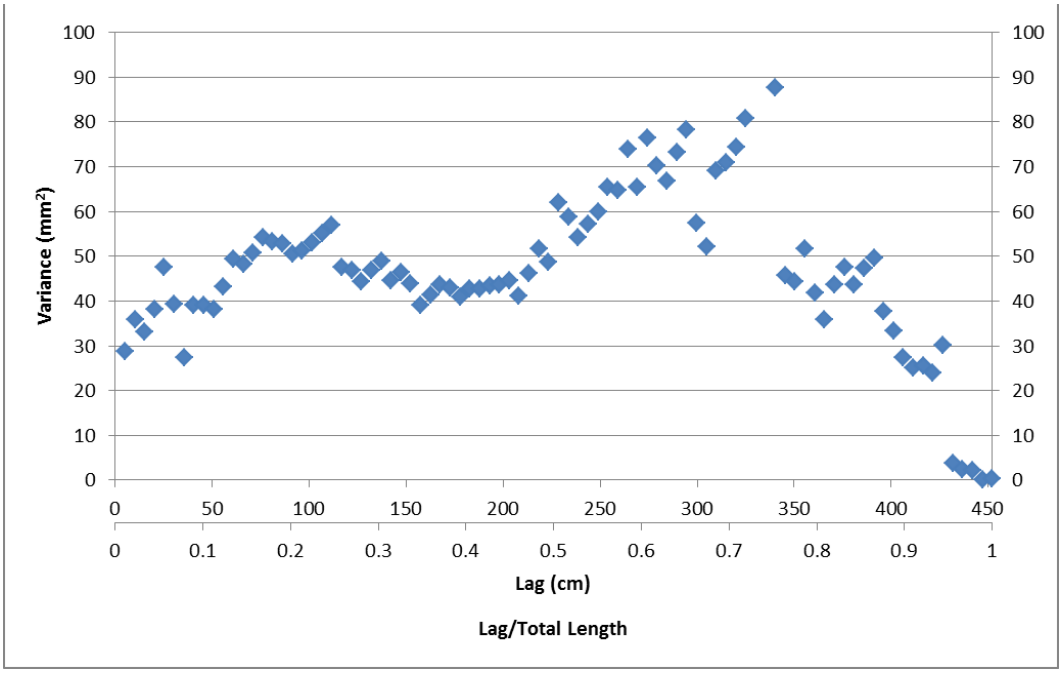

Figure 37: Variogram of the proppant thickness along the Cell 2 Trench 1 SE Wall. Two proppant thickness measurements were removed from the data set. These two points were located in the notch and were outliers in the data set.

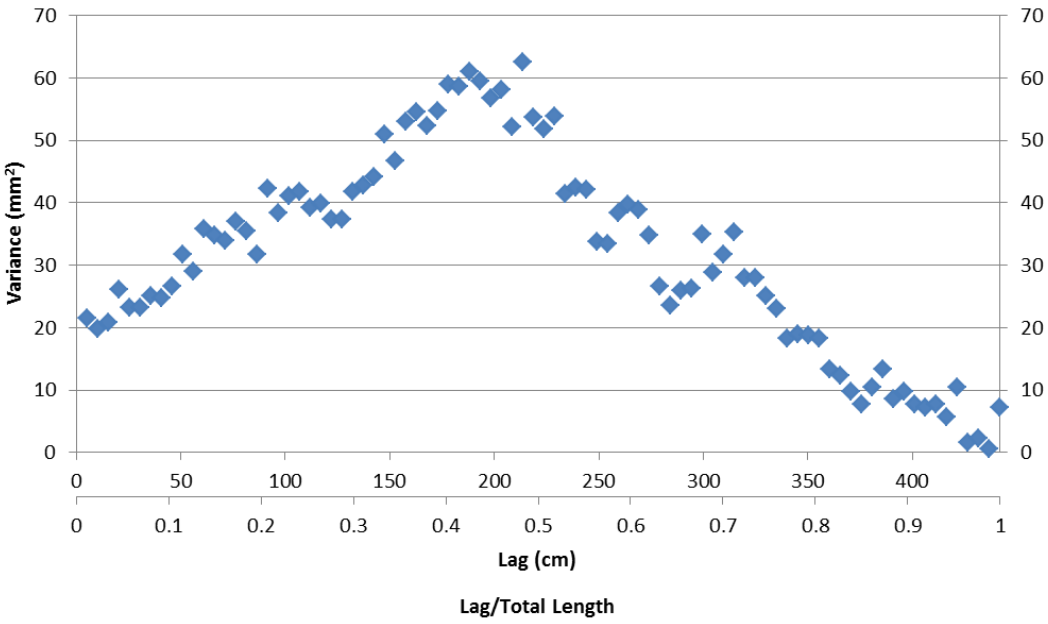

Figure 38: Variogram of the proppant thickness along the Cell 4 Trench 1 South Wall.

The small scale variability of the proppant thickness is likely the result of the internal form of the fracture. The proppant pinches out locally along the fracture. This seems to correspond to locations where adjacent fracture lobes have merged together (Murdoch et al., 2006). There are some locations along the trench wall where the proppant thickness decreases to zero. This is interpreted to be where the fracture broke into several different lobes. The length of these lobes seems to influence the sill in the variograms. When the length of the lag is less than the lobe width, the variance will increase, but the variance is not affected by lag lengths larger than the lobe size. When the lag distance becomes large enough, the variance will be controlled by the changes in the proppant thickness rather than the size of the lobes.

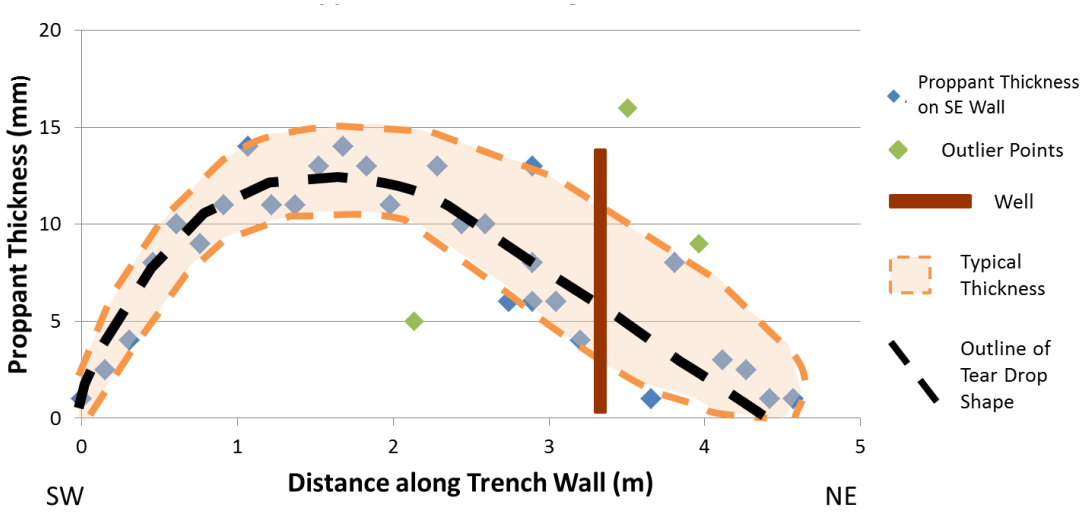

Figure 39: Proppant thickness along the SE wall of Trench 1 in Cell 2. Note the teardrop shape that fits the data.

Magnetometric Resistivity and Ground Penetrating Radar

Magnetometric resistivity and ground penetrating radar data were collected at the site, but only provided a secondary check of the data.

Magnetometric Resistivity Results

Magnetometric resistivity (MMR) data were collected at the site. To complete these surveys, magnetometers were set out at the same sixteen locations in each cell to collect data before and after fracture creation. The data were collected at 2.5 Hz, and 219 data points were collected (Multi-Phase Technologies, LLC, 2016). Multi-Phase Technologies analyzed the data to create map views of the electrical conductivity predicted at the site based on the MMR data.

Several challenges were encountered when collecting the MMR data. One challenge was that the magnetometers need to be placed in the same location and orientation for both the pre-fracture and post-fracture data collections. This was difficult to carry out due to the disturbances at the site from fracture creation. The equipment for fracture creation would knock over or shift the location markers set out for the magnetometers. A second challenge was the high contact resistance between the electrodes and the ground. This caused currents that were a few tens of milli-amperes and induced magnetic field measurements that were fractions of nT (Multi-Phase Technologies, LLC, 2016). The magnetic field background at the site is 50,000 nT. As a result, small errors in the orientation or location of the sensor can cause noise that is large relative to the induced signal (Multi-Phase Technologies, LLC, 2016). Another challenge encountered involved the proximity of the road to the field site (Figure 5). Cars may have caused vibrations that affected the sensors, and the cars themselves may have caused transient magnetic fields that increased the noise in the data (Multi-Phase Technologies, LLC, 2016).

Three datasets from Cell 6 were used in the 3D tomographic inversion to evaluate the contribution of MMR data: ERT alone, MMR alone, and combined ERT and MMR (Figure 40). Inversion of the electrical data alone predicts an equant zone of electrical conductivity that is greater than background over a region 4 m in diameter and approximately centered on the injection well. By contrast, inversion of the MMR data alone predicts no distinct anomaly (Figure 40b). This is likely because the uncertainty in the magnetic data was large compared to the signal. The electrical and magnetic data

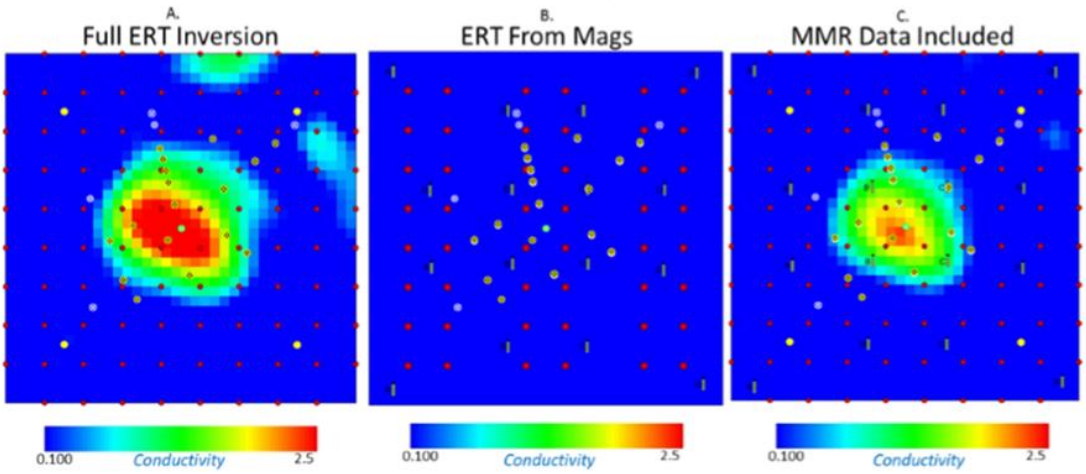

Figure 40: Electrical conductivity from inversion of ERT and MMR data sets from Cell 6 at a depth of 1.76 m. a.) inversion of electrical resistivity data alone. b.) inversion of magnetic data alone. c.) Inversion of both magnetic and electrical data. Image from Multi-Phase Technologies (2016, fig. 48).

were combined and inverted simultaneously, and the results are slightly different than when the electrical data was inverted alone. In particularly, inversion of the combined data predicts a zone of anomalous electrical conductivity that is slightly smaller than when the electrical data alone is used (Figure 40). We evaluated these results and concluded that inversion of the MMR data alone had negligible value and the uncertainty in the MMR data caused the combined ERT and MMR inversion to be less reliable than when ERT was used alone. As a result, the remainder of the study focused on the electrical data.

Ground Penetrating Radar

A group of our collaborators conducted GPR tests across the cells at the field site. The purpose of these tests was to evaluate the feasibility of using GPR to characterize the

location of proppant. The GPR data were analyzed by our collaborators and compared with the direct observations such as the soil core data. The complete analysis of this aspect of the project will be presented elsewhere.

CHAPTER 8: DISCUSSION

The proppant extent and depth based on the ERT data were evaluated by comparing them to the proppant extent and depth estimated by the soil core data and the excavation data. The soil core data was also compared to the uplift data. These results were then compared to the soil core/ERT analysis to determine whether the ERT or uplift gave a better predication of the fracture location.

Comparison of Estimated Proppant Extent

To evaluate the results of the geophysical test, the maps of the direct observations were overlain on the geophysical maps (Figure 41 through 45). Markers were placed on the plots to note the location where soil cores were taken and whether the fracture was present in the core or absent. The soil core locations that were the farthest from the injection well and that contained proppant were used to define the minimum extent of the proppant (Figure 41a through 45a). This thick square dotted outline is referred to as the proppant line. The soil core locations that did not contain proppant were then used to bound the maximum possible extent of the proppant. This thin dashed outline is called the no-proppant line (Figure 41b through 45b). It is inferred that the actual extent of the proppant is bounded by these two lines.

A grid was overlain on the maps to integrate the areas encompassed by the proppant line and no-proppant line. The difference in surface area between the no-proppant line and the proppant line was calculated. This information is listed in Table 4. The number of grid boxes located within the proppant line was counted and recorded.

Partial grid boxes were added together to approximate the number of full grid boxes they represented. This number was added to the number of full grid boxes within the proppant line. Using the scale bars on the map, the number of grid boxes encompassed by the proppant line was converted into the surface area enclosed by the proppant line. This was interpreted as the smallest surface area possible for the fracture. The same procedure was followed to determine the surface area enclosed by the no-proppant line. This was interpreted as the greatest surface area possible for the fracture. This was completed for the maps for Cells 1, 2, 4, 5, and 6.

The surface area of the proppant in each cell was estimated as the average of the areas in the proppant line and the no proppant line. The estimated uncertainty is half of the range (difference between the two areas).

On the ERT map for Cell 1, the proppant line creates an oval shape around the injection well and has an elongated tail extending out to the west of the injection well (Figure 41). The ERT indicates that the majority of the area within the proppant line has a high conductivity. However, there is a discrepancy north of the injection well. In this area, the ERT does not indicate that the proppant is present, but the proppant line based on the soil cores indicates that the fracture is present. The no-proppant line has the same shape as the proppant line and encompasses the proppant line. The majority of the high electrical conductivity indicated by the ERT is within the bounds of the no-proppant line.

The proppant extent indicated by the proppant line on the Cell 2 ERT plot is an oval shape that is oriented northeast to southwest (Figure 42). The majority of the area

encompassed by the proppant line has high electrical conductivity as indicated by the ERT data. The exception is to the northeast. The ERT indicates that this area within the proppant line has a low electrical conductivity. The no-proppant line encompasses the proppant line and the entire high electrical conductivity area. The outline of the no-proppant line is an irregular shape with both concave and convex curves.

The proppant line on the Cell 4 ERT plot is an irregular shape that has a slight northeast to southwest orientation (Figure 43). The high electrical conductivity area indicated by the ERT map extends past the proppant line along the entire outline. The no-proppant line is a circular shape that encompasses both the proppant line and the entire high electrical conductivity area. The center of the no-proppant outline is offset from the injection well.

The proppant line on the Cell 5 ERT map is a circular shape that is slightly offset from the injection well (Figure 44). The high electrical conductivity area indicated by the ERT data extends past the proppant line along the majority of the border. The no-proppant line is a semi-circular shape that encompasses the proppant line and the majority of the high electrical conductivity area. An area of high electrical conductivity extends past the no-proppant line to the southwest.

The proppant line on the Cell 6 ERT map is an irregular shape that has a northeast to southwest orientation (Figure 45). The majority of the area encompassed by the proppant line has high electrical conductivity. There is a small area to the northeast that has low electrical conductivity. The no-proppant line is an oval shape with a northeast to

southwest orientation. It encompasses the proppant line and the entire high electrical conductivity area. There are areas on the northeast and southwest extent of the no-proppant line that have low electrical conductivity.

Each of the five ERT maps was split into four quadrants: a NE quadrant, a NW quadrant, a SE quadrant, and a SW quadrant. This resulted in a total of 20 quadrants. The data indicate that the leading edge of the electrically conductive anomaly determined by the ERT was within the zone between the proppant and no proppant lines in 16 of the 20 quadrants. There were 4 quadrants where the ERT indicated that the fracture boundaries were outside of the zone between the proppant and no-proppant lines. In the NE quadrant of Cell 1, the NE quadrant of Cell 2, and the NE quadrant of Cell 6, the soil core data indicated that the fracture was present, but the ERT results indicate that the fracture is absent. The opposite discrepancy occurs in the SW quadrant of Cell 5. In this quadrant,

	Minimum Possible Area (m^2)	Maximum Possible Area (m^2)	Difference in Surface Areas (m^2)	Estimated Surface Area of Proppant (m^2)
Cell 1	9.1	24.1	15.1	17±8
Cell 2	8.4	20.9	12.4	14±6
Cell 4	8.6	26.9	18.3	18±9
Cell 5	8.1	18.9	10.8	14±5
Cell 6	12.9	24.2	11.3	18±5

Table 4 Calculations of Estimated Surface Area of the Proppant: Table of the minimum and maximum areas calculated for each cell and the difference between the two surface areas. The estimated surface area of the proppant is also given.

the ERT data indicates that the fracture is present, but the soil core data indicates that it is absent. This suggests that the ERT inversion correctly determines the edge of the conductive proppant within the resolution of the assessment method in most (80%) quadrants. The ERT appears to be biased to the southwest in the 20% of the quadrants where errors occur.

Comparison of Soil Core Occurrence with ERT and Uplift Data

A comparison analysis was carried out to compare the occurrence (location and proppant presence or absence) with the ERT data and the uplift data. These two analyses were then compared to each other to determine which method (ERT or uplift) was more consistent with the soil core data.

Evaluation of ERT Location of Proppant

The soil core locations were overlain on the ERT inversions with the goal of assessing the ability of ERT to locate proppant. The symbols used to mark the locations of the soil cores where proppant was present were different than the symbols used where proppant was absent (Figures 41 through 45). The soil core maps were superimposed on the ERT inversion maps, and four categories of core locations were identified (Table 5):

1. Proppant present in soil core & ERT predicts high electrical conductivity (T1)
2. Proppant present in soil core & ERT predicts low electrical conductivity (F1)
3. Proppant absent in soil core & ERT predicts high electrical conductivity (F2)
4. Proppant absent in soil core & ERT predicts low electrical conductivity (T2)

This gives two categories (T1 and T2) where the ERT predictions are correct and two categories (F1 and F2) where they are false. The total number of locations for categories T1 and F1 were normalized by the number of core locations where the proppant was present. The total number of locations for categories T2 and F2 were normalized by the number of core locations where the proppant was absent.

At the field site, there were a total of 95 soil cores collected. Of these 95 cores, 60 of the soil cores intersected the proppant. All of the remaining cores were deep enough to intersect the fracture if it was present, but proppant was absent in these soil cores

Category	# of Locations in Each Category by Cell					Total # of Locations	# of Locations / # of Core
	Cell 1	Cell 2	Cell 4	Cell 5	Cell 6		
T1	6	9	13	9	13	50	0.83
F1	3	2	0	1	4	10	0.17
# of Cores with Proppant Present	9	11	13	10	17	60	-
F2	1	0	0	1	0	2	0.06
T2	4	14	4	6	5	33	0.94
# of Cores with Proppant Absent	5	14	4	7	5	35	-
Total # of Cores	14	25	17	17	22	95	-

Table 5 Summary of ERT Performance Based on Soil Core Data: Summary of the number of soil cores that fall into each of the four categories. They are listed by cell. Below categories T1 and F1, the number of cores where proppant is present is totaled. Below categories T2 and F2, the number of cores where proppant is absent is totaled. At the bottom of the table, the total number of soil cores is calculated.

indicating that the fracture did not extend to this location. The number of soil cores collected in each cell varied from 14 (Cell 1) to 25 (Cell 2). The locations of the soil cores were chosen with one of two goals in mind: 1) determine the location of the outer edge of the proppant or 2) determine the internal form of the fracture. As a result, there were more soil cores that intersected the proppant than soil core where proppant was absent.

When the number of cores in the F1 and F2 categories was compared to the proppant type, the coke breeze proppant gave the best results. Pure coke breeze proppant was injected into Cell 4, and this cell had no soil core locations in the F1 or F2 categories. Both the coke breeze and sand proppant mix and the steel shot proppant had 2 to 4 soil cores in the F1 or F2 categories.

The results demonstrate that ERT is capable of determining the location of the proppant. In 83% of the locations where proppant was present in the soil cores, the ERT also correctly identified proppant (T1). In 94% of the locations where proppant was nonexistent in the soil cores, the ERT correctly identified an absence of proppant (T2). Some of the cells had even higher performance percentages. For example, 100% of the soil cores in Cell 4 fell into in the T1 or T2 categories. The cell with the poorest performance was Cell 1. In this cell, only 66% of the cores fell into the T1 category and only 80% were in the T2 category. The high percentage of soil cores in the T2 category is significant because these were the cores that were used to determine the location of the outer edge of the proppant and therefore are located very close to the edge of the

proppant. The ERT would have to be very accurate to correctly identify these locations. In contrast, the soil cores from the T1 category were initially employed to determine the internal form of the fracture. As a result, it is expected that it is less difficult for the ERT to correctly identify these locations.

Evaluation of Uplift Location of Proppant

An evaluation of the uplift data was then completed using similar categories to the ones listed above. To complete this evaluation, the soil core data was overlain on the uplift maps. The 3 mm contour line was included on all of the uplift maps and this was chosen to indicate the maximum extent of the proppant. The symbols used to mark the locations of the soil cores where proppant was present were different than the symbols used where proppant was absent (Figure 46). The locations were then placed in one of the following categories (Table 6):

1. Proppant present in soil core & uplift predicts proppant present (T1)
2. Proppant present in soil core & uplift predicts proppant absent (F1)
3. Proppant absent in soil core & uplift predicts proppant present (F2)
4. Proppant absent in soil core & uplift predicts proppant absent (T2)

This gives two categories (T1 and T2) where the uplift predictions are correct and two categories (F1 and F2) where they are false. The total number of locations for categories T1 and F1 were normalized by the number of core locations where the proppant was present. The total number of locations for categories T2 and F2 were normalized by the number of core locations where the proppant was absent.

These results demonstrate that all of the soil cores where proppant was present fell into the area of the uplift plot that indicated that the proppant was present. This was true for 100% of the soil cores where proppant was present. For the soil cores where proppant was absent, a different pattern occurs. In 66% of the locations where proppant was nonexistent in the soil cores, the uplift data predicted that the proppant was present. In 34% of the locations where proppant was absent in the soil cores, the uplift correctly predicted that the proppant was absent. The comparison between the uplift data and the soil core data varied in the individual cells. Cell 5 had the best results for the soil core locations with proppant absent. In this cell, 6 of the 7 soil cores with proppant absent were placed in the T2 category and only 1 core was placed in the F2 category. In the

Category	# of Locations in Each Category by Cell					Total # of Locations	# of Locations / # of Core
	Cell 1	Cell 2	Cell 4	Cell 5	Cell 6		
T1	9	11	13	10	17	60	1.00
F1	0	0	0	0	0	0	0.00
# of Cores with Proppant Present	9	11	13	10	17	60	-
F2	4	9	4	1	5	23	0.66
T2	1	5	0	6	0	12	0.34
# of Cores with Proppant Absent	5	14	4	7	5	35	-
Total # of Cores	14	25	17	17	22	95	-

Table 6: Summary of Uplift Performance Based on Soil Core Data: Summary of the number of soil cores that fall into each of the four categories compared to the uplift data. They are listed by cell. Below categories T1 and F1, the number of cores where proppant is present is totaled. Below categories T2 and F2, the number of cores where proppant is absent is totaled. At the bottom of the table, the total number of soil cores is calculated.

remaining cells, over half of the soil cores with proppant absent were placed in the F2 category. In Cell 4 and Cell 6, all of these soil cores were placed in the F2 category.

When the evaluation of the ERT location of the proppant was compared to the uplift location of the proppant, it was observed that the proppant prediction based on the ERT data gave better results than the uplift data. In the ERT data set, 83 of the 95 soil cores fell into either the T1 or T2 categories. In the uplift data set comparison, only 72 of the 95 soil cores were placed in the T1 or T2 categories. This was less than the ERT data. The number of soil cores in the uplift data set that were placed in the F1 or F2 categories was almost twice the number of soil cores that were placed in these categories when compared with the ERT data. This comparison between the ERT location of the proppant and the uplift location of the proppant indicates that the ERT data gives a better prediction of the location of the proppant.

Comparison of Estimated Fracture Depths

The cross sections from the ERT inversion were evaluated by comparing them to the soil core data. The soil core cross sections for Cells 1, 5, and 6 were overlain on their respective ERT cross sections (Figures 41, 44, and 45). For Cells 2 and 4, the soil core points and the cross section line from the excavation data were overlain on their respective ERT cross sections (Figure 42 and 43). For all cells, the injection well was included on the cross sections for reference. A thin white line named the ERT line was then drawn on the cross sections to indicate the location of the fracture according to the ERT data. The ERT inversions predict electrical conductivity above the background over

zones that are 0.2 m to 0.7 m thick, but the proppant is typically approximately 1 cm thick. The large thickness of the zones of elevated electrical conductivity is an artifact of the inversion procedure so the actual depth of the proppant was assumed to occur where the electrical conductivity was greatest. The white line was used to mark this location (Figures 41 through 45).

A total of 25 points were analyzed across the five cells (Table 7). The depth to the ERT line was measured at the same location on the cross section line as the soil core points. The depth to the proppant in the soil core was known from the field study. This data were used to calculate the absolute and relative errors between the observed depths of the proppant in the soil cores and the depth predicted by the ERT inversion.

This information was used to determine whether the ERT data indicated the fracture was above or below the soil core data. Five of the data points had a negative percent error. This means that the ERT data estimated a shallower fracture depth 20% of the cases. Eighteen of the points had a positive percent error. This means that 72% of the cases the ERT data estimated a greater fracture depth. There were also two locations (C1-4/50 and C2-4/41) where the soil core indicated the fracture was present, but the ERT data did not indicate the presence of the fracture. Therefore, this occurred for 8% of the data points. In the majority of the data, the ERT overestimated the fracture depth. In Cell 5, all of the ERT depths were greater than the depths indicated by the soil core data. Both Cell 2 and Cell 6 had one location where the ERT depth was shallower than the soil depth. In Cell 4, three of the five locations had ERT depths that were shallower than the

soil core data. In Cell 1 and Cell 2, there was one location where the soil core predicted that proppant was present, but the ERT data indicated that it was absent.

The average absolute error was then calculated and determined to be -0.17 meters. The absolute error data were then used to calculate the standard deviation. The following equation was employed.

$$Standard\ Deviation = \sqrt{\frac{\sum(average\ absolute\ error - absolute\ error)^2}{n-1}} \quad (3)$$

The standard deviation was calculated to be 0.19 meters. This means that the fracture depth predicted by the ERT will have an error of -0.17±0.19 meters. The negative value of the absolute error indicates that that the soil core location will be shallower than the ERT location depth.

The grid blocks used in the inversion range from 0.125 m in Cell 4 to 0.25 m in all the other cells. The standard deviation for the depth estimate is less than one of the grid blocks used in the inversion, and the absolute error is less than the size of most of the grid blocks. As a result, even though the ERT over predicts the depth of the proppant, the magnitude of this error is small compared to the resolution of the inversion analysis.

Several paired two sample Student's t-tests were completed to analyze the ERT and soil core fracture depth data. The t-test was run on the data for each cell and for all of the depth data collected (Table 8). The p-value for each cell was calculated. When the p-value for the individual cells were examined, all of the values were 0.98 or greater. In Cell 4, the p-value is 1.00. The p-value calculated for the entire data set was 0.90. These

Core#	Depth in Core (m)	Depth Predicted by ERT (m)	Absolute Error	Relative Error
Cell 1				
C1-4/50	-1.4	-1.9	-0.51	0.36
C1-2/230	-1.7	-1.8	-0.10	0.06
C1-4/230	-1.3	-1.6	-0.25	0.19
C1-6/230	-1.5	-1.6	-0.05	0.03
Cell 2				
C2-4/41	-1.4	-1.7	-0.34	0.25
C2-2/221	-1.5	-1.7	-0.14	0.09
C2-4/221	-1.3	-1.4	-0.13	0.10
C2-4.85/221 A	-1.6	-1.4	0.21	-0.13
C2-6/221	-1.4	-1.4	0.00	0.00
C2-10/221	-1.1	-1.4	-0.34	0.32
Cell 4				
C4-4/70	-1.8	-1.6	0.19	-0.11
C4-2/250	-1.6	-1.6	0.02	-0.01
C4-4/250	-1.3	-1.4	-0.16	0.13
C4-6/250	-1.2	-1.2	0.01	-0.01
C4-10/250	-0.4	-0.7	-0.29	0.77
Cell 5				
F5-4/0	-1.8	-2.0	-0.20	0.11
C5-3/0	-1.8	-2.0	-0.22	0.12
F5-2/180	-1.6	-2.0	-0.42	0.26
F5-4/180	-1.7	-2.0	-0.26	0.15
F5-5/180	-1.7	-2.0	-0.30	0.18
Cell 6	Soil core depths based on magnet readings			
C6-10.5/48	-0.7	-0.7	0.04	-0.06
C6-8.5/48	-0.9	-1.1	-0.18	0.20
C6-5/48	-1.2	-1.5	-0.29	0.24
C6-1.5/228	-1.6	-1.9	-0.30	0.19
C6-6.5/228	-1.5	-1.9	-0.39	0.26

Table 7 Error Calculations for Comparison of Soil Core and ERT Cross Section Data: The table lists the below ground surface depths for the fracture based on the soil core data and the ERT data. The data was then used to calculate the absolute error, relative error, and percent error. Positive percent error indicates that the ERT method estimated a greater depth than was observed in the soil core data. Negative percent error indicates that the ERT method estimated a shallower depth than was observed in the soil core data.

Cell #	Soil Core Mean Depth (m)	ERT Mean Depth (m)	p-value
1	-1.47 ± 0.16	-1.70 ± 0.18	0.98
2	-1.39 ± 0.19	-1.51 ± 0.16	0.98
4	-1.25 ± 0.54	-1.29 ± 0.38	1.00
5	-1.71 ± 0.09	-1.99 ± 0.02	0.98
6	-1.17 ± 0.37	-1.39 ± 0.52	0.97
All Cells	-1.39 ± 0.35	-1.57 ± 0.38	0.90

Table 8 Summary of the Standard Deviation of Soil Core and ERT Fracture Depths: Summary of the standard deviation of the soil core fracture depths and the ERT fracture depths for each cell and all the data. The p-value for each cell and for the total data set is listed in the far right column.

values are close to or equal to 1.00. This indicates that there is a high probability that the depths measured by the soil cores and the ERT in each cell come from the same population and have the same mean value.

Differences between the data sets are most likely due to chance and sampling of the data set. The discrepancies between the proppant depths indicated by the ERT and the soil core data could also be due to the way the ERT inversion was run. In the inversion process, the MMPT3D inversion algorithm is a difference inversion that determines how much the conductivity changed relative to the background level. If the inversion process was altered to constrain the changes in conductivity to a fracture form geometry with a set maximum thickness, it is possible that the discrepancies between the ERT predicted depths and the soil depths could be minimized.

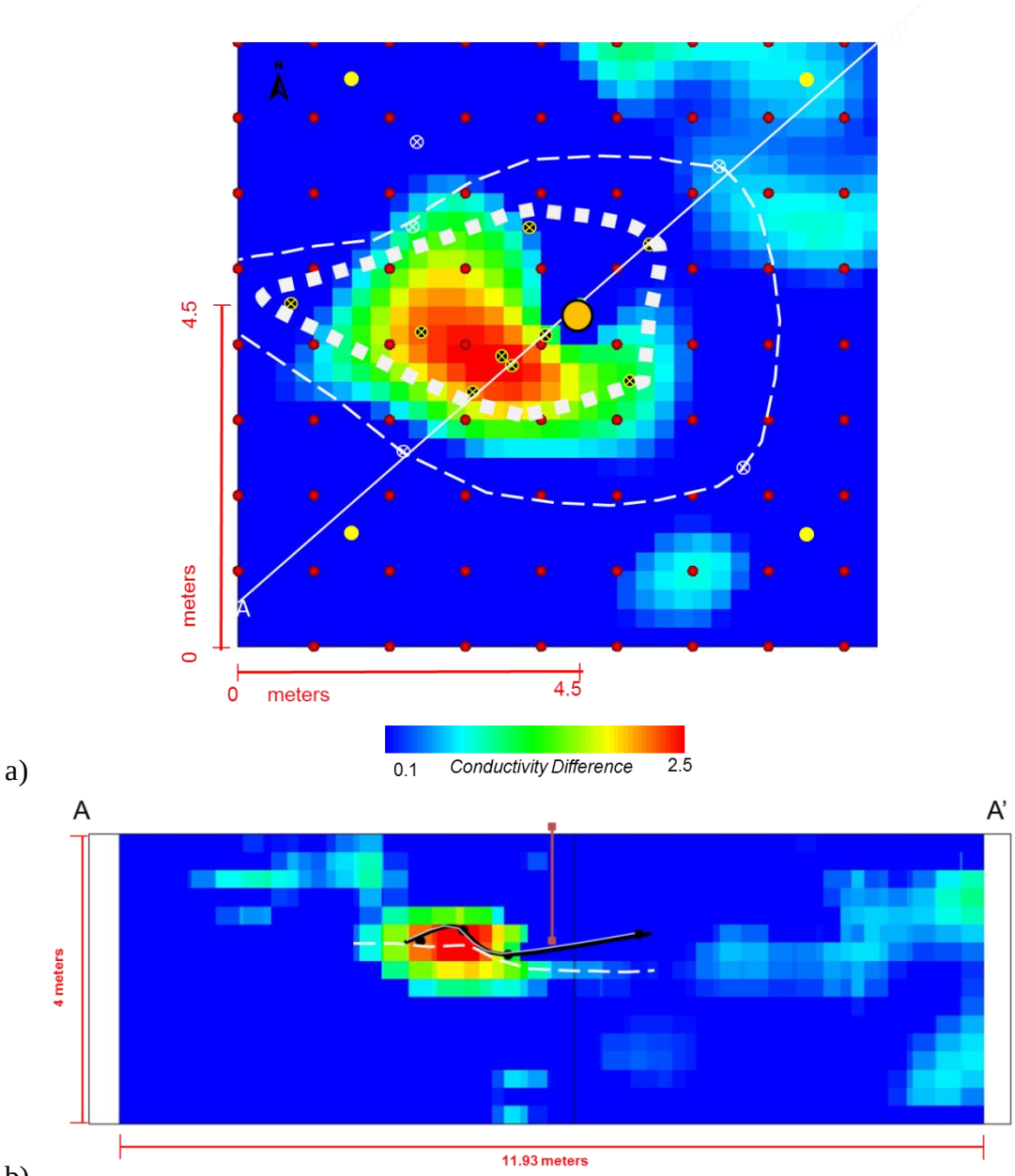

Figure 41: Comparison of ERT data and direct observation data in Cell 1 a) Map of electrical conductivity (color, in millisiemens log scale) at 1.6 m depth. The grid blocks are 0.25 m. Dots are soil core locations. The thick white square dotted line is the proppant line. The thin dashed line is the no proppant line. b) Cross section on 50° azimuth of electrical conductivity (color, in millisiemens log scale) and trace of hydraulic fracture (black and white line) interpolated from soil core observations (black dots). The thin white dashed line is the interpreted fracture location based on the ERT data.

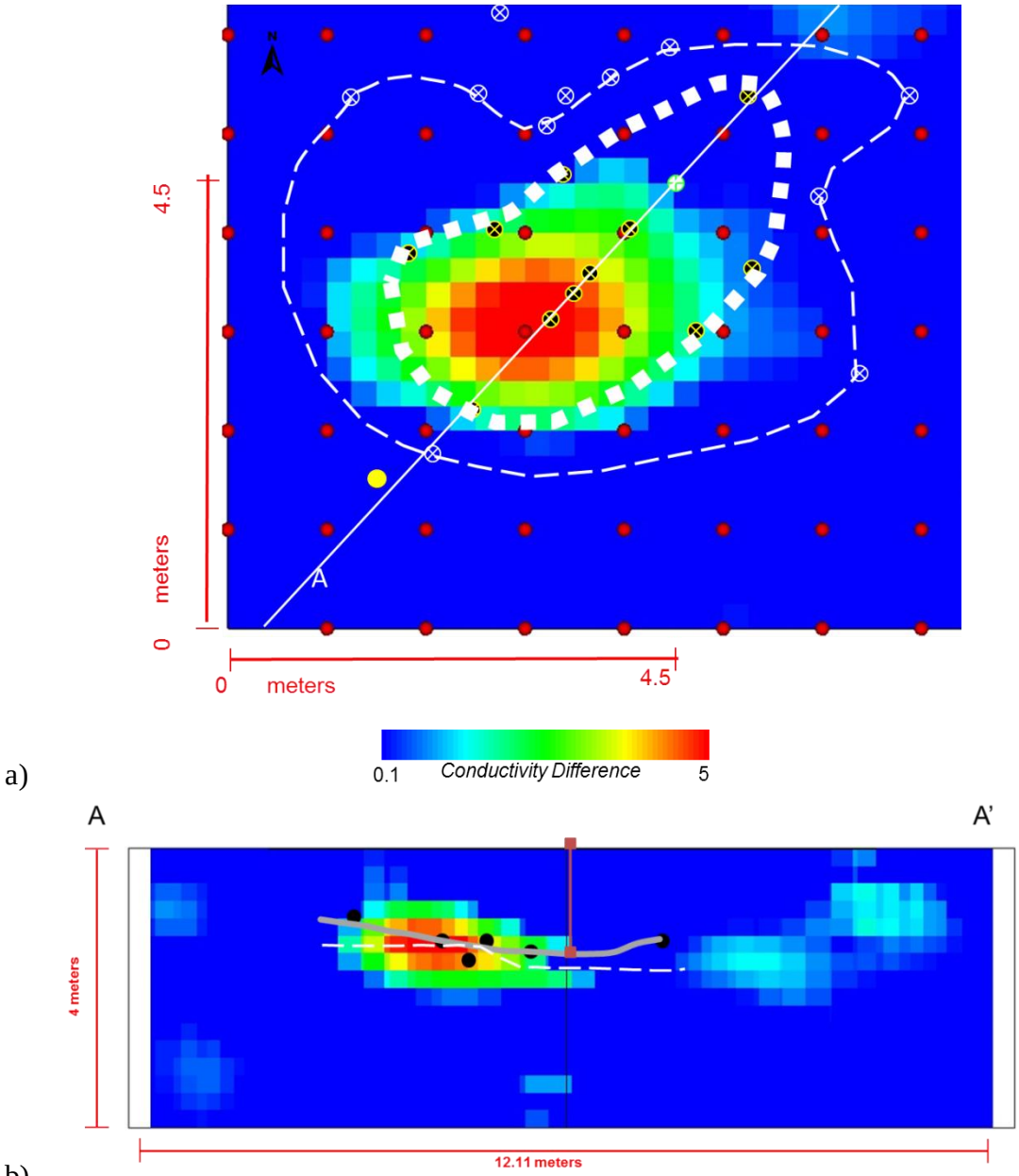

Figure 42: Comparison of ERT data and direct observation data in Cell 2 a) Map of electrical conductivity (color in millisiemens log scale) at 1.4 m depth. The edges of the map have been cropped to improve the resolution of the image. The grid blocks are 0.25 m. Dots are soil core locations. The thick white square dotted line is the proppant line. The thin dashed line is the no proppant line. b) Cross section on 47° azimuth of electrical conductivity (color, in millisiemens log scale) and trace of hydraulic fracture (gray line) interpolated from excavation data. The black dots are soil core observations. The points are soil core data. The thin white dashed line is the interpreted fracture location based on the ERT data.

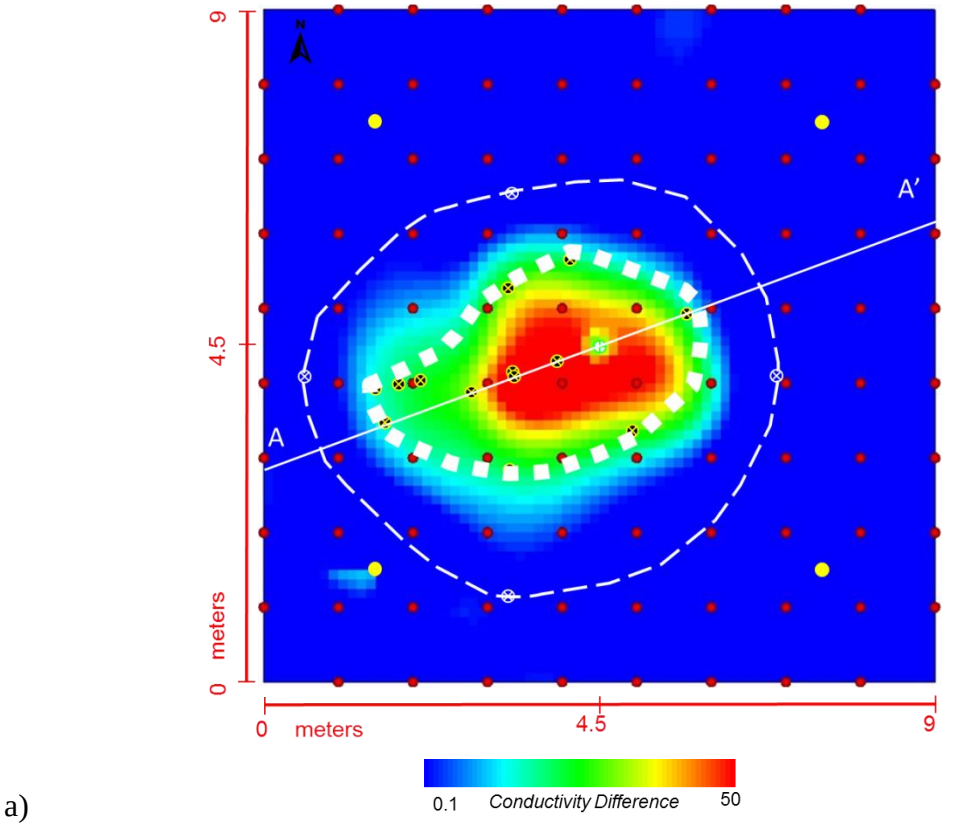

a)

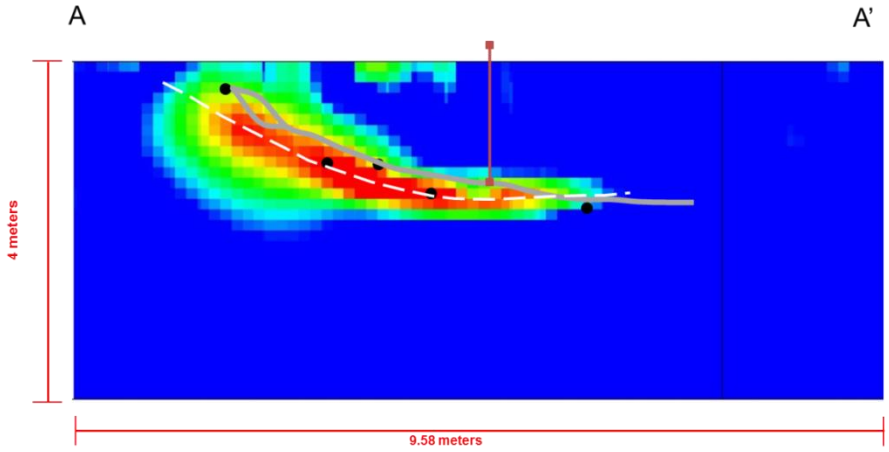

b)

Figure 43: Comparison of ERT data and direct observation data in Cell 4 a) Map of the electrical conductivity (color, in millisiemens log scale) at 1.6 m depth. The grid blocks are 0.125 m. Dots are soil core locations. The thick white square dotted line is the proppant line. The thin dashed line is the no proppant line. b) Cross section of electrical conductivity on NE/SW azimuth (color, in millisiemens log scale) and trace of hydraulic fracture (gray line) interpolated from excavation data. The black dots are soil core observations. The points are soil core data. The thin white dashed line is the interpreted fracture location based on the ERT data.

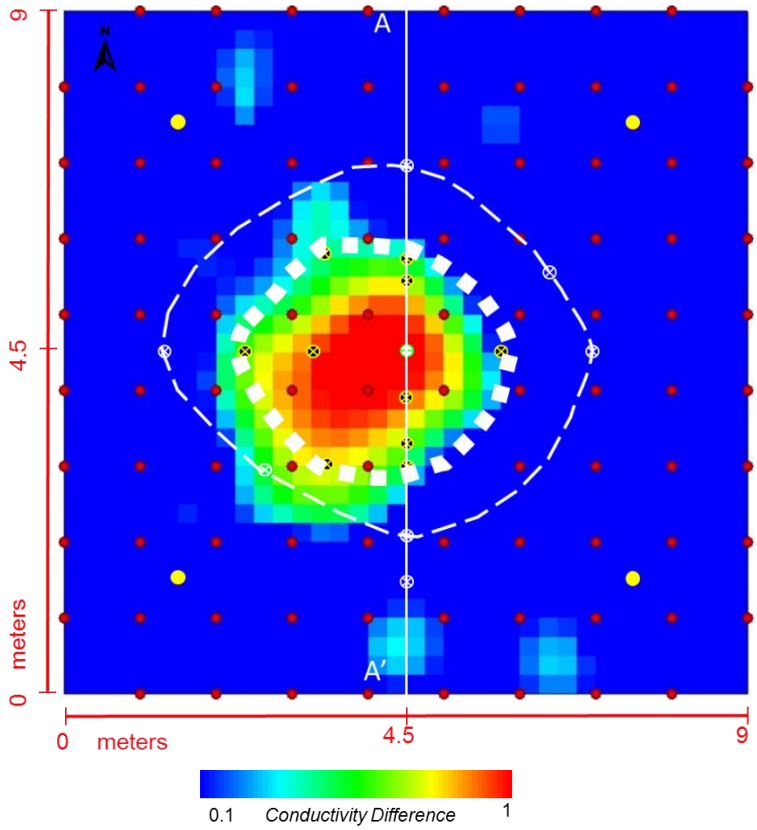

a)

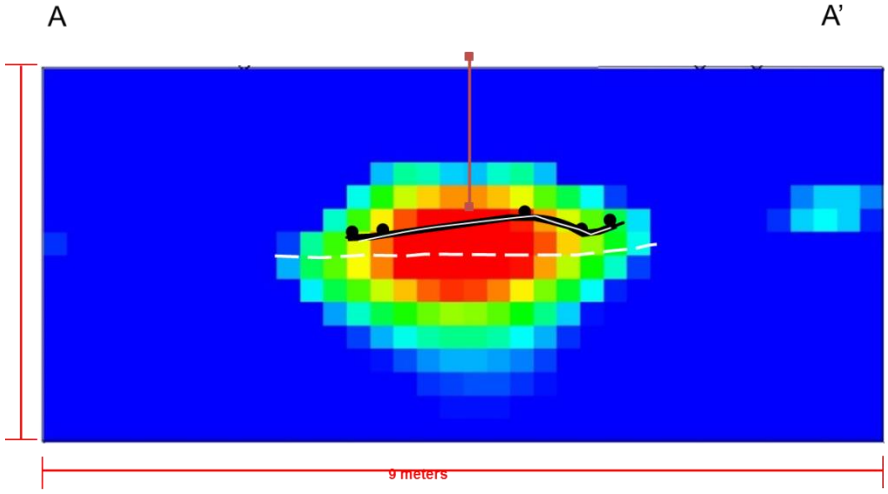

b)

Figure 44: Comparison of ERT data and direct observation data in Cell 5 a) Map of electrical conductivity (color, in millisiemens log scale) at 1.6 m depth. The grid blocks are 0.25 m. Dots are soil core locations. The thick white square dotted line is the proppant line. The thin dashed line is the no proppant line. b) Cross section on N/S azimuth of electrical conductivity (color, in millisiemens log scale) and trace of hydraulic fracture (black and white line) interpolated from soil core observations (black dots). The thin white dashed line is the interpreted fracture location based on the ERT data.

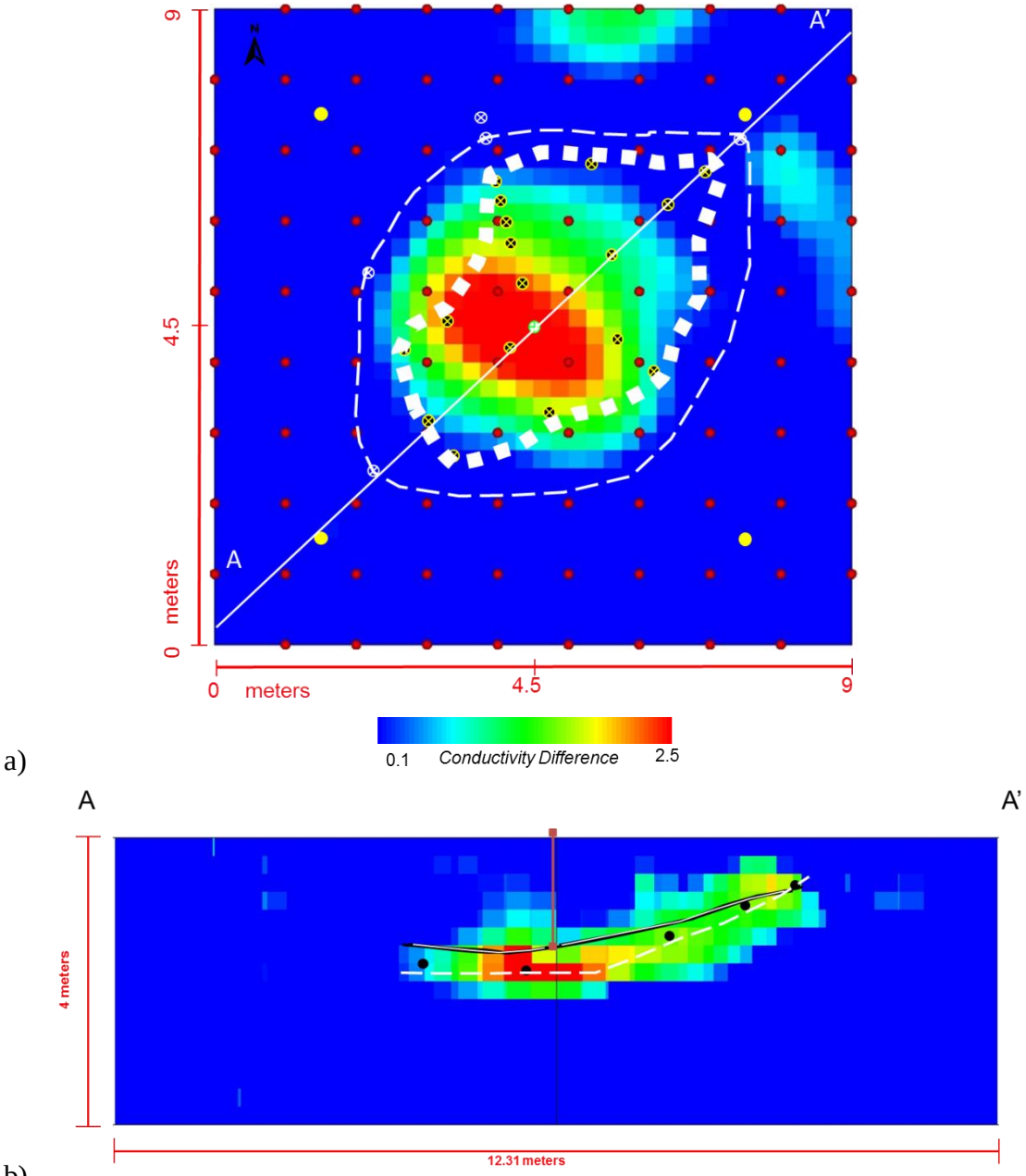

Figure 45: Comparison of ERT data and direct observation data in Cell 6 a) Map of electrical conductivity (color, in millisiemens log scale) at 1.76 m depth. The grid blocks are 0.25 m. Dots are soil core locations. The thick white square dotted line is the proppant line. The thin dashed line is the no proppant line. b) Cross section on 48° azimuth of electrical conductivity (color, in millisiemens log scale) and trace of hydraulic fracture (black and white line) interpolated from soil core observations (black dots). The thin white dashed line is the interpreted fracture location based on the ERT data.

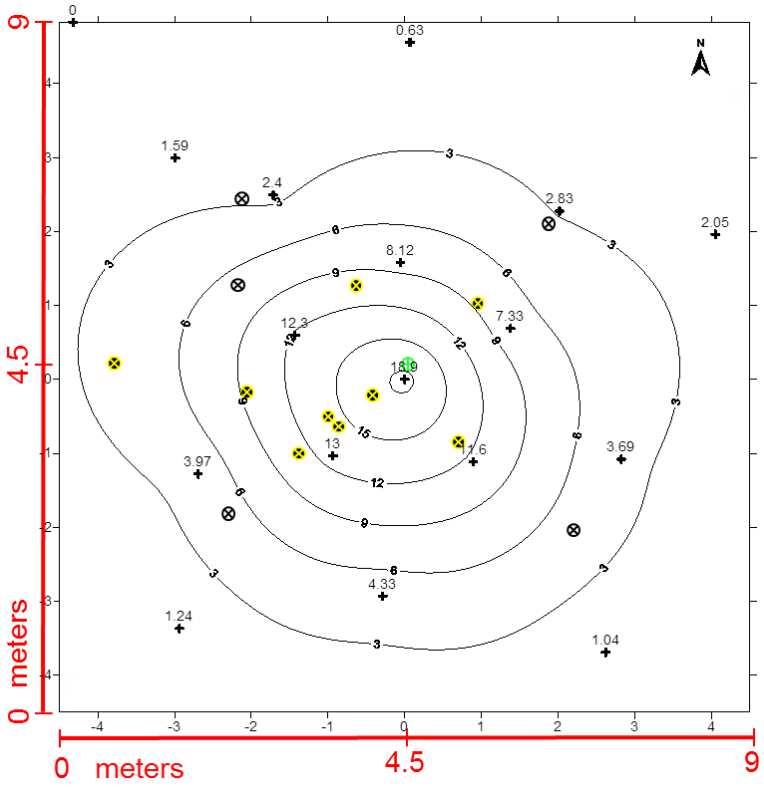
0
0.63
N
1.59
2.4
2.83
2.05
8.12
12.3
7.33
13
11.6
3.97
3.69
4.33
1.24
1.04
9
4.5
0 meters
0
4.5
9

a)

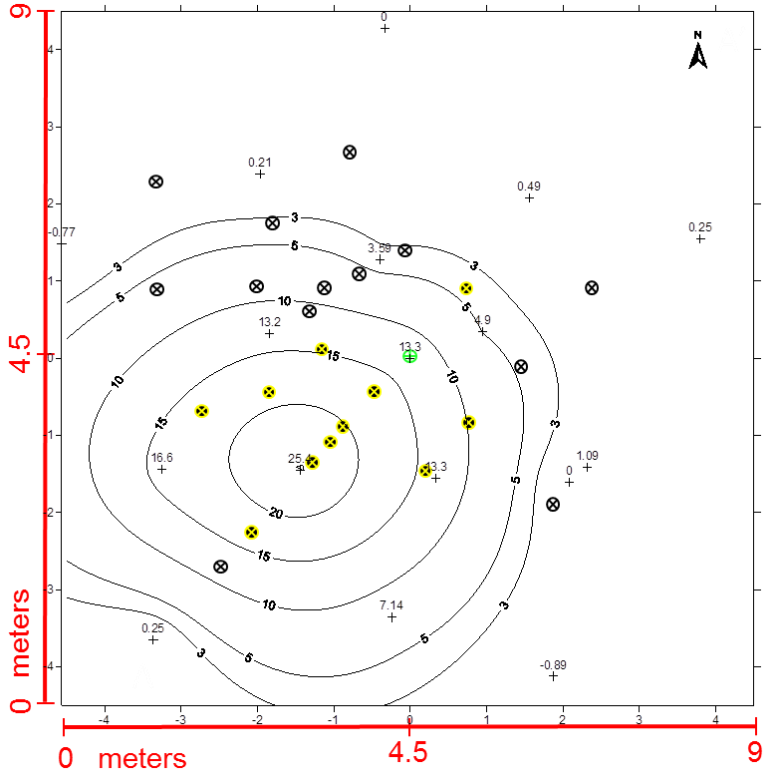
0
N
0.21
0.49
0.25
-0.77
3.59
13.2
13.3
4.9
16.6
25.4
13.3
1.09
0
7.14
0.25
-0.89
9
4.5
0 meters
0
4.5
9

b)

c)

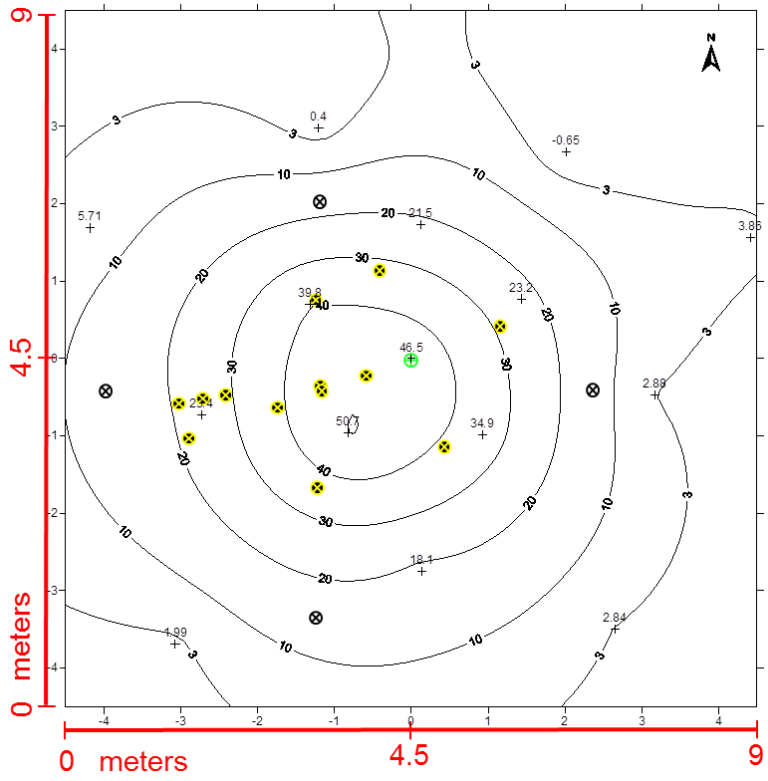
N
0.4
-0.65
5.71
21.5
3.86
39.8
23.2
46.5
2.89
25.4
50.7
34.9
18.1
1.99
2.84
0 meters
4.5
9
0 meters
4.5
9

d)

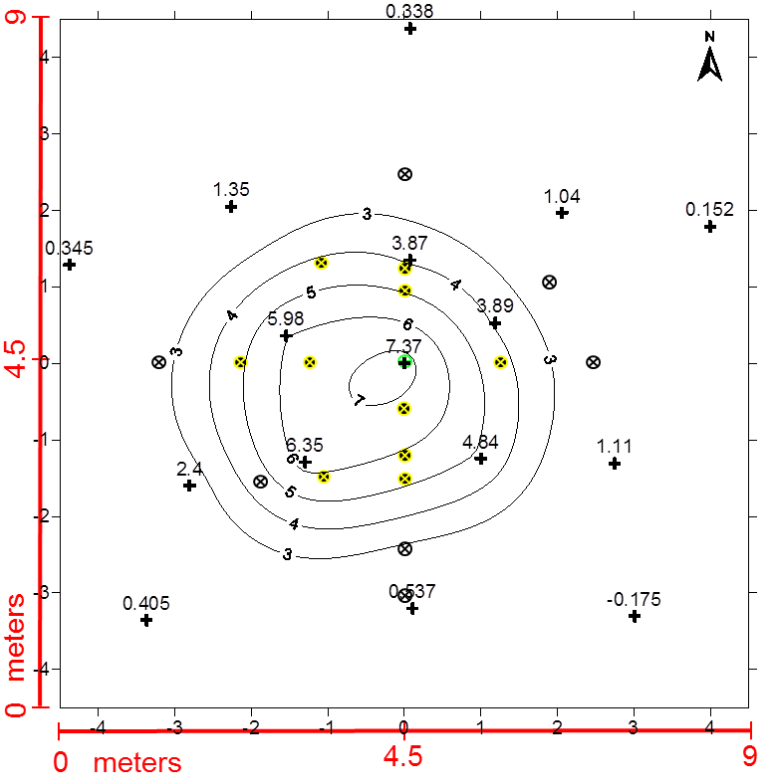
N
0.338
1.35
1.04
0.152
0.345
3.87
3.89
5.98
7.37
6.35
4.84
1.11
2.4
0.405
0.537
-0.175
0 meters
4.5
9
0 meters
4.5
9

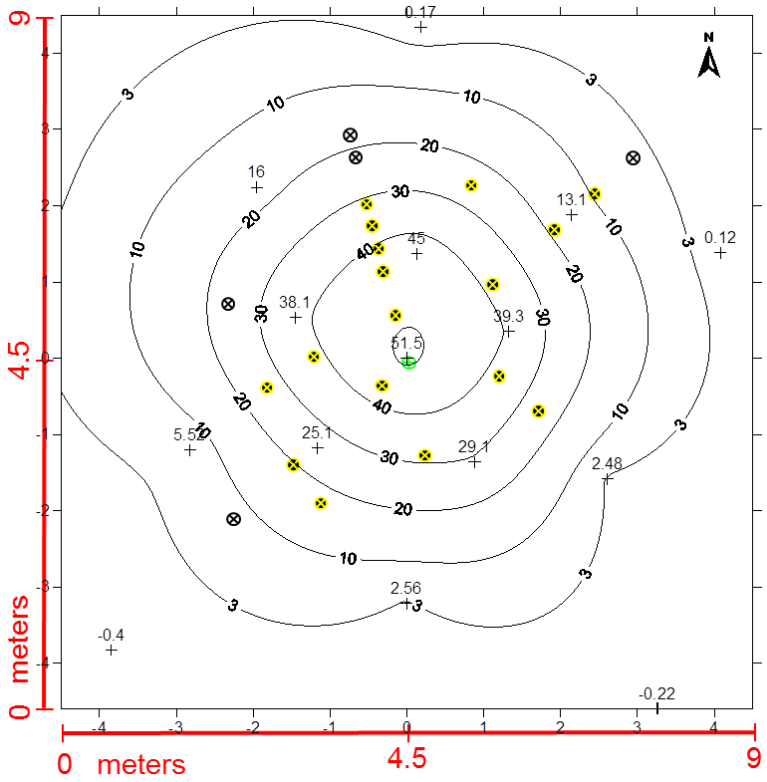

e)

Figure 46: Comparison of uplift data to soil core data. The green dot is the injection well. The yellow and black dots are the locations where the proppant was present in the soil core data. The black and white dots are the locations where proppant was absent in the soil core data. The cross symbols are the uplift data in mm. All contours are in mm. a) Cell 1 b) Cell 2 c) Cell 4 d) Cell 5 e) Cell 6

CHAPTER 9: CONCLUSION

The soil core and survey cross sections of the fractures illustrated that the fractures created shallow off center ellipsoids consistent with shallow fractures. Analysis of the uplift data from Powdersville and the Murdoch and Slack, 2002 data indicates that the fractures created at the Powdersville field site are comparable to previously created shallow hydraulic fractures even though they are more circular than those previously reported. Examination of the variograms created from the aperture measurements on the photo mosaic panoramas demonstrates that the variation across the maximum lobe can be determined. The small scale variance of the proppant thickness will be the result of the small scale internal form of the fracture while the maximum variance will be controlled by the size of the fracture lobes. The electrical resistivity tomography method was able to detect the location of the fractures by differentiating the electrically conductive proppants from the surrounding soil. The ERT data rounded the fractures as high conductivity anomalies in the subsurface.

When the ground checked data from the soil core and survey data were compared with the ERT results, the field observed data consistently matched the ERT. Based on the comparisons the leading edge of the proppant indicated by the geophysical data will consistently be located in-between the proppant and no-proppant lines. The location comparisons between the soil core data and the geophysical data also gave favorable results. This analysis demonstrated that when the soil core data indicated that the fracture was present the geophysical results would agree. In 94% of the cases where the soil core

data did not find the fracture, the ERT data would concur. The cross section comparisons demonstrate that the ERT can indicate the location of the fracture. In 72% of the cases, the fracture was shallower than indicated by the ERT data, and there was an error of -0.17±0.19 meters. The p-value calculated from the soil core and ERT t-test is 0.90 indicating that any discrepancies in the data are due to sampling errors. These results demonstrate that the ERT method is capable of locating fractures containing electrically conductive proppants and has the potential as a non-invasive method of determining fracture form, extent, and depth in environmental and industrial studies.

APPENDICES

Appendix A: Soil Core Information

This appendix contains information related to the soil core data. The first set of data included in Appendix A are the soil core description sheets that were filled out when each soil core was described. The next set of data included is the data taken from the soil description sheets organized into spreadsheets for comparison between the different soil cores.

Drill and Well Log

Sheet ___ of ___

Well ID C1-4/50

Date 6-8-15

Total Depth 6.11 (ft)

Casing Diameter ( )

Casing Elevation (MSL.) ( )

Casing Height (above g.s.) ( )

UTM Location

Site Description & Sketch Map:

Driller / (Geologist): Jessica Denison

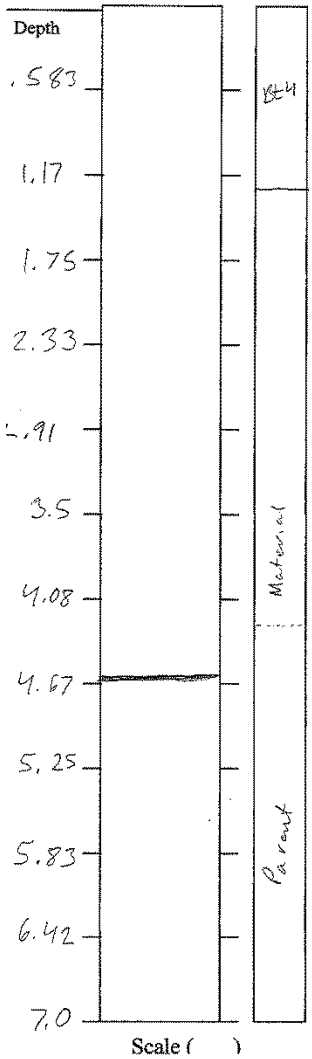

Color	Grain Size	Plasticity	Moisture	USCS / USDA	Comments

BE4 is a red (2.5 YR 4/6) clay loam. Mica flakes are common. It has a weak blocky structure. A few reddish yellow (7.5 YR 6/8) mottles are present. It is moderately plastic.

Parent material is a felsic rock such as a granite or a gneiss. Biotite, feldspars, and some quartz is present. Little structure is present and the material easily crumbles. The majority of the material is very pale brown (10 YR 8/3). The area surround the fracture (from dotted line to the bottom of the core) is a darker color. It is brownish yellow (10 YR 6/6). In the yellowish brown section, clear to bronze colored micas are present. The rest of the material is weathered to clays - most likely iron oxide clays such as goethite and/or limonite based on the color of the soil

Sand coke breeze fracture is 1.25 ft above the bottom of the core. 1.25 and shoe length of 0.25 ft are subtracted from total depth to give fracture location of 4.61 ft. Fracture is about 5mm thick.

Drill and Well Log

Sheet ___ of ___

Well ID C1-4/147

Date 6-8-15

Total Depth 7.0 (~~ft~~)

Casing Diameter ( )

Casing Elevation (MSL.) ( )

Casing Height (above g.s.) ( )

UTM Location

Site Description & Sketch Map:
- some dirt was lost out of this core 1

Driller / (Geologist): Jessica Denison

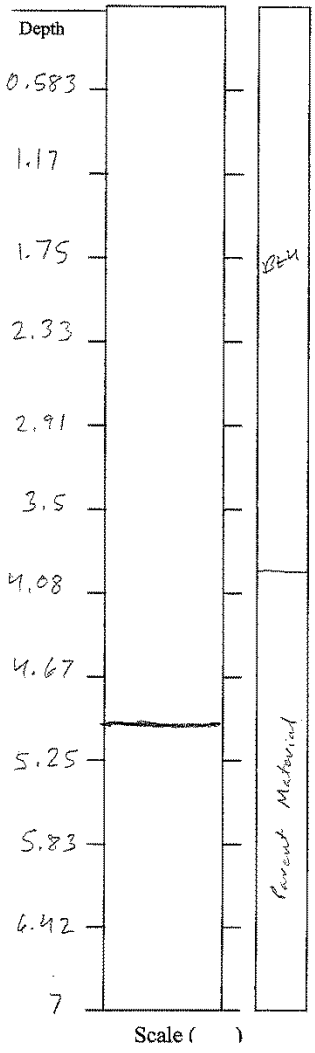

Color	Grain Size	Plasticity	Moisture	USCS / USDA	Comments

BEH is a red (2.5YR 4/6) clay loam. Mica flakes are common throughout. It has a weak blocky structure. It is moderately plastic. No obvious mottles are present.

Sand cake breccia ~~fracture~~ is 1.73 ~~ft~~ from the bottom of the core. This value and the shoe length are subtracted from the total depth to give a location of 5.07 ft below ground surface. Two fractures are present. The upper one is 4 to 10 mm thick. The lower fracture is 4 to 6 mm thick. Fractures are separated by 14 to 19 mm of soil.

Parent material is a felsic rock such as a granite or a gneiss. Quartz, feldspar, and biotite are present. The parent material has begun to weather to form clays such as kaolinite and possibly limonite or goethite. No structure is present. Some of the parent material is light gray (10YR 7/2) and some of it that has a greater amount of weathering is strong brown (7.5YR 5/8).

Drill and Well Log

Sheet ___ of ___

Well ID C1-2/230

Date 6-8-15

Total Depth 7.3 (ft)

Casing Diameter ( )

Casing Elevation (MSL.) ( )

Casing Height (above g.s.) ( )

UTM Location

Site Description & Sketch Map:

Driller / (Geologist): Jessica Denison

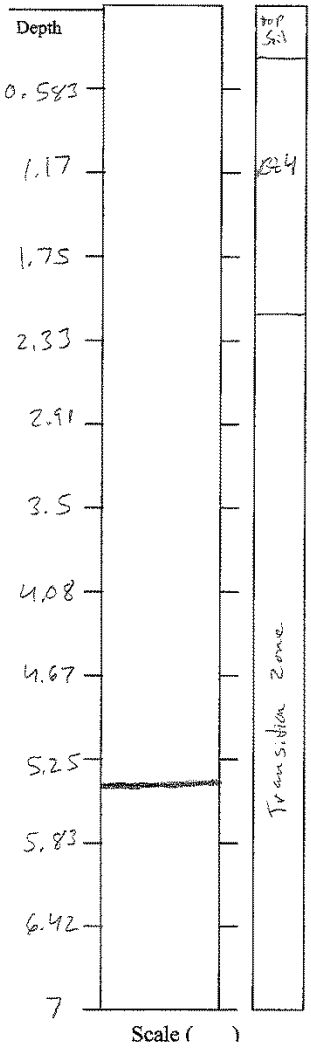

Color	Grain Size	Plasticity	Moisture	USCS / USDA	Comments

Fine grained material such as clays like kaolinite. Weathered micas are present. Material is yellowish brown (10YR 5/6).

Bt4 is a red (2.5YR 4/6) clay loam. Mica flakes are common. It has a weak medium subangular blocky structure. It is firm and moderately plastic. Reddish yellow (7.5YR 6/8) mottles are present.

Transition zone contains quartz, feldspar, and biotite. Feldspars are breaking down to clays such as kaolinite, limonite, and goethite. Manganese oxide is present within the section. Biotites are altering to a clear or bronze color. The soil is a yellowish brown (10YR 5/4) color.

Sand cake breeze fracture is 1.56ft above the bottom of the core. This value and the shoe length of 0.25 ft is subtracted from the total depth to give a location of 5.49 ft below ground surface. The fracture is 7 to 14 mm thick with mode thickness of 12 mm.

Drill and Well Log

Sheet ___ of ___

Well ID C1-6/230

Date 6-8-15

Total Depth 7.3 (ft)

Casing Diameter ( )

Casing Elevation (MSL.) ( )

Casing Height (above g.s.) ( )

UTM Location

Site Description & Sketch Map:

Driller / (Geologist): Jessica Denison

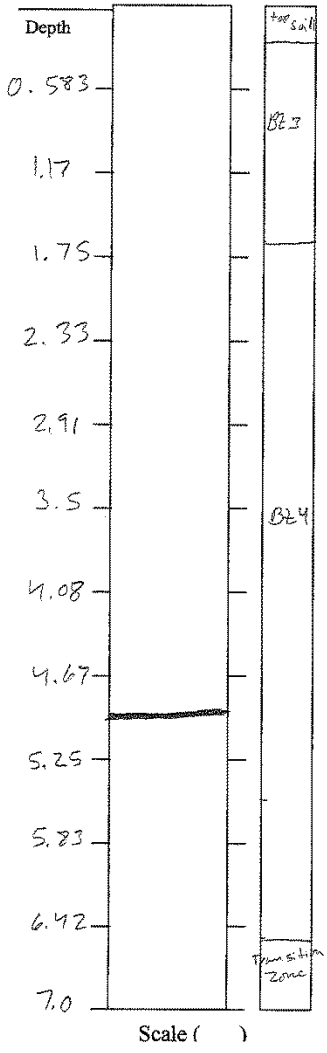

Color	Grain Size	Plasticity	Moisture	USCS / USDA	Comments

Top soil is loose material that is brown (7.5YR 4/3). Mica flakes common.

Bt3 is a red (2.5YR 4/6) clay. It has a moderate medium subangular blocky structure. Mica flakes are common throughout. Moderately plastic. No obvious mottles are present.

Bt4 is a red (2.5YR 4/6) clay loam. Mica flakes are common throughout. It has a weak medium, subangular blocky structure. Reddish yellow (7.5YR 6/8) mottles are present in the section.

Sand core breeze fracture is 2.1 ft above the bottom of the core. This value and the shoe length are subtracted from the total depth to give a location of 4.95 ft below ground surface. The fracture is 3mm to 10mm thick.

Transition zone contains quartz, feldspar, and micas such as biotite. The feldspars and micas are breaking down to clays such as kaolinite. It is yellowish brown (10YR 5/6).

Drill and Well Log

Sheet ___ of ___

Well ID C1 - 10/230
Date 6-8-15
Total Depth 7.2 (ft)
Casing Diameter ( )
Casing Elevation (MSL.) ( )
Casing Height (above g.s.) ( )

UTM Location
Site Description & Sketch Map:
- no fracture present

Driller / (Geologist): Jessica Denison

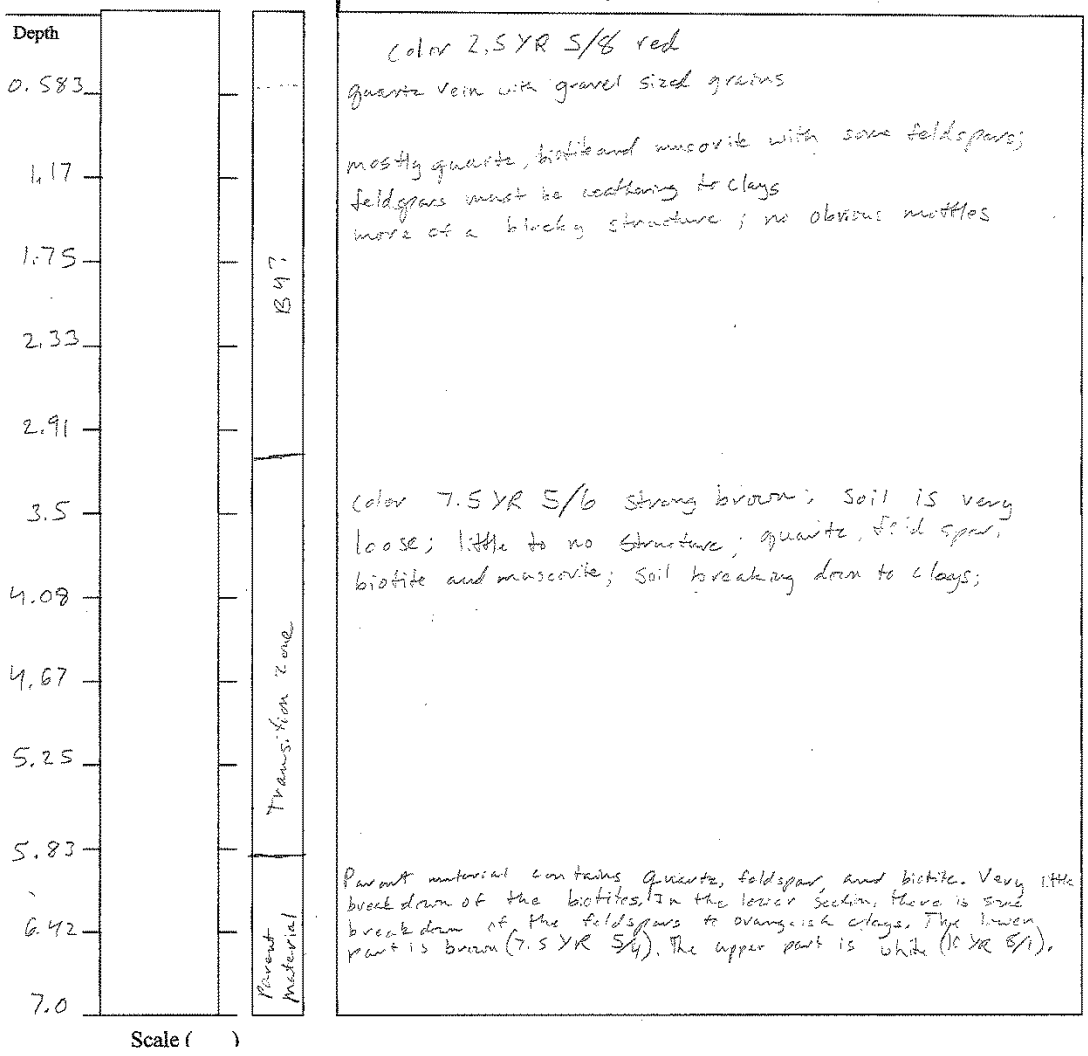

Drill and Well Log

Sheet ___ of ___

Well ID C1-4/327

Date 6-8-15

Total Depth 7.3 (~~FA~~)

Casing Diameter ( )

Casing Elevation (MSL.) ( )

Casing Height (above g.s.) ( )

UTM Location

Site Description & Sketch Map:

Driller/ Geologist: Jessica Morrison described 7-11-17

Well Construction | Lith. | Color | Grain Size | Plasticity | Moisture | USCS / USDA | Comments

Depth

0.583

1.17

1.75

2.33

2.91

3.5

4.08

4.67

5.25

5.83

6.42

7.0

Scale ( )

Transitional zone

Parent material (weathered)

Very degraded parent material

color 7.5YR 6/6 reddish yellow quartz, feldspars, muscovite and biotite present; feldspars easily break up; soil very loose; little structure

color 10YR 8/2 very pale brown; grain size ranges from gravel to very fine; soil appears to be broken down parent material perhaps a granite or a gneiss; quartz, feldspars, biotite + muscovite present

Second core breeze fracture is 1.67ft above the bottom of the core. This value and the shoe length are subtracted from the total depth to give a location of 5.38ft. The fracture is 5 to 7mm thick. Fracture does not appear to span entire core. Fracture projects 2/3 of the way across the core and stops. The other 1/3 of the fracture is about 10mm above it. They do not appear to be connected but it is difficult to tell.

Soil- color 7.5YR 7/6 reddish yellow; quartz, feldspar, biotite, muscovite present; not as many large feldspars as above - probably degraded to clays; grain size ranges from very fine to medium grained

Drill and Well Log

Sheet ___ of ___

Well ID C2-4/41

Date 6-4-15

Total Depth 7.05 ft ( )

Casing Diameter ( )

Casing Elevation (MSL.) ( )

Casing Height (above g.s.) ( )

UTM Location

Site Description & Sketch Map:

Driller / Geologist:

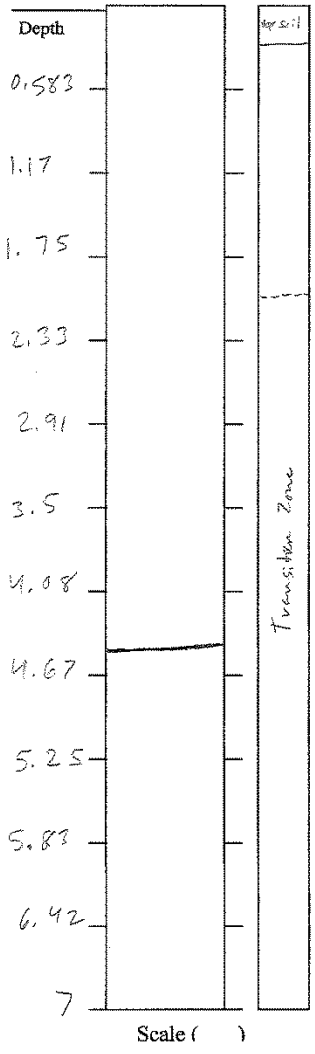

Color	Grain Size	Plasticity	Moisture	USCS / USDA	Comments

top soil is gravelly and sandy micaceous, most likely lost in shoe when last core and material in liner at the top of this core

Transition zone contains weathered parent material. Quartz, feldspar, and micas are present. At the bottom of the core, all three minerals are present as you move up section, the feldspars become more weathered and turn to clays and the biotite begins to break down. The color also changes as you move up section. At the bottom of the section it is yellowish brown (10YR 5/4). As you move up section, the color becomes more red. At the top the color is red (2.5YR 5/8). The soil is not plastic and is loose. It has little structure. The color is due to the feldspars breaking down to limonite/goethite (yellow) and hematite (red) clays.

dotted line is medium to coarse grained quartz vein.

Sand cake breeze fracture is 2.22 ft above the bottom of the core. The depth of the fracture is determined by subtracting 2.22 cm and the shoe length (0.25 ft) from the total depth of 7.05 ft to give a depth of 4.58 ft. Fracture is about 5mm wide

Drill and Well Log

Sheet ___ of ___

Well ID C2-4/136

Date 6-4-15

Total Depth 6.6 (ft)

Casing Diameter ( )

Casing Elevation (MSL.) ( )

Casing Height (above g.s.) ( )

UTM Location

Site Description & Sketch Map:
— core 1 at this location failed; I'm not certain of the details but I think the sediment fell out of the core as it was brought up from the borehole

Driller / (Geologist:) Jessica Denison

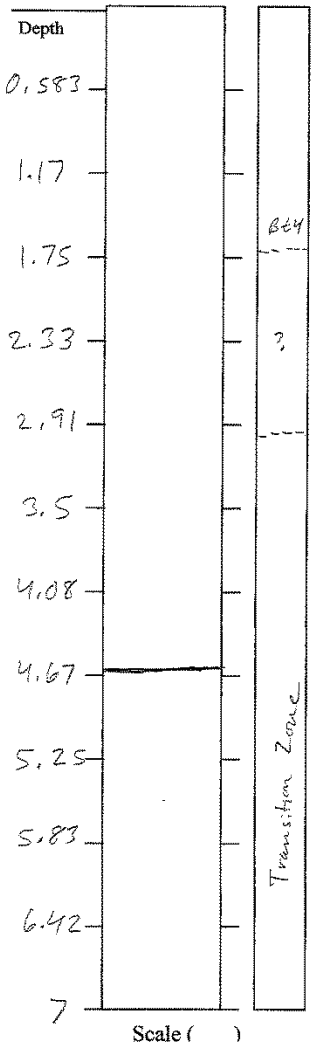

Color	Grain Size	Plasticity	Moisture	USCS / USDA	Comments

Btq is a clay loam that is red (2.5YR 4/6). It has a weak medium blocky structure. Clear to bronze colored mica flakes are common throughout. It is moderately plastic.

Sediment believed to be missing

Sand color breeze fracture is 1.75 ft above the bottom of the core. To get fracture location, 1.75ft and the shoe height is subtracted from the total depth to get a location of 4.6 ft. Fracture is 3mm to 4mm thick.

Transition zone contains weathered parent material. Quartz, feldspar, and mica are present. The feldspars are being weathered to oxide clays. Since the soil is a yellowish brown (10YR 5/6) iron oxide clays, since the feldspars are probably altering to iron oxides such as limonite and goethite. The micas appear to break down as you move up section and they have a bronze color. Manganese oxide layers are present in the section as well

Drill and Well Log

Sheet ___ of ___

Well ID C2-2/221

Date 6-4-15

Total Depth 7.0 (ft)

Casing Diameter ( )

Casing Elevation (MSL.) ( )

Casing Height (above g.s.) ( )

UTM Location

Site Description & Sketch Map:
- core compressed - only a single core available

Driller / (Geologist): Jessica Denison

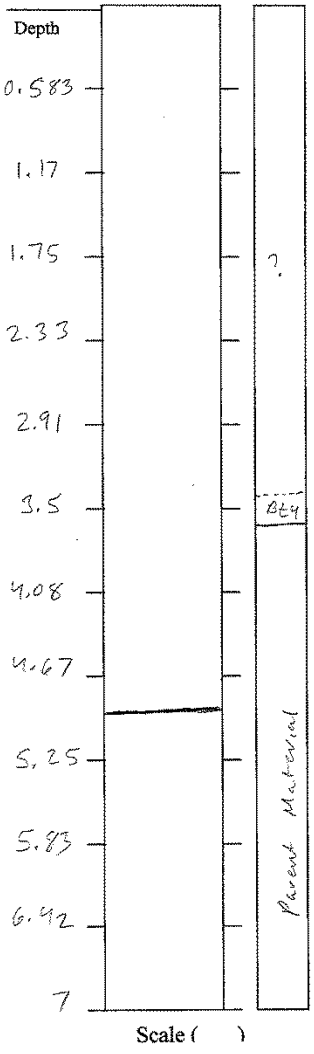

Color	Grain Size	Plasticity	Moisture	USCS / USDA	Comments

Bt4 is a red (2.5YR 4/6) clay loam. Mica flakes are common. Structure has been destroyed. No mottles present in section. It is moderately plastic.

Sand size breccia fracture is located 1.68 ft from the bottom of the core. To determine the fracture location, 1.68 ft and the shoe length are subtracted from the total depth to give a location of 5.07 ft. Fracture is 3 to 5 mm thick.

Parent material is a felsic material that contains quartz, feldspar, and biotite. No structure or layering is present in the section. Some clay material possibly kaolinite is present. This clay most likely results from the breakdown of feldspars. The soil is very pale brown (10YR 8/4).

Drill and Well Log

Sheet ___ of ___

Well ID C2-6/221

Date 6-4-15

Total Depth 7.0 (ft)

Casing Diameter ( )

Casing Elevation (MSL.) ( )

Casing Height (above g.s.) ( )

UTM Location

Site Description & Sketch Map:

Driller / (Geologist): Jessica Denison

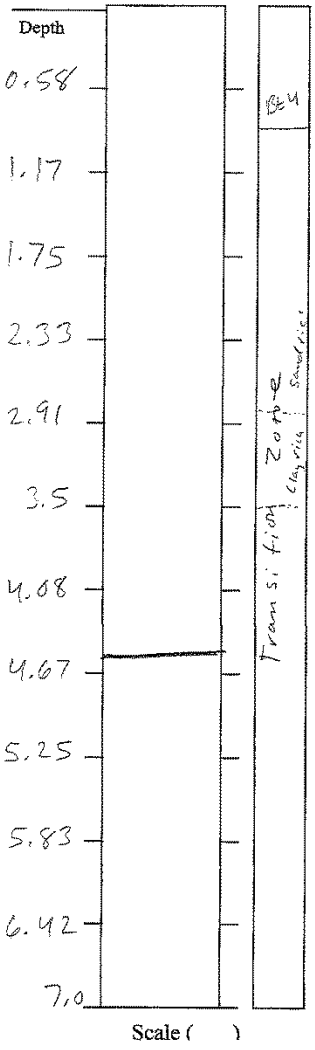

Color	Grain Size	Plasticity	Moisture	USCS / USDA	Comments

Btq is a clay loam that is red (2.5 YR 4/6). It has a weak, blocky structure and is plastic. Mica flakes are common. A few nodules are present that are reddish yellow (7.5 YR 6/8).

Transition zone contains weathered parent material. Quartz, feldspars and micas are present. The feldspars are highly weathered to iron oxide clays. The micas are also weathered and are often a bronze color. The color of the section becomes more reddish as you move up section. At the bottom, the color is brown (7.5YR 4/4). It then transitions to reddish yellow (5YR 6/8 or 7.5YR 6/6 further up section). The clay rich zone is yellowish red (5YR 5/8). The sand rich zone is light red (10R 6/4). Clay like kaolinite also appears to be present through the section.

Sand coke breeze fracture is 2.17 ft above the bottom of the core. The location is determined by subtracting 2.17ft and the shoe height from the total depth to get Location of 4.58 ft. Fracture is about 10mm wide

Drill and Well Log

Sheet ___ of ___

Well ID C2-10/221

Date 6-4-15

Total Depth 6.95 (ft)

Casing Diameter ( )

Casing Elevation (MSL.) ( )

Casing Height (above g.s.) ( )

UTM Location

Site Description & Sketch Map:

Driller / (Geologist): Jessica Denison

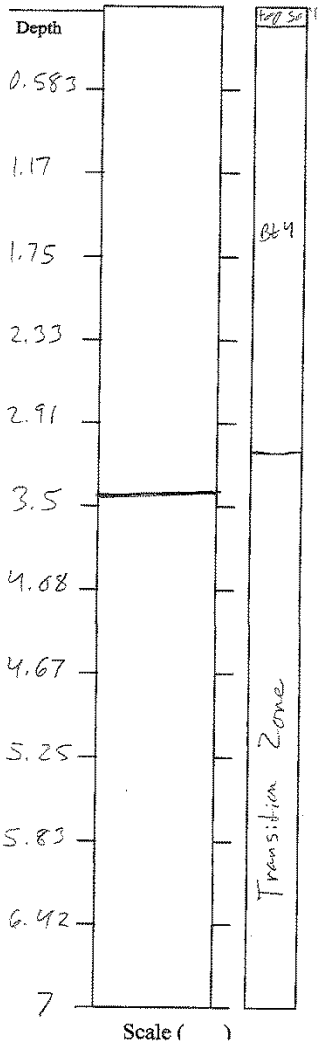

Color	Grain Size	Plasticity	Moisture	USCS / USDA	Comments

Very fine grained material present with some feldspar grains. Mica flakes are common. It is a reddish yellow (7.5YR 6/6)

Bt4 is a red (2.5YR 4/6) clay loam with mica flakes common throughout. It has a weak medium subangular blocky structure. It is moderately plastic. Mottles that are reddish yellow (7.5YR 6/8) are present.

The sand color breccia fracture is 3.25 ft above the bottom of the core. The location is determined by subtracting 3.25 and the shoe height from the total depth. This gives a location of 3.45 ft. Fracture thickness could not be determined because the sediment was so jumbled up. Fracture location is approximate due to this.

Transition Zone contains weathered parent material. Quartz, feldspar, and micas are present. At the bottom of the section, the material is very weathered and most of the feldspars have been weathered to iron oxide clays. This area is brown (7.5YR 4/4). Moving up section, a mica rich area is encountered. This area is mainly composed of clear to bronze colored micas and the iron oxide clays they are breaking down to. Above this is an area with relatively unweathered quartz, feldspar, and small white flakes are present. This section is a light reddish brown (5YR 6/4), coarse grained material to clay sized particles are present in this area.

Drill and Well Log

Sheet ___ of ___

Well ID C2-4/331

Date 6-4-15

Total Depth 6.6 (ft)

Casing Diameter ( )

Casing Elevation (MSL.) ( )

Casing Height (above g.s.) ( )

UTM Location

Site Description & Sketch Map:
- Fracture was not present in this core

Driller / (Geologist): Jessica Denison

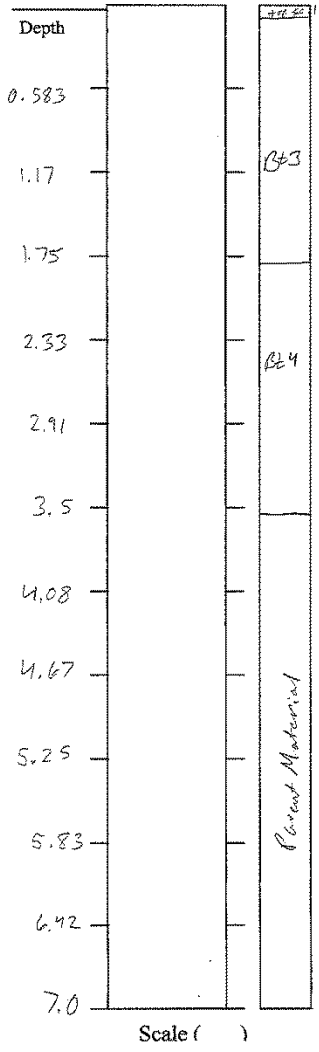

Color	Grain Size	Plasticity	Moisture	USCS / USDA	Comments

It is a brown color (10YR 4/3). It is very fine grained material.

Bt3 is a red (2.5 YR 4/6) clay. It has a moderate medium subangular blocky structure. It is firm and moderately plastic. Mica flakes are common

Bt4 is a clay loam that is red (2.5YR 4/6). It has a weak blocky structure. Mica flakes are common. Some mottles that are a reddish yellow (7.5 YR 6/8) are present

Parent material is a felsic rock such as a granite or a gneiss. Quartz, feldspar, and biotite are present. Some clays are present - possibly Kaolinite. The soil is white (10 YR 8/1). Two small sections are present where it appears that the feldspars and/or biotite are being weathered to iron oxide clays. The reddish color of the soil indicates this process is taking place. At the bottom of the section, manganese oxides are present.

Drill and Well Log

Sheet ___ of ___

Well ID C3A-4/0

Date 6-8-15 fracture description

Total Depth 7.0 (~~ft~~)

Casing Diameter ( )

Casing Elevation (MSL.) ( )

Casing Height (above g.s.) ( )

UTM Location

Site Description & Sketch Map:

described 7-12-17

Driller / (Geologist): Jessica Davison

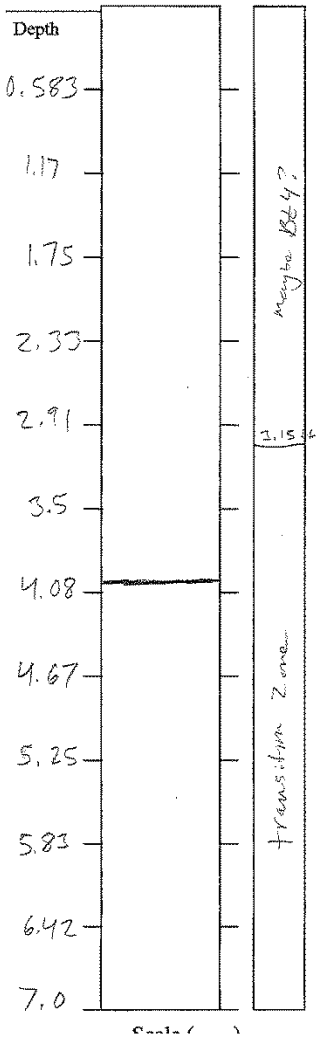

Well Construction	Lith.	Color	Grain Size	Plasticity	Moisture	USCS / USDA	Comments

color 5YR 5/8 yellowish red; micas primarily present along with red clay minerals; section contains some black layers that maybe manganese oxide; Soil loose but weak blocky structure; some layers near the bottom are 7.5YR 7/8 reddish yellow

Pure coke breeze fracture is 2.78 ft above the bottom of the core. This value and the shoe length are subtracted from the total depth to give a location of 2.97 ft below surface of earth. The fracture is about 15 mm thick.

color 7.5 YR 5/6 strong brown; in this zone, there are areas where micas are predominant along with yellowish clays and some quartz; there are some layers that are degraded parent material; degraded parent material contains feldspars, quartz, and micas; little structure except the few layers of degraded parent material

Drill and Well Log

Sheet ___ of ___

Well ID C3A - 4/90
Date 6-8-15
Total Depth 7.2 (ft)
Casing Diameter ( )
Casing Elevation (MSL.) ( )
Casing Height (above g.s.) ( )

UTM Location
Site Description & Sketch Map: description 7-10-17

Driller / (Geologist): Jessica Denison

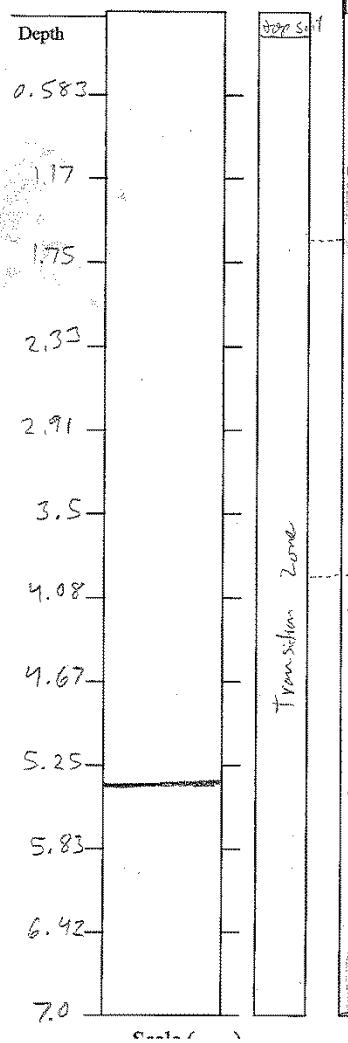

Color	Grain Size	Plasticity	Moisture	USCS / USDA	Comments

top soil - 7.5YR 5/4 strong brown - loose structure

Transition zone - color and structure changes as more clasts of grains of quartz, feldspar, and mica present; little to weak structure; color 5 YR 5/8 yellowish red; decrease in clay content; easily friable quartz + feldspar have red coating on them; a few mottles (color 7.5 YR 7/8 reddish yellow) present;

color 5 YR 5/8 yellowish red

yellow mottles are present; blocky structure is present; higher clay content than below; high mica content
mottles color is 7.5YR 6/8 reddish yellow

Transition zone - color 5 YR 6/8 reddish yellow
mica flakes biotite + muscovite present; material is sandy; grains too fine to distinguish other minerals

Rare core breaks fracture is 1,51 ft above the bottom of the core. This value and the shoe length are subtracted from the total depth to give a location of 5,44 ft. The fracture is 3 to 6 mm thick. Fracture is dipping at an angle of about 14°.

Drill and Well Log

Sheet ___ of ___

Well ID C3A-2/180
Date 6-9-15
Total Depth 7.05 (ft)
Casing Diameter ( )
Casing Elevation (MSL.) ( )
Casing Height (above g.s.) ( )

UTM Location
Site Description & Sketch Map:

described 7/24/17
Driller / (Geologist): Jessica Denison

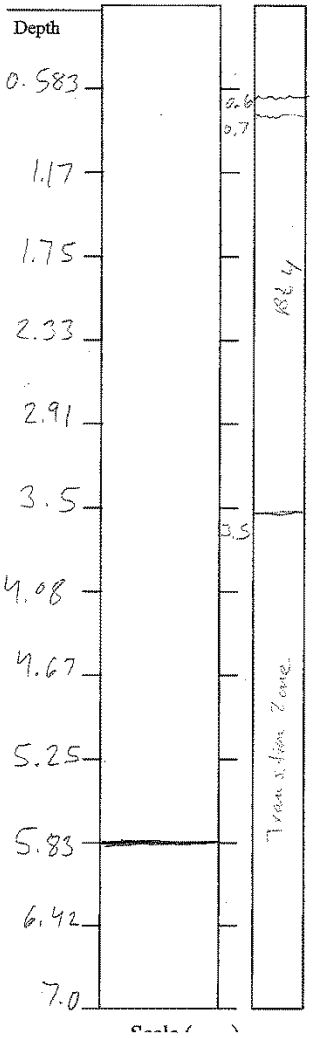

Color	Grain Size	Plasticity	Moisture	USCS / USDA	Comments

Color 10R 5/8 red; quartz and micas present and reddish clays; quartz and micas have reddish tinge on them - micas probably weathering to iron oxide clays; slight blocky structure; no visible mottles

Bt4 is silty clay loam or clay loam - felt slightly gritty

Quartz vein present from 0.6 ft to 0.7 ft; quartz peices are gravel sized and therefore easily seen without a hand lens; grains have reddish coating and mica grains attached to them

color at bottom of core is 5YR 5/6 yellowish red; color at top of zone is 5YR 4/6 yellowish red; quartz, feldspar and micas present; feldspars look like they are weathering to micas and micas have reddish tinge like they are weathering to iron oxides; no structure; possibly a loam; some layers of manganese oxide

The coke breeze fracture is 0.97 ft above the bottom of the core. This value and the shoe length are subtracted from the total depth to give a location of 5.83 ft. The fracture is 4 to 10 mm thick. It is dipping at an angle of about 14°.

Drill and Well Log

Sheet ___ of ___

Well ID C3A-4/180

Date 6-9-15

Total Depth 7.1 (ft)

Casing Diameter ( )

Casing Elevation (MSL.) ( )

Casing Height (above g.s.) ( )

UTM Location

Site Description & Sketch Map:

described 7-24/17

Driller / (Geologist) Jessica Denison

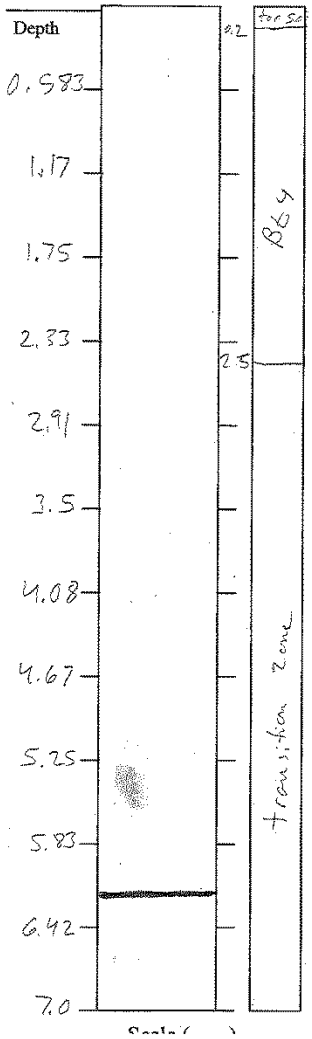

Well Construction	Lith.	Color	Grain Size	Plasticity	Moisture	USCS / USDA	Comments

- Bt4 - color 10R 4/8 red; predominately micas and red clays; maybe some small feldspars present; micas might be weathering to iron oxide clays; slight blocky structure

  it is a silty clay loam or clay loam - it was slightly gritty

- top soil - loose; color 10YR 4/6 dark yellowish brown

- color is at the bottom of the zone is 5YR 5/6 yellowish red; in the middle of the zone the color is 2.5YR 5/8 red; at the top of the zone 5YR 5/6 yellowish red; quartz and micas present; some small weathered feldspars present; all minerals have reddish tinge on them - may indicate that minerals are weathering to iron oxide clays; no structure at the bottom or top of the zone; middle of zone has weak blocky structure;

  loam to silt loam

The pave color breeze fracture is 0.61 ft above the bottom of the core. This value and the shoe length are subtracted from the total depth to give a location of 6.24 ft. The fracture is 3 to 4 mm thick.

Drill and Well Log

Sheet ___ of ___

Well ID C3A-6/180
Date 6-9-15
Total Depth 6.95 (ft)
Casing Diameter ( )
Casing Elevation (MSL.) ( )
Casing Height (above g.s.) ( )

UTM Location
Site Description & Sketch Map:
- No evidence of fracture in core

described 7-24-17
Driller / (Geologist): Jessica Denison

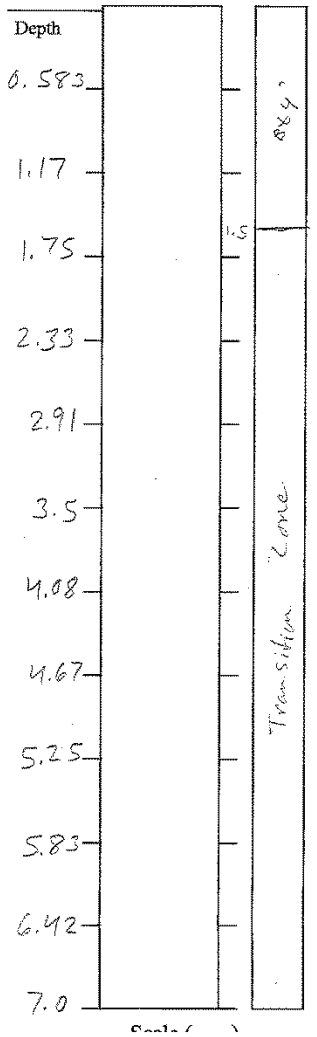

Color	Grain Size	Plasticity	Moisture	USCS / USDA	Comments

color 2.5 YR 5/8 red
sandy clay loam
mainly micas present; micas appear to be weathering to reddish iron oxide clays
weak blocky structure
possibly some mottles but too small to distinguish color

upper part of transition zone is 5YR 5/8 yellowish red; micas are larger and can be seen without hand lens

possibly is loam or silt loam

color is 7.5YR 5/6 strong brown; Slight blocky structure near the bottom of the core; no structure near the boundary; Quartz present; majority micas with red orange tinge; there are some small feldspars that are degrading; the reddish orange tinge of the micas indicates that they may be altering to iron oxides; grains are tiny and can only be seen with a hand lens

Drill and Well Log

Sheet ___ of ___

Well ID C3A-10/180
Date 6-9-15
Total Depth 7.4 (ft)
Casing Diameter ( )
Casing Elevation (MSL.) ( )
Casing Height (above g.s.) ( )

UTM Location
Site Description & Sketch Map: - No evidence of fracture in cores described 7-25-17
Driller / (Geologist): Jessica Denison

Well Construction	Lith.	Color	Grain Size	Plasticity	Moisture	USCS / USDA	Comments

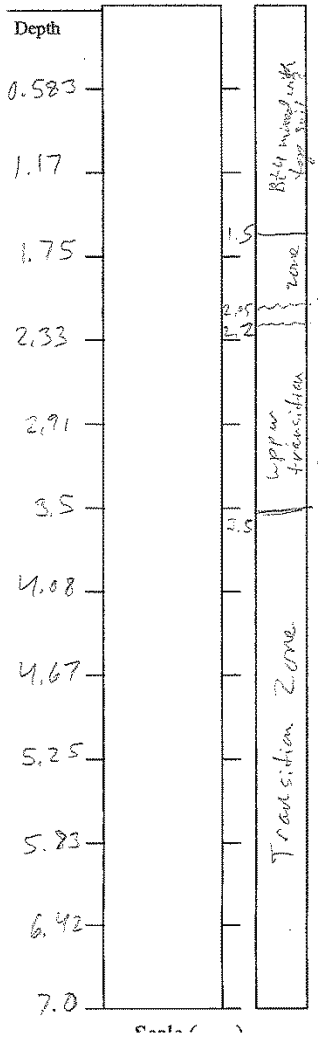

Color 2.5YR 4/4 red, mostly micas present with some weathered feldspars; all minerals have reddish tinge like weathering to iron oxide clays; slight blocky texture; very firm soil
Not possible to complete USDA soil chart - too many pieces >2mm present

Quartz vein - gravel to sand sized quartz veins; vein dip at angle of ~ 39°
Color 5YR 5/6 yellowish red; mostly quartz and micas with some degraded feldspars; all minerals have a reddish tinge - maybe weathering to iron oxide clays; slight blocky structure;

loam to silt loam

Color 7.5YR 5/4 brown; Quartz, feldspars, and micas present; fine material mostly looks like broken down minerals that haven't started weathering to clays yet or very minimally weathered to clays; could be some magnesium oxide present; no structure present; Soil very loose;

felt sandy - Sandy loam or loam

Drill and Well Log

Sheet ___ of ___

Well ID C3A-4/270 | UTM Location

Date 6-9-15 | Site Description & Sketch Map:

Total Depth 7.1 (~~ft~~)

Casing Diameter ( )

Casing Elevation (MSL.) ( )

Casing Height (above g.s.) ( )

described 7-12-17

Driller / (Geologist): Jessica Dawson

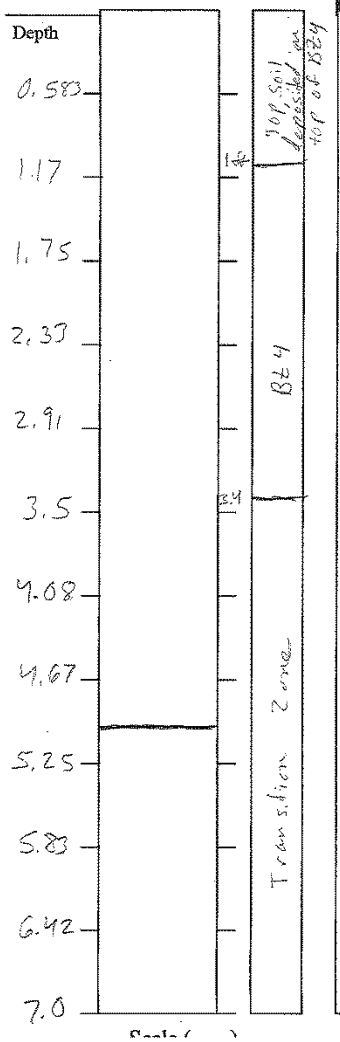

Color	Grain Size	Plasticity	Moisture	USCS / USDA	Comments

color 5YR 5/8 yellowish red; mica flakers common with red clays; alternating layers of loose soil and what appears to be thin layers of schist; this layering comprises the structure

color 2.5 YR 5/8 red; mostly micas and red clays present with a small percentage of quartz; weak blocky structure; very small number of mottles; mottles are 7.5 YR 7/8 reddish yellow

rare cobble breccia fracture is located 1.8 ft above the bottom of the core. This value and the shoe length are subtracted from the total depth to give a location of 5.05 ft. The fracture is 9 to 10 mm thick

Transition Zone - color at the bottom of the section is 7.5 YR 6/6 reddish yellow; the color changes as you move up section to 5 YR 5/8 yellowish red; quartz, weathered feldspars, biotite and muscovite present in bottom of section; in top of section mostly micas present with little quartz or feldspars; has been weathered to clays; loose soil with little structure

Drill and Well Log

Sheet ___ of ___

Well ID C4-4/70

Date 5-3-15

Total Depth 7.3 (ft)

Casing Diameter ( )

Casing Elevation (MSL.) ( )

Casing Height (above g.s.) ( )

UTM Location

Site Description & Sketch Map:

Driller / (Geologist): Jessica Denison

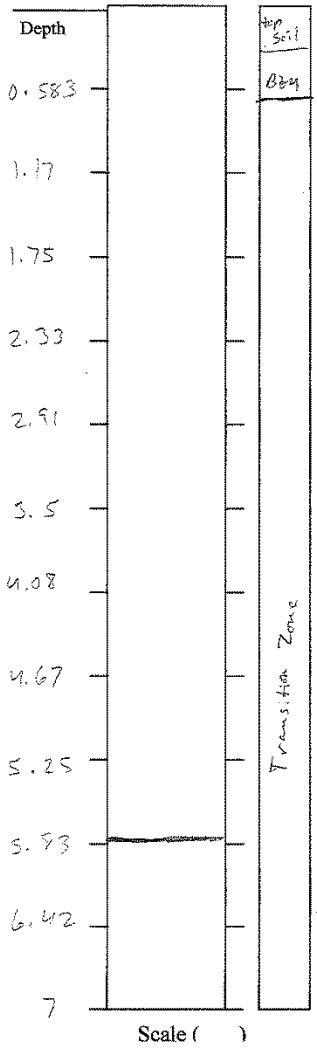

Color	Grain Size	Plasticity	Moisture	USCS / USDA	Comments

Material probably left over from drilling the previous hole

Bay is a clay loam that is red 2.5 YR 4/6. Mica flakes are common, Blocky structure. Some larger grains of quartz + feldspar present

Transition zone contains quartz, feldspars, and biotite. The color changes as you move up section, at the bottom of the section, the color is more of a yellowish brown (10 YR 5/6) to a more reddish yellow (7.5 YR 6/8). Mica flakes are common throughout. The color change is probably due to the breakdown of feldspars to iron oxides. At the bottom of the section, remnants of goethite is formed, at the top, an iron oxide such as hematite is formed.

100% Coke breeze fracture is 1.25 ft from the bottom of the core. Total depth was measured to be 7.3. Fracture Location is Total depth minus the shoe height and distance of fracture is from the bottom of the core. This equals 5.8 ft. Fracture thickness ranges from 1 mm to 11 mm

Drill and Well Log

Sheet ___ of ___

Well ID C4-4/160

Date 6-3-15

Total Depth 7.1 (ft)

Casing Diameter ( )

Casing Elevation (MSL.) ( )

Casing Height (above g.s.) ( )

UTM Location

Site Description & Sketch Map:

Driller / (Geologist): Jessica Denison

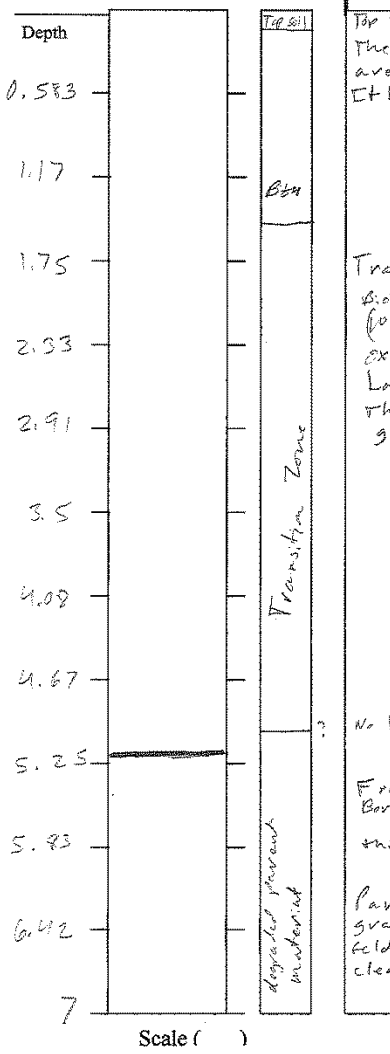

Color	Grain Size	Plasticity	Moisture	USCS / USDA	Comments

Top soil is sandy material that is red (10R 4/6). It is loose material with no structure.

The soil is a clay loam that is red (2.5YR 4/6). Mica flakes are common. Some reddish yellow mottles (7.5 YR 6/8) present. It has a blocky structure. It is also moderately sticky

Transition zone contains quartz, feldspar, and biotite. Biotite is very common. The soil is light yellowish brown (10YR 6/4). The feldspars appear to be degrading to iron oxides such as limonite and goethite and possibly hematite. Large grains of feldspars are present in some areas. These large grains are easily broken apart to smaller grains

No breaks?

Fracture is 1.625ft above the bottom of the core. Borehole total depth is 7.1ft. To determine fracture location 7.1ft − 1.625ft − 0.25ft = 5.225ft. Fracture is 8mm thick.

Parent material appears to be a felsic rock such as a granite. Feldspars, quartz, and biotite are present. The feldspars are starting to become degraded but are still clearly visible when soil is viewed with hand lens.

Drill and Well Log

Sheet ___ of ___

Well ID C4-2/250

Date 6-4-15

Total Depth 7.2 (ft)

Casing Diameter ( )

Casing Elevation (MSL.) ( )

Casing Height (above g.s.) ( )

UTM Location

Site Description & Sketch Map:

Driller / (Geologist): Jessica Denison

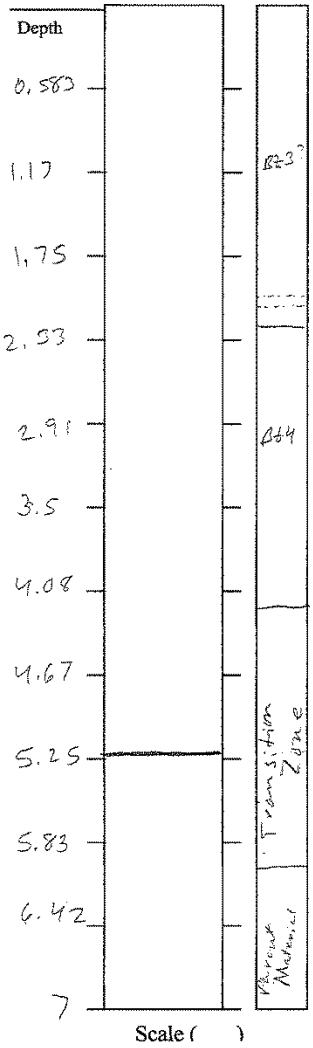

Color	Grain Size	Plasticity	Moisture	USCS / USDA	Comments

It is a clay that is red (2.5YR 4/6) with reddish yellow (2.5YR 6/6) mottles. It has a blocky structure. Mica flakes are common.

layer of larger grains of feldspar (medium to fine grained)

Bt4 is a clay loam that is red (2.5YR 4/6) in color. It has a blocky structure with reddish yellow (7.5YR 6/8) mottles. Mica flakes are common.

Transition zone contains altered parent material. Quartz, feldspar, and micas are present. Micas appear to have a bronze color. There are sections with large feldspars and granite and it is mostly micas and reddish clumps probably weathered from the feldspars. It is light red (2.5YR 6/6)

100% Coke breeze fracture is 1.71 ft above the bottom of the core. Total depth was measured to be 7.2 ft. Fracture location was determined by subtracting 1.71 ft and the shoe height (0.25 ft) from the total depth to give 5.24 ft. There appears to be 2 different fractures. Each one is about 6mm thick and are separated by about 4mm of soil

Parent material is a felsic material containing quartz, feldspar and biotite. Some veins containing larger feldspar grains are present. Feldspars have yellow orange tone on them indicating that they are being altered to iron oxides such as goethite and limonite.

Drill and Well Log

Sheet ___ of ___

Well ID C4-6/250

Date 6-4-15

Total Depth 7.3 (ft)

Casing Diameter ( )

Casing Elevation (MSL.) ( )

Casing Height (above g.s.) ( )

UTM Location

Site Description & Sketch Map:

Driller / Geologist:

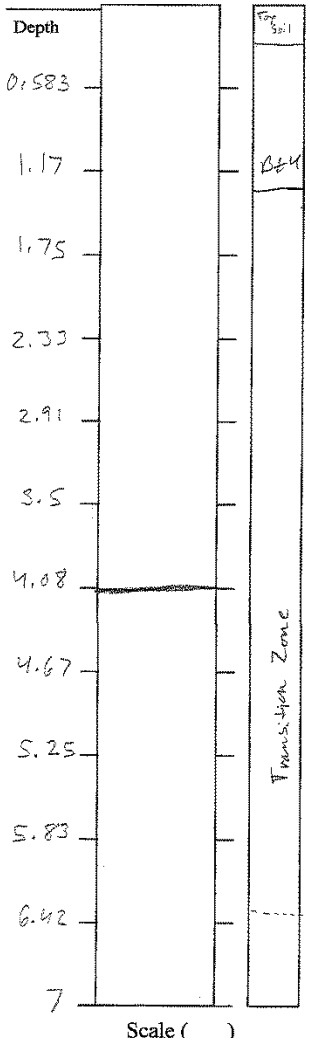

Color	Grain Size	Plasticity	Moisture	USCS / USDA	Comments

Manganese oxide present. It is strong brown (7.5YR 4/3). It can easily be crumbled between your fingers

It is a clay loam that is red (2.5YR 4/6). It has some reddish yellow (7.5 YR 6/8) mottles and a blocky structure. Mica flakes are common.

Transition zone contains felsic parent material that is weathering. Quartz, feldspar, biotite, and muscovite are present. Section at first is dark in color. At the bottom, it is a dark color due to the manganese oxide present. It then alters to a reddish color and then to a yellowish brown color. It then alternates between the dark color, reddish color, and yellowish brown color as it moves up section. In the reddish section, the feldspars seem to be breaking down to iron oxides like hematite. In the yellowish brown sections, the feldspars seem to be breaking down to iron oxides such as limonite and goethite. Biotites seem to be breaking down as you move up section.

100% coke breeze fracture is 2.95ft above the bottom of the core. Fracture location was determined by subtracting 2.95ft and the shoe height (0.25ft) from the total depth to give a location of 4.09 feet. Fracture thickness ranges from 5mm to 10mm. The thinner area appears to be going over a mottle in the soil. Fracture is dipping at an angle of about 40°.

even with a lot of manganese oxide present

Drill and Well Log

Sheet ___ of ___

Well ID C4-10/250

Date 6-4-15

Total Depth 7.4 (ft)

Casing Diameter ( )

Casing Elevation (MSL.) ( )

Casing Height (above g.s.) ( )

UTM Location

Site Description & Sketch Map:

Driller / (Geologist): Jessica Denison

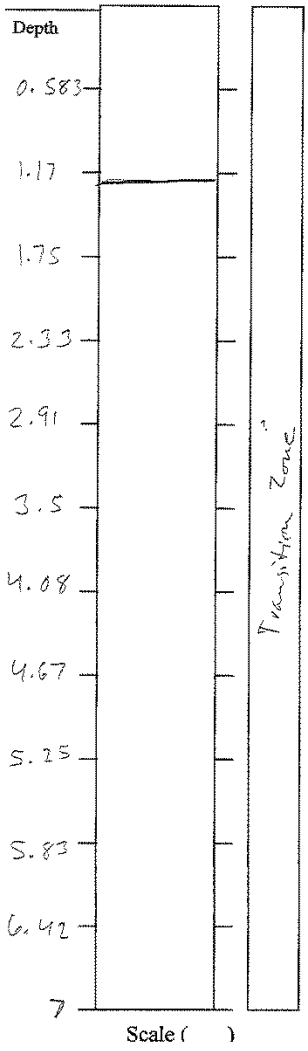

Color	Grain Size	Plasticity	Moisture	USCS / USDA	Comments

100% core breeze fracture was measured to be 1.21 ft below ground surface. Fracture is in the first core and was so thin, it is not visible without cutting open the core. Fracture is 1.5 to 2 mm thick.

Transition zone contains quartz, feldspar, and biotite. Another mica that is more bronze in color is also present. This could either be muscovite or phlogopite. As you go up section, the soil alternates between clay rich areas and very silty areas. Due to this characteristic, the whole section was characterized as a transition zone. Manganese oxide layers are fairly common throughout. Mica flakes are also common throughout, the soil is red (10R 5/8). Kaolinite is also present in some sections.

Drill and Well Log

Sheet ___ of ___

Well ID C4-8/259

Date 6-4-15

Total Depth 7.22 (ft)

Casing Diameter ( )

Casing Elevation (MSL.) ( )

Casing Height (above g.s.) ( )

UTM Location

Site Description & Sketch Map:

- The 2nd core was collected but was not kept.
- It is known that the unlabeled core is not the 2nd core of this location because the fracture was present in the unlabeled core. The fracture would not be in core 2 at this location.

Driller / Geologist: Jessica Denison See C4-9/259

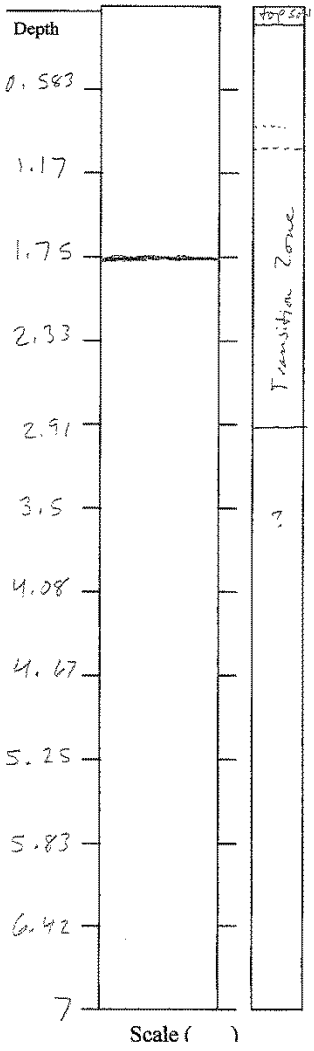

Color	Grain Size	Plasticity	Moisture	USCS / USDA	Comments

felsic material that contains light colored micas. Large amount of clay material such as kaolinite present. Possibly due to material left in shute from other test hole

Transition zone is composed of weathered parent material. Quartz, feldspar, and micas (biotite) are present. As you move up section, the amount of clays increases and the amount of feldspars decreases. The feldspars are most likely degrading to clays. As you move up section, the micas become a more bronze color. It is possible that the biotite is altering to phlogopite. The color changes from a brownish yellow (10YR 6/4) to red (2.5YR 5/8). The soil is not plastic. Mica flakes present throughout, dotted lines are prominent manganese oxide layers.

100% core between fracture was measured to be 1.79 ft from the top of the core or below ground surface. Fracture is thin and not possible to see without cutting open the core. Fracture is 2mm to 5mm thick and is dipping at an angle of about 30°.

Drill and Well Log

Sheet ___ of ___

Well ID C4-9/25a ?

Date 6-4-15

Total Depth 2.75 (ft)

Casing Diameter ( )

Casing Elevation (MSL.) ( )

Casing Height (above g.s.) ( )

UTM Location

Site Description & Sketch Map:
- This core was unlabeled. However it is assumed to be C4-9/25a since the fracture is present in the core and there was not a core with this label.
- Location of BGS was approximated based on location of top of sediment

Driller / (Geologist): Jessica Denison

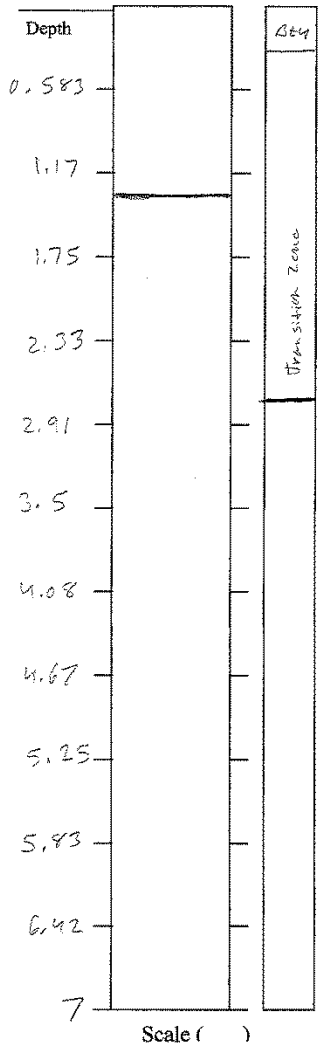

Color	Grain Size	Plasticity	Moisture	USCS / USDA	Comments

BGS is a clay loam that is red (2.5 YR 5/6). Mica flakes are common. It is moderately plastic, and has a blocky structure. Some reddish yellow mottles (7.5 YR 6/8) present.

Based on the approximated line of BGS, the fracture is 1.4 ft below the surface. The fracture is about 3 mm thick.

The total length of the soil core including the shoe height is 3.36 ft base on measuring the core.

bottom of borehole

Transition zone contains weathered parent material. Quartz, feldspar, and micas are present. At the bottom of the section, feldspars are small and rare and appear to have mostly broken down into clays. Such as hematite. A large part of the section is made up of parent material that has only been degraded a minimal amount. This section contains very fine clay particles to coarse grained material. One very coarse grained granite grain is present. Some clays are present where the feldspars have degraded. A clay rich section is present in the section as well. This soil is not very plastic. The more weathered section are red (10R 5/8) while the coarse grained material is reddish yellow (5YR 7/6).

Drill and Well Log

Sheet ___ of ___

Well ID C4-10/259

Date 6-4-15

Total Depth 2.2 (ft)

Casing Diameter ( )

Casing Elevation (MSL.) ( )

Casing Height (above g.s.) ( )

UTM Location

Site Description & Sketch Map:
- only a single core was taken from this site
- total core length is 3.37 ft

Driller / (Geologist): Jessica Denison

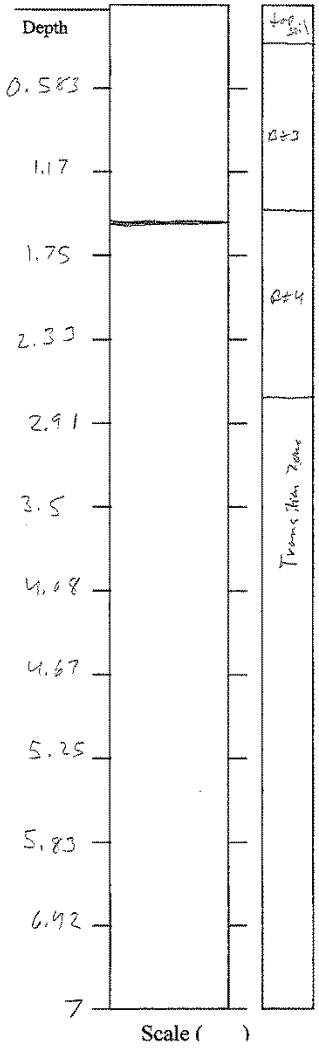

Color	Grain Size	Plasticity	Moisture	USCS / USDA	Comments

loose material in liner, gravelly material with 1 or 2 clay layers present. Material is generally mottled with some bronze micas present. It is strong brown (7.5 YR 5/6). It is not plastic

B+3 is a red color (2.5 YR 4/6) with reddish yellow (7.5 YR 6/6) mottles. Mica flakes are common throughout. It is a clay with a medium sub angular blocky structure. It is moderately plastic.

100% coke breeze fracture is 1.5 ft below ground surface. Fracture is 6mm thick.
Based on direct measurement of the core, the total length is 3.58 ft

B+4 is a clay loam that is red (2.5 YR 4/6) with reddish yellow (7.5 YR 6/6) mottles. It has a weak medium blocky structure. Mica flakes are common. It is moderately plastic

Transition zone contains the broken down parent material. Quartz, feldspars, and micas are present, a lot of red clay material is also present. This red clay material is probably due to the breakdown of feldspars to iron oxides like hematite. Material is not very plastic. Micas are often a bronze color which means they could be muscovite or phlogopite. Soil is red (2.5 YR 5/6).

Drill and Well Log

Sheet ___ of ___

Well ID CH-4/340

Date 6-4-15

Total Depth 7.4 (ft)

Casing Diameter ( )

Casing Elevation (MSL.) ( )

Casing Height (above g.s.) ( )

UTM Location

Site Description & Sketch Map:

Driller / Geologist: Jessica Denison

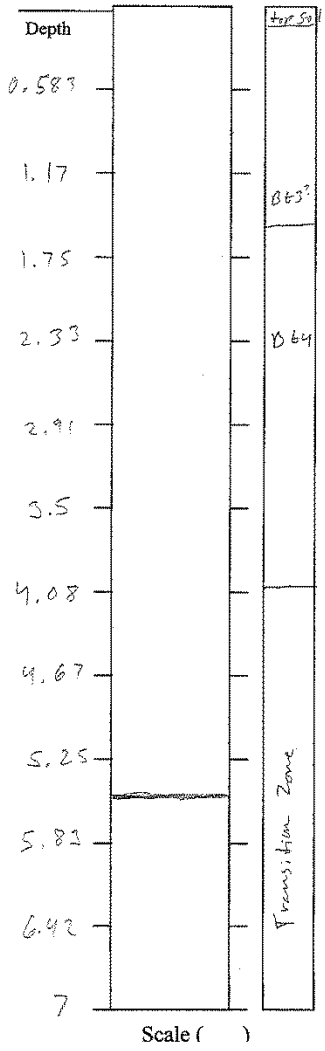

Color	Grain Size	Plasticity	Moisture	USCS / USDA	Comments

Similar to parent material. Quartz, feldspar, biotite common.

Bt3 is clay that is red (2.5YR 4/6) with reddish yellow (7.5YR 6/8) mottles. It has a blocky structure and mica flakes are common.

Bt4 is clay loam that is red (2.5YR 4/6) with reddish yellow mottles (7.5YR 6/8). It has a blocky structure and mica flakes are common.

Soil is degraded parent material. Quartz, feldspar, and biotite are present. Areas of high clay content (such as kaolinite) are present at random intervals throughout the section. The feldspars seem to be weathering out to iron oxides such as limonite, goethite, and hematite. The color of the section varies based on the predominant iron oxide present. Mica flakes are present throughout.

100% core breeze fracture is 1.62 ft above the bottom of the core. Total depth was measured to be 7.46 ft. Fracture location is the total depth minus the shoe height and distance fracture is from the bottom of the core, this equals 5.53 ft. Fracture thickness ranges from 2 mm to 10 mm where it was smeared against the sides of the tube.

Drill and Well Log

Sheet ___ of ___

Well ID F5-4/0

Date 6-5-15

Total Depth 7.42 (ft)

Casing Diameter ( )

Casing Elevation (MSL.) ( )

Casing Height (above g.s.) ( )

UTM Location

Site Description & Sketch Map:

Driller / (Geologist): Jessica Denison

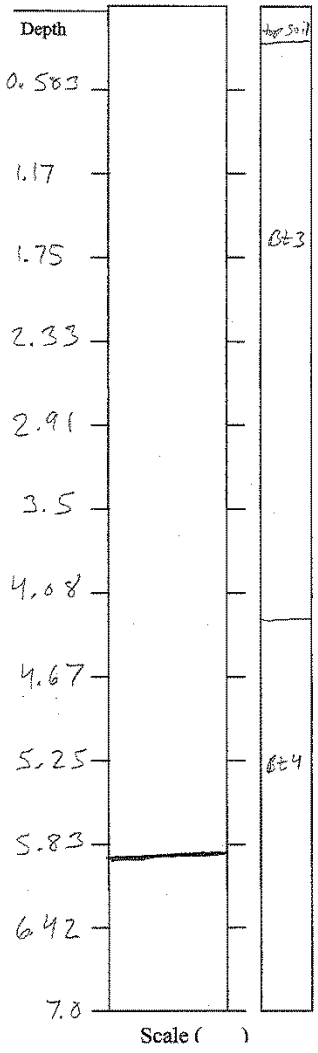

Color	Grain Size	Plasticity	Moisture	USCS / USDA	Comments

Soil is strong brown (7.5 YR 5/6). It has a lot of black grains in it that are probably manganese oxide. Bronze colored micas and iron oxide clays are also common

Bt3 is a red (2.5 YR 4/6) clay. Micas flakes are common. It is moderately plastic and has a moderate medium subangular blocky structure. It is firm. Small reddish yellow (7.5 YR 6/6) mottles are present. Lower in the section, they give the soil a striped appearance.

Bt4 is a clay loam that is red (2.5 YR 4/6). Several reddish yellow (7.5 YR 6/8) mottles are present. The mottles in this section are large and form a layered appearance with the rest of the soil. Mica flakes are common throughout. Soil has a weak blocky structure. A large manganese oxide layer is present about 1 1/2 inches above the fracture.

Fracture is 1.27 ft above the bottom of the core. To get fracture location, 1.27 ft and 0.25 for shoe length were subtracted from the total depth. This gives a location of 5.9 ft below ground surface. No Strike magnet data is available because the hole filled in before data could be collected. Fracture is about 9 mm thick.

Drill and Well Log

Sheet ___ of ___

Well ID FS-4/90
Date 6-5-15
Total Depth 7.0 (~~ft~~)
Casing Diameter ( )
Casing Elevation (MSL.) ( )
Casing Height (above g.s.) ( )

UTM Location
Site Description & Sketch Map:

Driller / (Geologist): Jessica Denison

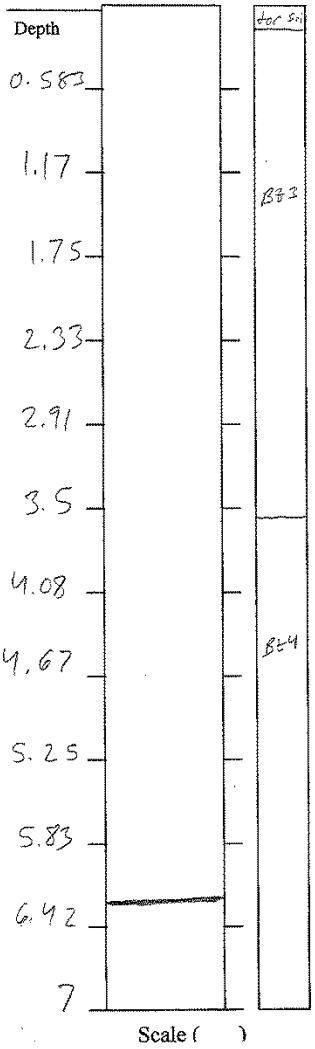

Color	Grain Size	Plasticity	Moisture	USCS / USDA	Comments

Contains more silt by. No structure. It is yellowish red (5 YR 5/6)

Bt3 is a red (2.5 YR 4/6) clay. Mica flakes are common. It is firm and has a moderate medium subangular blocky structure. Small reddish yellow (7.5 YR 6/6) mottles are present. Moderately Plastic.

Bt4 is a red (2.5 YR 4/6) clay loam. Several reddish yellow (7.5 YR 6/8) mottles are present. The mottles in this section are thick and form a layered appearance with the rest of the soil. Mica flakes are common and the soil has a weak medium subangular blocky structure. A thick section of manganese oxide is present below the fracture.

Steel shot fracture is 0.54ft above the bottom of the core. This value and the length of the shoe are subtracted from the total depth to give a fracture Location. ie 6.2 ft below ground surface. String magnet fracture depth is 6.42 ft below ground surface. The String magnet depth is added to 0.75 the curved 0.5 shoe to give another estimate of total depth of 7.2 ft.

Fracture is about 10 mm thick

Drill and Well Log

Sheet ___ of ___

Well ID FS-2/180

Date 6-5-15

Total Depth 7.2 (ft)

Casing Diameter ( )

Casing Elevation (MSL.) ( )

Casing Height (above g.s.) ( )

UTM Location

Site Description & Sketch Map:
- only one core (core 2) available
- core 1 is missing
- unknown core could possibly be core 1 for this location or the core 1 for FS-3/180

Driller / Geologist: Jessica Denison

Well Construction	Lith.	Color	Grain Size	Plasticity	Moisture	USCS / USDA	Comments

Depth

0.583

1.17

1.75

2.33

2.91

3.5

4.08

4.67

5.25

5.83

6.42

7.0

Scale ( )

Bt3

Bt4

Bt3 is a red (2.5YR 4/6) clay. Clear to bronze colored mica flakes are common throughout. It has a moderate medium subangular blocky structure. It is firm and moderately plastic. No mottles are visible in the very small (1.5in) section available for study.

Bt4 is a red (2.5YR 4/6) clay loam. It is made up of reddish iron oxides clays. Clear to bronze colored mica flakes are common throughout. It has a weak medium blocky structure. Some reddish yellow (7.5YK 6/8) mottles are present particularly further down in the section. Manganese oxide layers are present throughout the section.

Steel shot fracture is 1.75ft above the bottom of the core. This value and shoe height is subtracted from the total depth to give a fracture depth of 5.2 ft. The string magnet depth is 5.04 ft and is added to 0.25ft and 1.75ft to give another total depth estimate of 7.04 ft. Fracture is 15 to 20mm thick

Drill and Well Log

Sheet ___ of ___

Well ID FS-5/180

Date 6-5-15

Total Depth 7.5 (ft)

Casing Diameter ( )

Casing Elevation (MSL.) ( )

Casing Height (above g.s.) ( )

UTM Location

Site Description & Sketch Map:
- only core 2 is present. core 1 is missing.
- there is one unlabeled core that could be the core 1 for this borehole or core 1 for FS-2/180

Driller / (Geologist) Jessica Denison

Well Construction	Lith.	Color	Grain Size	Plasticity	Moisture	USCS / USDA	Comments

Depth

0.583

1.17

1.75

2.33

2.91

3.5

4.08

4.67

5.25

5.83

6.42

7.0

?

Bt4

potted line - it is known Bt4 extends this far but it is not known whether the boundary is here or somewhere further up the core

Bt4 is a red (2.5YR 4/6) clay loam. It is composed of reddish iron oxide clays. Clear to bronze micas are common throughout. It has a weak blocky structure. Some reddish yellow (7.5YR 6/8) mottles are present but they are difficult to distinguish. Moderately plastic. Manganese oxide layers are present throughout the section.

Steel shoe fracture is 1.83 ft above the bottom of the core. This value and the shoe length are subtracted from the total depth to give a fracture location of 5.42 ft. The magnet string depth is 5.38 ft. This is added to the shoe length and 1.83 ft to give another measure of the total depth = 7.46 ft. Fracture is 3 to 4 mm thick

Scale ( )

Drill and Well Log

Sheet ___ of ___

Well ID FS-10/180

Date 6-5-15

Total Depth 7.3 (FA)

Casing Diameter ( )

Casing Elevation (MSL.) ( )

Casing Height (above g.s.) ( )

UTM Location

Site Description & Sketch Map:
- Fracture not present in cores or when magnet string was put down bore hole

Driller / (Geologist): Jessica Denison

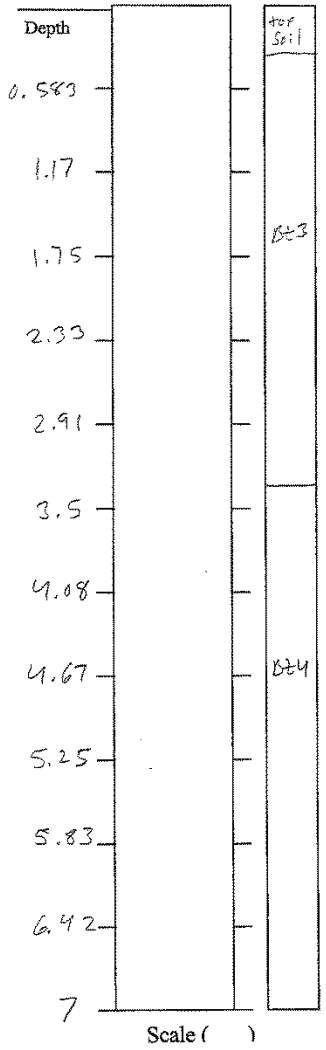

Color	Grain Size	Plasticity	Moisture	USCS / USDA	Comments

clay material possibly kaolinite is present, clear to bronze mica is also common. It is dark yellowish brown (10YR 4/4).

Bt3 is a red (2.5YR 4/6) clay. Mica flakes are common in it. Reddish yellow (7.5 YR 6/6) mottles are present. It has a moderate blocky structure. It is moderately plastic. Reddish iron oxide clays are present.

Bt4 is a red (2.5YR 4/6) clay loam. It has a weak blocky structure. Iron oxide clays are present along with clear to bronze mica. Some quartz grains are also present. Reddish yellow (7.5 YR 6/8) mottles are present. Some manganese oxide layers are present in the section. The boundary with Bt3 is approximate since the section containing the boundary was not cut open.

Drill and Well Log

Sheet ___ of ___

Well ID FS-4/270

Date 6-5-15

Total Depth 7.2 (ft)

Casing Diameter ( )

Casing Elevation (MSL.) ( )

Casing Height (above g.s.) ( )

UTM Location

Site Description & Sketch Map:

Driller / Geologist: Jessica Denison

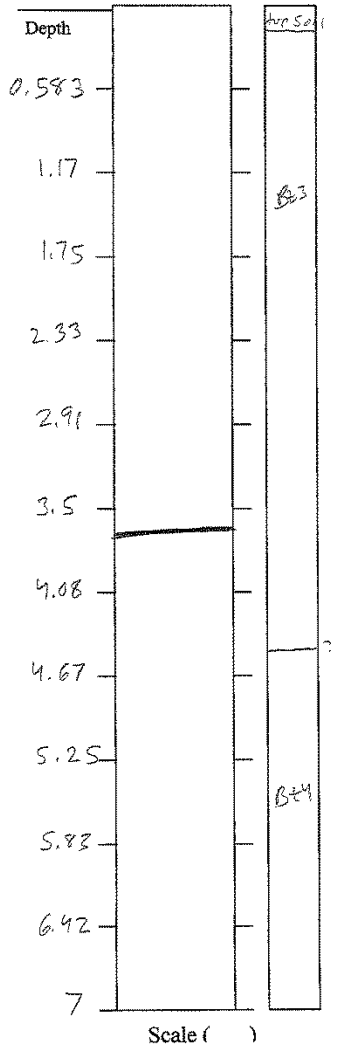

Color	Grain Size	Plasticity	Moisture	USCS / USDA	Comments

Soil is reddish brown (5YR 4/4). It has no structure and easily crumbles.

Bt3 is a red (2.5YR 4/6) clay. Some reddish yellow (7.5YR 6/6) mottles are present. It is moderately plastic and has a moderate blocky structure. Mica flakes are common. See notes on Bt4 regarding boundary. Some manganese oxide present in section.

Steel shot fracture is 3.25 ft above the bottom of the core. 3.25 ft and the shot length are subtracted from the total depth to give a fracture location of 3.7 ft below ground surface. A string magnet depth of 3.96 ft was determined. This was added to 3.25 ft and 0.25 ft to give a second total depth measurement of 7.46 ft. Fracture is 5 to 8 mm thick.

Bt4 is a red (2.5YR 4/6) clay loam. Mica flakes are common. Red iron oxide clays are present. Reddish yellow (7.5YR 6/8) mottles are present. The mottles sometimes create a layered appearance with the soil. It has a weak medium subangular blocky structure. It is moderately plastic. Some manganese oxide is present as well.

The boundary between Bt4 and Bt3 is somewhat arbitrary. There is a gradual increase in clay as you move up section resulting in an unclear boundary between the layers

Drill and Well Log

Sheet ___ of ___

Well ID FS- unknown

Date 6-25-15

Total Depth ? ( )

Casing Diameter ( )

Casing Elevation (MSL.) ( )

Casing Height (above g.s.) ( )

UTM Location

Site Description & Sketch Map:
- This core is unlabeled. It is most likely the core 1 of either FS-2/180 or FS-5/180

Driller / (Geologist): Jessica Denison

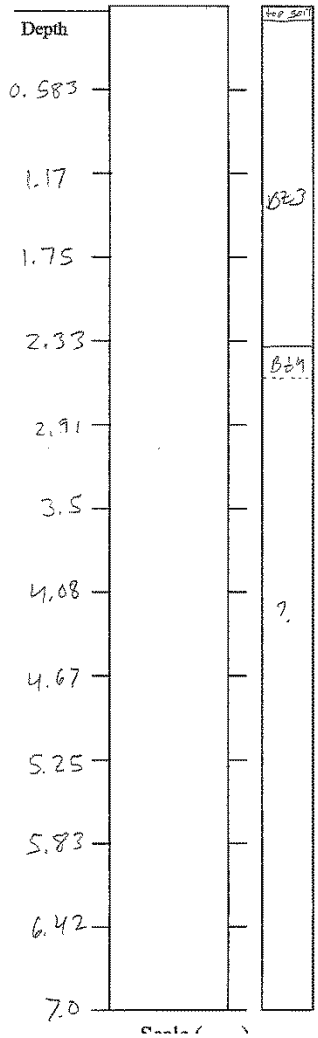

Color	Grain Size	Plasticity	Moisture	USCS / USDA	Comments

Lacks structure and easily crumbles. It is dark brown (7.5YR 3/2) and mica flakes are common.

Bt3 is a red (2.5YR 4/6) clay. Mica flakes are common. Roots are present. It is medium blocky structure. Some reddish yellow (2.5YR 6/6) mottles present. Moderately plastic

Bt4 is a red (2.5YR 4/6) clay loam. Mica flakes are common. Difficult to determine structure with such a small amount of sample - it is somewhat blocky. Moderately plastic. Some reddish yellow (7.5YR 6/8) mottles.

Drill and Well Log

Sheet ___ of ___

Well ID F6-4/98 | UTM Location _____

Date 6-2-15 (Rescribed) | Site Description & Sketch Map:

Total Depth 7.11 (ft)

Casing Diameter ( )

Casing Elevation (MSL.) ( )

Casing Height (above g.s.) ( )

Driller / (Geologist) Jessica Denison

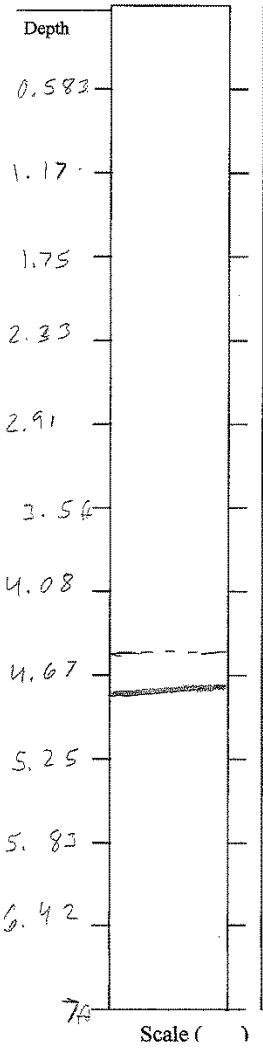

Color	Grain Size	Plasticity	Moisture	USCS / USDA	Comments

R(2.5 YR 4/6) clay loam with some medium reddish yellow (7.5 YR 6/8) mottles. It is firm. Mica flakes are common. Plant roots common in upper sections. Material similar to the Saprolite present in first 3.25 inches below ground surface of the core

contacts between units are gradational

possible manganese oxide layer

Fracture is 2.13 ft or 2 ft 1.5 in from the bottom of the core. 4.5 ft + 2.125 ft + 0.25 = 6.88 ft for total depth. Total depth measured was 7.11 ft. There is a difference of 0.23 ft or 2.82 inches. Fracture is about 8 mm thick

Saprolite or parent material appears to be felsic rock with some platy structure. Course quartz veins are present. Yellowish brown color about 10YR 5/6 but is varies throughout. Mica flakes are present throughout

Drill and Well Log

Sheet ___ of ___

Well ID F6-4/169

Date 6-3-15 (described)

Total Depth 7.2 (ft)

Casing Diameter ( )

Casing Elevation (MSL.) ( )

Casing Height (above g.s.) ( )

UTM Location

Site Description & Sketch Map:

Driller / (Geologist) Jessica Denison

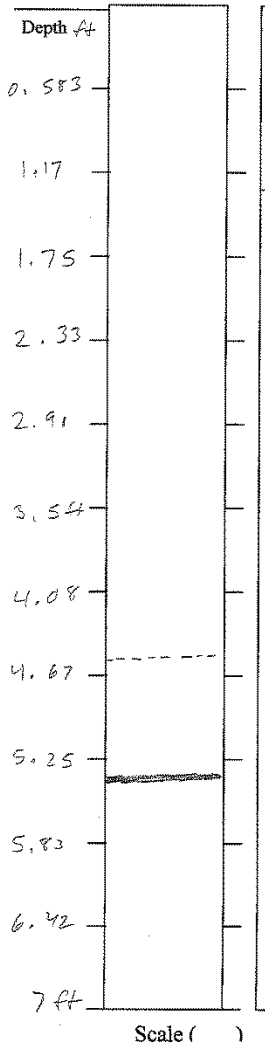

Color	Grain Size	Plasticity	Moisture	USCS / USDA	Comments

Red (2.5YR 4/6) clay loam. One possible mottle present. Mica flakes are common. Soil is firm with blocky structure.

Sharp contact between units

Saprolite is felsic rock that was been greatly broken down. Some layered structure present. Saprolite grades upward from felsic material to alternating layers of yellowish brown and red. Mica flakes are present throughout

possible manganese oxide layer

Steel shot fracture is at 5.225ft below ground surface when magnet was dropped down bore hole. In the core, the fracture is 1.625ft from the bottom. These are added together along with the shoe height (0.25 ft) to give total depth of 7.1 ft. The actual measured depth was 7.2 ft, a difference of 1.2 inches. Fracture is about 8 mm wide.

Drill and Well Log

Sheet ___ of ___

Well ID F6-4/275

Date 6-3-15 (describer)

Total Depth 7.25 (ft)

Casing Diameter ( )

Casing Elevation (MSL.) ( )

Casing Height (above g.s.) ( )

UTM Location

Site Description & Sketch Map:

Driller / (Geologist): Jessica Denison

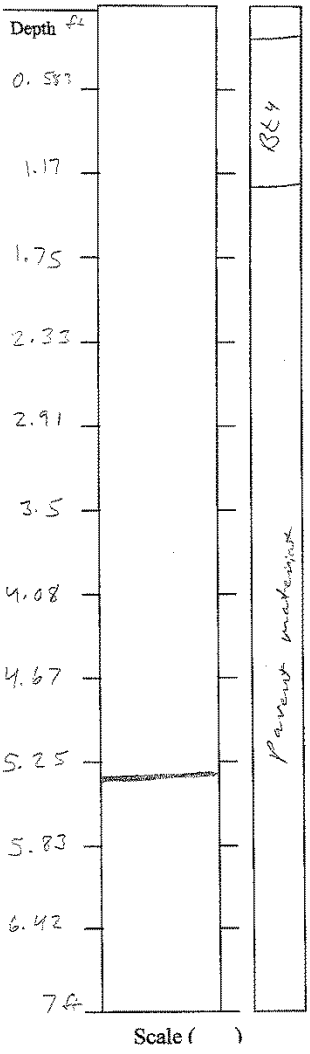

Color	Grain Size	Plasticity	Moisture	USCS / USDA	Comments

light gray (10YR 7/2) Kaolinite rich material with medium grained material in it
Sharp contact
red (2.5 YR 4/6). Mica flakes present throughout. It's a clay loam. Some reddish yellow mottles present. Blocky structure present

gradational contact between units

Saprolite is felsic rock that is highly weathered. Igneous fabric is still present along with medium to coarse grained feldspar veins. Large amounts of mica flakes are present throughout. Color is yellowish brown (10YR 5/6) but varies throughout

Steel shot fracture is at 5.104 ft when magnet was dropped down the bore hole. In the core, the fracture is 1.667 ft from the bottom of the core. These are added together along with the shoe height to give a total depth of 7.02 ft. The measured total depth is 7.25 which is a difference of 0.23 ft or 2.76 inches. The fracture thickness varies from 8mm to 10mm

Drill and Well Log

Sheet ___ of ___

Well ID F6-2/346

Date 6-3-15 (described)

Total Depth 7.5 (ft)

Casing Diameter ( )

Casing Elevation (MSL.) ( )

Casing Height (above g.s.) ( )

UTM Location

Site Description & Sketch Map:

Driller / Geologist: Jessica Denison

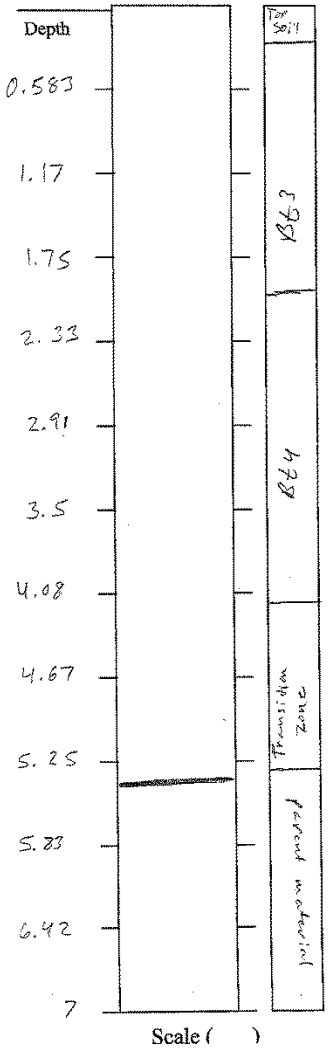

Color	Grain Size	Plasticity	Moisture	USCS / USDA	Comments

Large grains that crumple when pressure applied, are a white/gray color. Biotite appears to be present.

Clay with a red (2.5 YR 4/6) color. It is firm and blocky. Small roots present in soil. No mottles present in this core. Fine mica flakes common through out.

clay loam that is red on 2.5 YR 4/6. Mica flakes are common. Mottles of a 7.5 YR 6/8 color are present as well.

Transition between the parent material and the Bt horizon. Zone has a color of 7.5 YR 5/6 or strong brown. Biotite seem to be degrading

Fracture is 1.8125 ft from bottom of the core. The depth to the fracture with the string magnet was 4.79 ft. These numbers are added together along with the shoe height (0.25 ft) to give a total depth of the hole of 6.85 ft. The measured depth of the hole was 7.5 ft. The thickness of the fracture is 10 mm to 12 mm

Parent material appears to be felsic rock possibly granite or gneiss. Some possible faint banding is present between the felsic material and biotite micas. Quartz and large amounts of feldspars are also present. Some yellow coloring is present in spots possibly indicative of more reducing conditions. Kaolinite present in some areas.

Drill and Well Log

Sheet ___ of ___

Well ID F6-6/346

Date 6-3-15 (described)

Total Depth 7.25 (ft)

Casing Diameter ( )

Casing Elevation (MSL.) ( )

Casing Height (above g.s.) ( )

UTM Location

Site Description & Sketch Map: Core 1 failed in this hole so only core 2 was obtained

Driller / (Geologist): Jessica Denison

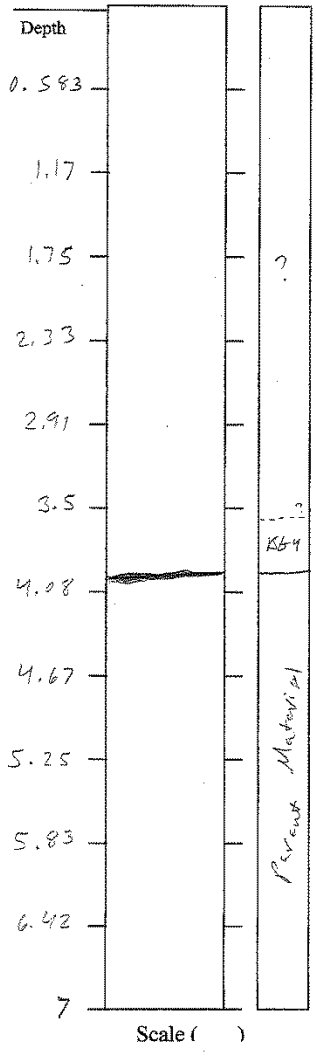

Color	Grain Size	Plasticity	Moisture	USCS / USDA	Comments

Clay loam that is red (2.5YR 4/6). Mica flakes are common in the section. Upper boundary is unknown since core 1 failed.

Fracture is located at the top of core 2 but this area is very jumbled and the structure has been destroyed. Measurement of 2.08 ft from the bottom of the core is approximate. Fracture depth using string magnet was 1.875 ft. These numbers are added together with a shoe height of 0.25 ft to give a total depth of 5.205 which is not close to the measured total depth of 7.25 ft. Thickness not available due to jumbled nature of that section of the core

Parent material appears to be felsic rock possibly a granite or gneiss. No layering is apparent. Quartz is present along with large amounts of biotite and feldspars. Feldspars have yellow orange films on them and appear to be weathering to some type of iron oxide such as goethite or limonite. Some yellow colored layers are present in some sections. This is probably where a large amount of the feldspars have weathered to iron oxides

Drill and Well Log

Sheet ___ of ___

Well ID F6-10/346

Date 6-3-15 (described)

Total Depth 7.4 (ft)

Casing Diameter ( )

Casing Elevation (MSL.) ( )

Casing Height (above g.s.) ( )

UTM Location

Site Description & Sketch Map:
No evidence of fracture in the core or with the strong magnet in the bore hole

Driller / (Geologist): Jessica Denison

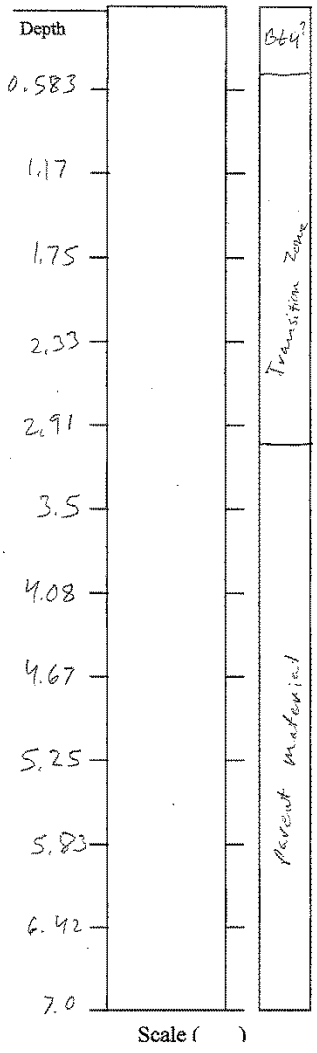

Color	Grain Size	Plasticity	Moisture	USCS / USDA	Comments

clay loam that is red (2.5 YR 4/6). Mica flakes are common. Roots are present, a manganese layer is present in this section and the soil around it is more yellowish brown.

Transition zone has a yellowish brown color. It is a clay loam with some bands of feldspars present. Mica flakes are common. Some sections of the zone are more reddish in color.

Parent material appears to be felsic rock such as granite or gneiss. No layering is apparent in the parent material between the light and dark minerals. A gray clay like kaolinite is present in the section - most likely due to the breakdown of the feldspars. Quartz, feldspars and biotite are present. The color becomes more yellowish brown (10YR 5/6) as you move up section. This color change is probably due to an increase in the amount of iron oxides such as limonite and goethite.

The following table gives the locations of each soil core in relation to the injection well in the center of each cell and the location of each soil core in relation to a coordinate system where the injection well in the center of cell 2 is the origin.

Core Name	Feet from Well	Azimuth	North/South (ft)	East/West (ft)	North/South (m)	East/West (m)	North/South (m) in single coordinate system	East/West (m) in single coordinate system
Cell 1 Data							**Cell 2 injection well is (0,0)**	
C1-4/50	4	50	2.57	3.06	0.78	0.93	0.78	9.93
C1-4/147	4	147	-3.35	2.18	-1.02	0.66	-1.02	9.66
C1-2/230	2	230	-1.29	-1.53	-0.39	-0.47	-0.39	8.53
C1-6/230	6	230	-3.86	-4.60	-1.18	-1.40	-1.18	7.60
C1-10/230	10	230	-6.43	-7.66	-1.96	-2.33	-1.96	6.67
C1-4/327	4	327	3.35	-2.18	1.02	-0.66	1.02	8.34
Cell 2 Data								
C2-4/41	4	41	3.02	2.62	0.92	0.80	0.92	0.80
C2-4/136	4	136	-2.88	2.78	-0.88	0.85	-0.88	0.85
C2-2/221	2	221	-1.51	-1.31	-0.46	-0.40	-0.46	-0.40
C2-6/221	6	221	-4.53	-3.94	-1.38	-1.20	-1.38	-1.20
C2-10/221	10	221	-7.55	-6.56	-2.30	-2.00	-2.30	-2.00
C2-4/331	4	331	3.50	-1.94	1.07	-0.59	1.07	-0.59
Cell 3A Data								
C3A-4/0	4	0	4	0	1.22	0.00	3.22	-6.00
C3A-4/90	4	90	0	4	0.00	1.22	2.00	-4.78
C3A-	2	180	-2	0	-0.61	0.00	1.39	-6.00

2/180								
C3A-4/180	4	180	-4	0	-1.22	0.00	0.78	-6.00
C3A-6/180	6	180	-6	0	-1.83	0.00	0.17	-6.00
C3A-10/180	10	180	-10	0	-3.05	0.00	-1.05	-6.00
C3A-4/270	4	270	0	-4	0.00	-1.22	2.00	-7.22
Cell 4 Data								
C4-4/70	4	70	1.37	3.76	0.42	1.15	-8.58	10.15
C4-4/160	4	160	-3.76	1.37	-1.15	0.42	-10.15	9.42
C4-2/250	2	250	-0.68	-1.88	-0.21	-0.57	-9.21	8.43
C4-6/250	6	250	-2.05	-5.64	-0.63	-1.72	-9.63	7.28
C4-10/250	10	250	-3.42	-9.40	-1.04	-2.86	-10.04	6.14
C4-8-259	8	259	-1.53	-7.85	-0.47	-2.39	-9.47	6.61
C4-9/259	9	259	-1.72	-8.83	-0.52	-2.69	-9.52	6.31
C4-10/259	10	259	-1.91	-9.82	-0.58	-2.99	-9.58	6.01
C4-4/340	4	340	3.76	-1.37	1.15	-0.42	-7.85	8.58
Cell 5 Data								
F5-4/0	4	0	4	0	1.22	0.00	5.25	-18.93
F5-4/90	4	90	0	4	0.00	1.22	4.03	-17.71
F5-2/180	2	180	-2	0	-0.61	0.00	3.42	-18.93
F5-5/180	5	180	-5	0	-1.52	0.00	2.51	-18.93
F5-	10	180	-10	0	-3.05	0.00	0.98	-18.93

10/180								
F5-4/270	4	270	0	-4	0.00	-1.22	4.03	-20.15
F5-unknown	-	-	-	-	-	-	-	-
Cell 6 Data								
F6-4/98	4	98	-0.56	3.96	-0.17	1.21	11.13	-55.27
F6-4/169	4	169	-3.93	0.76	-1.20	0.23	10.10	-56.25
F6-4/275	4	275	0.35	-3.98	0.11	-1.21	11.41	-57.69
F6-2/346	2	346	1.94	-0.48	0.59	-0.15	11.89	-56.63
F6-6/346	6	346	5.82	-1.45	1.77	-0.44	13.07	-56.92
F6-10/346	10	346	9.70	-2.42	2.96	-0.74	14.26	-57.22

The following table gives the depth of each soil unit as feet below ground surface.

Core Name	Total Depth (ft)	Top Soil (ft) bgs	Top L3 (ft) bgs	Top L4 (ft) bgs	Top Upper Transition (ft) bgs	Top of Saprolite (ft) bgs	Top Highly Degraded Saprolite (ft) bgs
Cell 1 Data							
C1-4/50	6.11	-	-	0	1.25	-	
C1-4/147	7	-	-	0	3.9	-	
C1-2/230	7.3	0	-	0.37	2.1	-	
C1-6/230	7.3	0	0.26	1.66	6.5	-	
C1-10/230	7.2	-	-	0	3.1	5.9	
C1-4/327	7.3	-	-	-	0	0.59	5.01
Cell 2 Data							
C2-4/41	7.05	0	-	-	0.26	-	-
C2-4/136	6.6	-	-	0	3	-	-
C2-2/221	7	-	-	3.4	3.6	-	-
C2-6/221	7	-	-	0	0.85	-	-
C2-10/221	6.95	0	-	0.13	3.1	-	-
C2-4/331	6.6	0	0.11	1.8	-	3.53	-
Cell 3A Data							
C3A-4/0	7	-	-	0	3.15	-	
C3A-4/90	7.2	0	-	-	0.17	-	
C3A-2/180	7.05	-	-	0	3.5	-	
C3A-4/180	7.1	0	-	0.2	2.5	-	
C3A-6/180	6.95	-	-	0	1.5	-	
C3A-10/180	7.4	0	-	0	1.5	-	
C3A-4/270	7.1	0	-	1	3.4	-	

Cell 4 Data							
C4-4/70	7.3	0	-	0.29	0.64	-	-
C4-4/160	7.1	0	-	0.15	1.47	5.01	-
C4-2/250	7.2	-	0	2.21	4.2	6	-
C4-6/250	7.3	0	-	0.26	1.29	-	-
C4-10/250	7.4	-	-	-	0	-	-
C4-8-259	7.22	0	-	-	0.11	-	-
C4-9/259	2.75	-	-	0	0.29	-	-
C4-10/259	2.2	0	0.26	1.42	2.73	-	-
C4-4/340	7.4	0	0.15	1.55	4.02	-	-
Cell 5 Data							
F5-4/0	7.42	0	0.44	4.24	-	-	-
F5-4/90	7	0	0.15	3.56	-	-	-
F5-2/180	7.2	?	present	3.61	-	-	-
F5-5/180	7.5	?	?	3.6?	-	-	-
F5-10/180	7.3	0	0.33	3.33	-	-	-
F5-4/270	7.2	0	0.18	4.5	-	-	-
F5-unknown	?	0	0.09	2.36	-	-	-
Cell 6 Data							
F6-4/98	7.11	0	-	0.15	-	3.32	-
F6-4/169	7.2	-	-	0	-	1.29	-
F6-4/275	7.25	0	-	0.22	-	1.25	-
F6-2/346	7.5	0	0.26	1.99	4.16	5.3	-
F6-6/346	7.25	?	?	present	-	3.94	-
F6-10/346	7.4	-	-	0	0.48	3.06	-

The following table gives the elevations of the top surface of each soil unit as elevation above sea level. Notes on each soil core are also included.

Core Name	Elevation of L3 (m)	Elevation of L4 (m)	Elevation of Upper Transition (m)	Elevation of Saprolite Material (m)	Notes
Cell 1 Data					
C1-4/50	-	273.41	273.02	-	
C1-4/147	-	273.41	272.22	-	
C1-2/230	-	273.29	272.77	-	
C1-6/230	273.33	272.90	271.42	-	
C1-10/230	-	273.41	272.46	271.61	
C1-4/327	-	-	273.41	273.23	
Cell 2 Data					
C2-4/41	-	-	273.94	-	
C2-4/136	-	274.02	273.10	-	Bottom of Core 1 Missing; therefore depths/thickness are uncertain
C2-2/221	-	272.98	272.92	-	Core compressed and only a single core available; therefore depths/thicknesses are uncertain
C2-6/221	-	274.02	273.76	-	
C2-10/221	-	273.98	273.07	-	
C2-4/331	273.98	273.47	-	272.94	
Cell 3A Data					
C3A-4/0		274.02	273.06		
C3A-4/90			273.96		
C3A-2/180		274.02	272.95		

C3A-4/180		273.95	273.25		
C3A-6/180		274.02	273.56		
C3A-10/180		274.02	273.56		Bt4 mixed with top soil
C3A-4/270		273.71	272.98		
Cell 4 Data					
C4-4/70	-	273.01	272.91	-	
C4-4/160	-	273.06	272.65	271.57	
C4-2/250	273.10	272.43	271.82	271.27	
C4-6/250	-	273.02	272.71	-	
C4-10/250	-	-	273.10	-	Entire core is upper transition unit
C4-8-259	-	-	273.07	-	Core 2 was not kept so thickness and layers present are uncertain
C4-9/259	-	273.10	273.01	-	Core was unlabeled but was assumed to be this core since there wasn't a core with this label
C4-10/259	273.02	272.67	272.27	-	Single core taken; hole was 2.2 ft but core was 3.3 ft (expansion occurred)
C4-4/340	273.06	272.63	271.88	-	
Cell 5 Data					
F5-4/0	274.19	273.03	-	-	
F5-4/90	274.27	273.23	-	-	
F5-2/180	-	273.22	-	-	Only core 2 available; depth/thicknesses are uncertain; Bt3 and Bt4 present
F5-5/180	-	-	-	-	Only core 2 available; depth/thicknesses are uncertain; only Bt4 present
F5-10/180	274.22	273.31	-	-	
F5-4/270	274.27	272.95	-	-	
F5-unknown	274.29	273.60	-	-	The single core was unlabeled so it is unknown whether it belongs to F5-2/180 or

					F5-5/180
Cell 6 Data					
F6-4/98	-	274.88	-	273.92	
F6-4/169	-	274.93	-	274.54	
F6-4/275	-	274.86	-	274.55	
F6-2/346	274.85	274.32	273.66	273.31	
F6-6/346	-	-	-	273.73	Core 1 failed so only core 2 was obtained; depths/thicknesses uncertain
F6-10/346	-	274.93	274.78	274.00	

The following tables contain data about the fracture found in each of the soil cores collected during the first round of coring.

Cell 1

Core Name	# Cores Collected	Total Borehole Depth (ft)*	Feet from Top of Core to Fracture	Feet from Bottom of Core to Fracture	Shoe Length (ft)	Fracture Depth Below Ground Surface (ft)	Fracture Thickness (mm)	Notes
C1-4/50	2	6.11	-	1.25	0.25	4.61	5	
C1-4/147	2	7.0	-	1.73	0.25	5.02	4 to 10 and 4 to 6	Two fracture are present in this core and they run parallel to each other. The upper one is 4 mm to 10 mm thick, and the lower fracture is 4 mm to 6 mm thick. The fracture are separated by 14 mm to 19 mm of soil.
C1-2/230	2	7.3	-	1.56	0.25	5.49	7 to 14	The mode thickness is 12 mm.
C1-4/230	2	7.1	4.29	-	0.25	4.29	11 to 30	This core was sent to UNC and was not cut open for analysis. The thickness was difficult to determine, and the larger thickness values were probably due to smearing on the sides of the cores.
C1-6/230	2	7.3	-	2.1	0.25	4.95	3 to 10	

C1-10/230	2	7.2	-	-	0.25	-	-	Fracture not present in core.
C1-4/327	2	7.3	-	1.67	0.25	5.38	5 to 7	Fracture does not appear to span the entire core. Fracture projects 2/3 of the way across the core and stops. The other 1/3 of the fracture is about 10 mm above it. They do not appear to be connected, but it is difficult to tell.

Cell 2

Core Name	# Cores Collected	Total Borehole Depth (ft)*	Feet from Top of Core to Fracture	Feet from Bottom of Core to Fracture	Shoe Length (ft)	Fracture Depth Below Ground Surface (ft)	Fracture Thickness (mm)	Notes
C2-4/41	2	7.05	-	2.22	0.25	4.58	5	
C2-4/136	2	6.6	-	1.75	0.25	4.60	3 to 4	
C2-2/221	1	7.0	-	1.68	0.25	5.07	3 to 5	Note on the core stated that the core compressed and only a single core was available
C2-4/221	2	7.1	4.3	-	0.25	4.33	≈10	This core was sent to UNC and was not cut open for analysis. The thickness is most likely

								fairly accurate since the fracture thickness was pretty consistant all the way around the core tube.
C2-6/221	2	7.0	-	2.17	0.25	4.58	10	
C2-10/221	2	6.95	-	3.25	0.25	3.45	-	Fracture was located at the top of the second core. Soil was very jumbled in this section so the thickness of the fracture could not be determined. Fracture distance from the bottom of the core is also somewhat approximated +/- 0.5 inches
C2-4/331	2	6.6	-	-	0.25	-	-	No fracture was identified in this core.

Cell 3A

Core Name	# Cores Collected	Total Borehole Depth (ft)*	Feet from Top of Core to Fracture	Feet from Bottom of Core to Fracture	Shoe Length (ft)	Fracture Depth Below Ground Surface (ft)	Fracture Thickness (mm)	Notes
C3A-4/0	2	7.0	-	2.78	0.25	3.97	15	
C3A-4/90	2	7.2	-	1.51	0.25	5.44	3 to 6	Fracture is dipping at an angle of about 14°.

C3A-2/180	2	7.05	-	0.97	0.25	5.83	4 to 10	Fracture is dipping at an angle of about 14°.
C3A-4/180	2	7.1	-	0.61	0.25	6.24	3 to 4	
C3A-6/180	2	6.95	-	-	0.25	-	-	Fracture is not present in this core.
C3A-10/180	2	7.4	-	-	0.25	-	-	Fracture is not present in this core.
C3A-4/190	2	7.1	6.54	-	0.25	6.54	5 to 10	This core was sent to UNC and was not cut open for analysis. There did not appear to be much smearing on the sides of the core.
C3A-4/270	2	7.1	-	1.8	0.25	5.05	9 to 10	

Cell 4

Core Name	# Cores Collected	Total Borehole Depth (ft)*	Feet from Top of Core to Fracture	Feet from Bottom of Core to Fracture	Shoe Length (ft)	Fracture Depth Below Ground Surface (ft)	Fracture Thickness (mm)	Notes
C4-4/70	2	7.3	-	1.25	0.25	5.80	3 to 11	
C4-4/160	2	7.1	-	1.62	0.25	5.23	8	

C4-2/250	2	7.2	-	1.71	0.25	5.24	6	It appears that two 6 mm thick fractures are present. They run parallel to each other and are separated by about 4 mm of soil
C4-4/250	2	7.3	4.17	-	0.25	4.17	≈15 to 20	This core was sent to UNC and was not cut open for analysis. Therefore, smearing on the sides of the core could make the fracture appear thicker than it really is. This also means that the depth to the fracture is somewhat approximate since the fracture could not be clearly seen through the tube.
C4-6/250	2	7.3	-	2.95	0.25	4.10	5 to 10	The thinner section of the fracture appears to be lying on top of a mottle in the soil. Fracture is dipping at an angle of about 40°
C4-10/250	2	7.4	1.21	-	0.25	1.21	1.5 to 2	
C4-8/259	2	7.22	1.79	-	0.25	1.79	2 to 5	Even though 2 cores were taken, only the first core was kept since the fracture was present in the first core. The total depth measurement accounts for both cores. The fracture is dipping at an angle of about 30°.
C4-9/259	1	2.75	1.4	-	0.25	1.4	3	This core was unlabeled. It is assumed to be C4-9/259 because it was known that it was from cell 4 andC4-9/259 was the only core

								that was missing from this group. Ground surface on this core was estimated based on the current top of the soil in the core
C4-10/259	1	2.2	1.5	-	0.25	1.5	6	
C4-4/340	2	7.4	-	1.62	0.25	5.53	2 to 10	

Cell 5

Core Name	# Cores Collected	Total Borehole Depth (ft)*	Feet from Top of Core to Fracture	Feet from Bottom of Core to Fracture	Shoe Length (ft)	Fracture Depth Below Ground Surface (ft)	Fracture Thickness (mm)	Notes
F5-4/0	2	7.42	-	1.27	0.25	5.90	9	No string magnet data is available because the hole filled in before this data could be collected.
F5-4/90	2	7.0	-	0.54	0.25	6.21	10	
F5-2/180	1	7.2	-	1.75	0.25	5.20	15 to 20	Only core 2 was recovered from this borehole. Core 1 is missing.
F5-4/180	2	7.0	5.71	-	0.25	5.71	≈15	This core was sent to UNC and was not cut open for analysis. It was difficult to determine fracture thickness due to a large

								amount of smearing. The thickness listed is based on the area with the highest magnetism. The smearing makes the fracture appear to be 30 mm to 40 mm thick.
F5-5/180	1	7.5	-	1.83	0.25	5.42	3 to 4	Only core 2 was recovered from this borehole. Core 1 is missing. There is an unlabeled core that might be core 1 for this hole.
F5-10/180	2	7.3	-	-	0.25	-	-	Fracture is not present in this core, and the magnet was not attrached to the side of the borehole when it was dropped down borehole.
F5-4/270	2	7.2	-	3.25	0.25	3.70	5 to 8	

Cell 6

Core Name	# Cores Collected	Total Borehole Depth (ft)*	Feet from Top of Core to Fracture	Feet from Bottom of Core to Fracture	Shoe Length (ft)	Fracture Depth Below Ground Surface (ft)	Fracture Thickness (mm)	Notes
F6-4/98	2	7.11	-	2.13	0.25	4.73	8	
F6-	2	7.2	-	1.63	0.25	5.32	8	

4/169								
F6-4/275	2	7.25	-	1.67	0.25	5.33	8 to 10	
F6-2/346	2	7.5	-	1.81	0.25	5.44	10 to 12	
F6-4/346	2	7.0	4.35	-	0.25	4.35	≈20	This core was sent to UNC and was not cut open for analysis. It was difficult to determine fracture thickness due to a large amount of smearing.
F6-6/346	2	7.25	-	3.08	0.25	3.92	-	Core 1 failed at this location so only core 2 was obtained. Fracture is located at the top of the second core where the sediment is very jumbled. Since the structure was destroyed in this section of the core, it was not possible to obtain the fracture thickness.
F6-10/346	2	7.4	-	-	0.25	-	-	Fracture is not present in this core.

The following extra data was taken in cells 5 and 6 since the proppant was magnetic.

Cell 5

Core Name	Depth from Surface to Fracture with Magnet**	Borehole Depth from Measurements^	Difference between total borehole depth and borehole depth from measurements (ft)	Difference between total borehole depth and borehole depth from measurements (in)
F5-4/0	-	-	-	-
F5-4/90	6.42	7.21	-0.21	-2.52
F5-2/180	5.04	7.04	0.16	1.92
F5-4/180	5.38	-	-	-
F5-5/180	5.38	7.46	0.04	0.48
F5-10/180	-	-	-	-
F5-4/270	3.96	7.46	-0.26	-3.12

Cell 6

Core Name	Depth from Surface to Fracture with Magnet**	Borehole Depth from Measurements^	Difference between total borehole depth and borehole depth from measurements (ft)	Difference between total borehole depth and borehole depth from measurements (in)
F6-4/98	4.5	6.88	0.23	2.76
F6-4/169	5.23	7.11	0.09	1.08
F6-4/275	5.1	7.02	0.23	2.76
F6-2/346	4.79	6.85	0.65	7.8
F6-4/346	4.17	-	-	-
F6-6/346	1.88	5.21	2.04	24.48
F6-10/346	-	-	-	-

*Measured in the field by placing a tape measure down the borehole

**Measured in the field by dropping a magnet tied to a string down the borehole. The magnet would stick to the fracture location and the depth to that location from the surface was measured.

^Based on depth from surface to fracture with magnet, depth from bottom of the core to the fracture, and the shoe length.

The following tables contain data about the fracture found in each of the soil cores collected during the second round of coring.

Cell 1

Core Name	Feet From Injection Well	Bearing from Well (Azimuth)	Fracture Present	Expected Result
C1-10/315	10	315	No	Not present
C1-8/295	8	295	No	Present
C1-7/260	7	260	Yes	Present
C1-12.5/270	12.5	270	No	Possible
C1-8.5/45	8.5	45	No	Not present
C1-10/135	10	135	No	Not present
C1-4/236	4	236	Yes	Present

Core Name	Total Borehole Depth (ft)*	Feet from Top of Core to Fracture	Feet from Bottom of Core 1 to Fracture	Feet from Bottom of Core 2 to Fracture	Fracture Depth Below Ground Surface (ft)	Fracture Thickness (mm)	Notes
C1-10/315	7.95	-	-	-	-	-	
C1-8/295	7.9	-	-	-	-	-	Discrepancy between

							expected result and observed result.
C1-7/260	7.8	3.75	-	-	3.75	-	Thickness unable to be obtained due to compression
C1-12.5/270	7.95	-	-	-	-	-	
C1-8.5/45	8.05	-	-	-	-	-	
C1-10/135	8.0	-	-	-	-	-	
C1-4/236	7.95	-	-	2.42	5.33	5 to 10	The fracture is dipping at an angle of about 25°. Compression of the core probably affects the results.

Cell 2

Core Name	Feet From Injection Well	Bearing from Well (Azimuth)	Fracture Present	Expected Result
C2-4.5/310	4.5	310	No	Present
C2-3.5/275	3.5	275	Yes	Present
C2-7/295	7	295	No	Present
C2-11/285	11	285	No	Possible

C2-13/305	13	305	No	Not present
C2-9/345	9	345	No	Possible
C2-11.5/45	11.5	45	No	Not present
C2-8.5/70	8.5	70	No	Not present
C2-9/135	9	135	No	Not present
C2-12/221	12	221	No	-
C2-4.85/221	4.85	221	Yes	-
C2-4.5/0	4.5	0	No	-
C2-4.5/295	4.5	295	No	-
C2-8/315	8	315	No	Possible
C2-6/255	6	255	Yes	Present
C2-9/255	9	255	Yes	Not Present
C2-5/95	5	95	No	Possible
C2-5/170	5	170	Yes	Not Present

Core Name	Total Borehole Depth (ft)*	Feet from Top of Core to Fracture	Feet from Bottom of Core 1 to Fracture	Feet from Bottom of Core 2 to Fracture	Fracture Depth Below Ground Surface (ft)	Fracture Thickness (mm)	Notes
C2-4.5/310	7.90	-	-	-	-	-	Discrepancy between expected result and observed result.
C2-3.5/275	7.90	-	-	2.09	5.66	15	A large amount of compression occurred

							so measurements may be off some.
C2-7/295	7.90	-	-	-	-	-	Discrepancy between expected result and observed result.
C2-11/285	7.40	-	-	-	-	-	
C2-13/305	7.85	-	-	-	-	-	
C2-9/345	7.85	-	-	-	-	-	
C2-11.5/45	7.90	-	-	-	-	-	
C2-8.5/70	7.85	-	-	-	-	-	
C2-9/135	7.60	-	-	-	-	-	
C2-12/221	7.85	-	-	-	-	-	
C2-4.85/221	7.7	-	-	2.49 and 2.31	5.26 and 5.44 respectively	8 to 10 and 20 max	The first fracture listed is the main fracture that is 8 to 10 mm thick. The second fracture 5.44 ft. below ground surface only protrudes about 8 mm into the core and its maximum thickness is 20 mm.
C2-4.5/0	-	-	-	-	-	-	A total depth measurement was not obtained for this borehole.
C2-	-	-	-	-	-	-	A total depth

4.5/295							measurement was not obtained for this borehole.
C2-8/315	8.00	-	-	-	-	-	
C2-6/255	-	-	-	2.29	5.46	12	A total depth measurement was not obtained for this borehole.
C2-9/255	7.83	-	0.67	-	3.08	5 to 7	Part of the fracture is horizontal, and part of the fracture is dipping at an angle of 45°. Discrepancy between expected result and observed result.
C2-5/95	7.83	-	-	-	-	-	
C2-5/170	7.92	-	-	2.04	5.71	6	The fracture is dipping at an angle of about 30°. Discrepancy between expected result and observed result.

Cells 3 and 3A

Core Name	Feet From Injection Well	Bearing from Well (Azimuth)	Fracture Present	Expected Result
C3-8/265	8	265	No	Possible
C3-3.5/300	3.5	300	No	Present
C3-3.5/20	3.5	20	Yes	Present
C3-10.5/10	10.5	10	Yes	Present
C3-11.5/335	11.5	335	No	Possible
C3-17/55	17	55	No	Possible
C3A-7/0	7	0	Yes	Possible
C3A-7/90	7	90	Yes	Possible
C3A-7/270	7	270	No	Possible

Core Name	Total Borehole Depth (ft)*	Feet from Top of Core to Fracture	Feet from Bottom of Core 1 to Fracture	Feet from Bottom of Core 2 to Fracture	Fracture Depth Below Ground Surface (ft)	Fracture Thickness (mm)	Notes
C3-8/265	7.8	-	-	-	-	-	
C3-3.5/300	7.7	-	-	-	-	-	Discrepancy between expected result and observed result.
C3-3.5/20	7.5	1.54	-	-	1.54	3	Large amount of compression present.
C3-10.5/10	8.0	-	-	3.5	4.25	≈10	Minimal expansion present.
C3-11.5/335	7.95	-	-	-	-	-	
C3-17/55	7.83	-	-	-	-	-	
C3A-7/0	8.00	-	0.28	3.61	3.47 and 4.14	4 to 5 and ≈3 respectively	Two fractures were present in this core. One fracture is 3.47 ft. below the surface of the earth

							and the other fracture is 4.14 ft. below the surface of the earth.
C3A-7/90	7.17	-	-	2.54	5.21	5	The fracture is dipping at about a 25° angle.
C3A-7/270	8.00	-	-	-	-	-	

Cell 4

Core Name	Feet From Injection Well	Bearing from Well (Azimuth)	Fracture Present	Expected Result
C4-11.75/200	11.75	200	No	Not Present
C4-6.75/216	6.75	216	Yes	Present
C4-4.75/302	4.75	302	Yes	Present
C4-7.75/330	7.75	330	No	Not Present
C4-13/264	13	264	No	Not Present
C4-7.75/100	7.75	100	No	Not Present
C4-4/253	4	253	Possibly	Yes

Core Name	Total Borehole Depth (ft)*	Feet from Top of Core to Fracture	Feet from Bottom of Core 1 to Fracture	Feet from Bottom of Core 2 to Fracture	Fracture Depth Below Ground Surface (ft)	Fracture Thickness (mm)	Notes

C4-11.75/200	8.75	-	-	-	-	-	
C4-6.75/216	7.65	-	0.35	-	3.40	15	
C4-4.75/302	7.9	-	-	3.09	4.66	≈ 8	
C4-7.75/330	7.83	-	-	-	-	-	
C4-13/264	7.9	-	-	-	-	-	
C4-7.75/100	8.05	-	-	-	-	-	
C4-4/253	7.95	-	-	2.29????	5.46???	Unknown	It is difficult to determine the thickness and location of the fracture. Coke breeze is scattered through the core but no fracture is present. The numbers given are estimations with a high possibility of error.

Cell 5

Core Name	Feet From Injection Well	Bearing from Well (Azimuth)	Fracture Present	Expected Result
C5-10.5/270	10.5	270	No	Possible
C5-7/270	7	270	Yes	Present
C5-8/90	8	90	No	Possible
C5-6/215	6	215	Yes	Present
C5-5.5/320	5.5	320	Yes	Present
C5-8/0	8	0	No	Possible
C5-8/180	8	180	No	Possible
C5-8/230	8	230	No	Possible
C5-3/0	3	0	Yes	Present
C5-7/61	7	61	No	Possible

Core Name	Total Borehole Depth (ft)*	Depth from Surface to Fracture with Magnet**	Feet from Top of Core to Fracture	Feet from Bottom of Core 1 to Fracture	Feet from Bottom of Core 2 to Fracture	Fracture Depth Below Ground Surface (ft)	Fracture Thickness (mm)	Notes
C5-10.5/270	7.67	-	-	-	-	-	-	
C5-7/270	8.0	3.40	-	0.17	-	3.58	≈ 8	It is difficult to determine the thickness due to separation of the core at the fracture.
C5-8/90	8.0	-	-	-	-	-	-	
C5-6/215	7.83	4.33	-	-	3.29	4.46	6 to 7	
C5-5.5/320	7.92	4.58	-	-	3.0	4.75	6	
C5-8/0	7.92	-	-	-	-	-	-	
C5-8/180	8.0	-	-	-	-	-	-	
C5-8/230	7.83	3.75	-	-	-	-	-	Huge discrepancy with this core. Magnet test says that the fracture is there, but it was not seen in the soil core. This could be due to about 3 inches of soil missing from the soil cores at about the location the magnet indicated the fracture

								is located. See note under ^.
C5-3/0	8	5.5	-	-	1.9	5.85	≈20	The thickness was difficult to determine since the area containing the fracture was very broken up so the fracture may actually be smaller.
C5-7/61	7.92	-	-	-	-	-	-	

Cell 6

Core Name	Feet From Injection Well	Bearing from Well (Azimuth)	Fracture Present	Expected Result
C6-6.5/228	6.5	228	Yes	Not Present
C6-1.5/228	1.5	228	Yes	Present
C6-5/48	5	48	Yes	Present
C6-8.5/48	8.5	48	Yes	Not Present
C6-10.5/48	10.8	48	Yes	Not Present
C6-8/288	8	288	No	Not Present
C6-7/212	7	212	Yes	Not Present
C6-10/228	10	228	No	Not Present
C6-13/48	13	48	No	Not Present
C6-6/260	6	260	Yes	-
C6-5/346	5	346	Yes	-
C6-7/346	7	346	Yes	-
C6-9/346	9	346	No	-
C6-8/20	8	20	Yes	-
C6-6/110	6	110	Yes	-

Core Name	Total Borehole Depth (ft)*	Depth from Surface to Fracture with Magnet**	Feet from Top of Core to Fracture	Feet from Bottom of Core 1 to Fracture	Feet from Bottom of Core 2 to Fracture	Fracture Depth Below Ground Surface (ft)	Fracture Thickness (mm)	Notes
C6-6.5/228	8.0	4.83	-	-	1.96	5.79	4 to 6	Discrepancy here because the fracture was present even though it was not expected to be.
C6-1.5/228	8.0	5.13	-	-	1.65	6.1	14	A large amount of compression is present which could affect the core measurements.
C6-5/48	8.0	3.96	-	-	3.14	4.61	5 to 18	The area around the fracture is very jumbled so it is difficult to tell how thick the fracture is.
C6-8.5/48	8.0	2.88	-	0.56	-	3.19	2 to 5	It was difficult to determine the thickness of the fracture. Discrepancy here because the fracture was present even though it was not expected to be.
C6-10.5/48	9.50	2.33	-	1.47	-	2.28	3	Discrepancy here because the fracture was present even

								though it was not expected to be.
C6-8/288	8.0	-	-	-	-	-	-	
C6-7/212	8.0	4.63	-	-	2.38	5.37	4	Discrepancy here because the fracture was present even though it was not expected to be.
C6-10/228	7.67	-	-	-	-	-	-	
C6-13/48	7.92	-	-	-	-	-	-	
C6-6/260	7.92	4.83	-	-	2.36	5.39	6 to 7	
C6-5/346	7.83	4.08	-	-	3.28	4.47	10	Some expansion occurred in this core.
C6-7/346	7.83	3.33	-	0.17	-	3.58	≈7	
C6-9/346	8.17	-	-	-	-	-	-	
C6-8/20	8.0	3.00	-	0.53	-	3.22	≈9	
C6-6/110	8.0	4.08	-	-	2.46	5.29	Unknown	The area around the fracture was very jumbled, and it was not possible to determine the thickness of the fracture.

*Measured in the field by placing a tape measure down the borehole.
^Theoretically the first sleeve contained 45 inches of soil and the second sleeve contained everything from 4 feet below ground surface to 7.75 feet below ground surface. These assumptions were used for the calculations in column J.

Appendix B: Excavation Data

This appendix contains the survey data collected in Cells 2 and 4 during the excavation of the trenches. The first group of tables contains the survey data that was collected from the trenches during excavation. The depth of the fracture calculated from this data is also included. In these tables, the elevation datum is set so that the surface of the earth at the field site has a value of 0 meters. The next set of tables contains the fracture apertures that were measured on the walls of the trenches.

Cell 2 Trench 1 Northwest Wall Survey Data							
Station	Feet Along Fracture	Meters Along Fracture	Horizontal Angle	Vertical Angle	Distance (m)	Vertical Elevation (m)	Corrected Elevation (m)
REF1	-	-	1234010	335511	11.47	-0.64	-
REF2	-	-	864940	337064	9.10	-0.58	-
REF3	-	-	799196	342137	9.54	-0.84	-
C2T10	0	0	897906	457286	3.79	-2.28	-0.99
C2T11	1	0.30	912871	454992	3.95	-2.34	-1.05
C2T12	2	0.61	929222	449465	4.06	-2.32	-1.03
C2T13	3	0.91	944022	445576	4.23	-2.35	-1.06
C2T14	4	1.22	956860	445202	4.45	-2.47	-1.17
C2T15	5	1.52	969507	441986	4.64	-2.51	-1.22
C2T16	6	1.83	981505	439038	4.87	-2.58	-1.29
C2T17	7	2.13	990532	435119	5.06	-2.60	-1.30
C2T18	8	2.44	999141	432275	5.29	-2.65	-1.36
C2T19	9	2.74	1006595	428488	5.52	-2.68	-1.39
C2T210	10	3.05	1013626	423837	5.75	-2.68	-1.38
C2T211	11	3.35	1019498	420286	5.99	-2.69	-1.40
C2T212	12	3.66	1024398	416759	6.26	-2.72	-1.43
C2T213	13	3.96	1027668	408904	6.47	-2.59	-1.29
C2T214A	14	4.27	1033018	407149	6.73	-2.64	-1.35
C2T214B	14	4.27	1033041	412196	6.80	-2.82	-1.53
REF1	-	-	1233970	335507	11.47	-0.64	-
REF2	-	-	864879	337064	9.10	-0.58	-
REF3	-	-	799141	342124	9.54	-0.84	-

The corrected elevation calculated in the last column corrects for the fact that the survey station was a set height above the ground surface. This is the elevation value used for all cross sections. The REF values are the reference points that were taken at the beginning and end of each survey collection period.

Cell 2 Trench 1 Southeast Wall							
Station	Feet Along Fracture	Meters Along Fracture	Horizontal Angle	Vertical Angle	Distance (m)	Vertical Elevation (m)	Corrected Elevation (m)
REF1	-	-	793921	320614	12.99	0.21	-
REF2	-	-	369194	312947	5.18	0.28	-
REF3	-	-	259390	323437	5.85	0.02	-
C2T1SE0	0	0	890184	469794	2.38	-1.54	-1.04
C2T1SE1	1	0.30	862967	467910	2.48	-1.59	-1.09
C2T1SE2	2	0.61	833370	462010	2.63	-1.63	-1.13
C2T1SE3	3	0.91	812861	458404	2.81	-1.70	-1.20
C2T1SE4	4	1.22	793263	452811	2.99	-1.75	-1.25
C2T1SE5	5	1.52	775506	447008	3.24	-1.82	-1.32
C2T1SE6	6	1.83	761183	442091	3.46	-1.87	-1.37
C2T1SE7	7	2.13	749527	436033	3.72	-1.92	-1.42
C2T1SE8	8	2.44	740198	426347	4.15	-1.97	-1.47
C2T1SE9	9	2.74	730041	419307	4.45	-1.99	-1.49
C2T1SE10	10	3.05	718380	414576	4.71	-2.00	-1.50
C2T1SE11	11	3.35	709013	411237	4.93	-2.02	-1.52
C2T1SE12	12	3.66	709096	411242	4.92	-2.02	-1.52
C2T1SE13	13	3.96	702253	406081	5.15	-2.00	-1.50
C2T1SE14	14	4.27	698520	397566	5.37	-1.88	-1.38
C2T1SE15	15	4.57	693706	391646	5.64	-1.82	-1.32
REF1	-	-	793932	320615	12.99	0.21	-
REF2	-	-	369153	312929	5.18	0.28	-
REF3	-	-	259413	323424	5.85	0.02	-

The corrected elevation calculated in the last column corrects for the fact that the survey station was a set height above the ground surface. This is the elevation value used for all cross sections. The REF values are the reference points that were taken at the beginning and end of each survey collection period.

Cell 2 Trench 2 North Wall							
Station	Feet Along Fracture	Meters Along Fracture	Horizontal Angle	Vertical Angle	Distance (m)	Vertical Elevation (m)	Corrected Elevation (m)
REF1	-	-	1187974	330676	11.00	-0.36	-
REF2	-	-	774918	331493	8.02	-0.29	-
REF3	-	-	704001	336997	8.79	-0.55	-
C2T2N0	0	0	1128673	465328	3.80	-2.40	-1.39
C2T2N1	1	0.30	1108085	468409	3.74	-2.41	-1.39
C2T2N2	2	0.61	1086622	471218	3.72	-2.44	-1.42
C2T2N3	3	0.91	1064861	472984	3.70	-2.44	-1.43
C2T2N4	4	1.22	1043454	465932	3.71	-2.35	-1.34
C2T2N5	5	1.52	1021568	470509	3.80	-2.48	-1.46
C2T2N6	6	1.83	1002049	468020	3.88	-2.49	-1.47
C2T2N10	10	3.05	927278	448763	4.17	-2.37	-1.36
C2T2N11	11	3.35	911809	441045	4.23	-2.27	-1.25
C2T2N12	12	3.66	901631	427884	4.39	-2.12	-1.10
REF1	-	-	1187855	330670	11.00	-0.36	-
REF2	-	-	774847	331484	8.02	-0.29	-
REF3	-	-	703902	336985	8.78	-0.55	-

The corrected elevation calculated in the last column corrects for the fact that the survey station was a set height above the ground surface. This is the elevation value used for all cross sections. The REF values are the reference points that were taken at the beginning and end of each survey collection period.

Cell 2 Trench 2 South Wall							
Station	Feet Along Fracture	Meters Along Fracture	Horizontal Angle	Vertical Angle	Distance (m)	Vertical Elevation (m)	Corrected Elevation (m)
REF1	-	-	1030288	346049	5.37	-0.57	-
REF2	-	-	604298	332144	12.87	-0.51	-
REF3	-	-	565921	335022	14.43	-0.77	-
C2T2S0	0	0	558562	432833	4.98	-2.51	-1.23
C2T2S1	1	0.30	562936	429989	5.26	-2.59	-1.31
C2T2S2	2	0.61	567221	424836	5.53	-2.60	-1.32
C2T2S3	3	0.91	569360	417837	5.75	-2.53	-1.25
C2T2S4	4	1.22	573529	416390	6.04	-2.62	-1.34
C2T2S5	5	1.52	576680	412123	6.34	-2.63	-1.35
C2T2S6	6	1.83	579367	408337	6.60	-2.62	-1.34
C2T2S10	10	3.05	588235	391433	7.57	-2.43	-1.15
C2T2S11	11	3.35	590173	386316	7.81	-2.32	-1.04
C2T2S12	12	3.66	589433	380451	7.98	-2.16	-0.88
REF1	-	-	1030209	346065	5.37	-0.57	-
REF2	-	-	604337	332158	12.87	-0.51	-
REF3	-	-	565893	335022	14.43	-0.77	-

The corrected elevation calculated in the last column corrects for the fact that the survey station was a set height above the ground surface. This is the elevation value used for all cross sections. The REF values are the reference points that were taken at the beginning and end of each survey collection period.

Cell 2 Trench 3 Southeast Wall							
Station	Feet Along Fracture	Meters Along Fracture	Horizontal Angle	Vertical Angle	Distance (m)	Vertical Elevation (m)	Corrected Elevation (m)
REF1	-	-	596949	355300	4.22	-0.64	-
REF2	-	-	24323	333725	12.14	-0.57	-
REF3	-	-	1285723	336157	14.16	-0.83	-
C2T3SE0	0	0	25806	466705	4.29	-2.74	-1.27
C2T3SE1	1	0.30	33742	457226	4.52	-2.72	-1.25
C2T3SE2	2	0.61	39442	452740	4.80	-2.80	-1.33
C2T3SE3	3	0.91	44369	445048	5.00	-2.77	-1.30
C2T3SE4	4	1.22	47946	439093	5.26	-2.79	-1.32
REF1	-	-	596936	355300	4.22	-0.64	-
REF2	-	-	24351	333709	12.14	-0.57	-
REF3	-	-	1285901	336155	14.16	-0.83	-

The corrected elevation calculated in the last column corrects for the fact that the survey station was a set height above the ground surface. This is the elevation value used for all cross sections. The REF values are the reference points that were taken at the beginning and end of each survey collection period.

Cell 2 Trench 3 Southwest Wall							
Station	Feet Along Fracture	Meters Along Fracture	Horizontal Angle	Vertical Angle	Distance (m)	Vertical Elevation (m)	Corrected Elevation (m)
REF1	-	-	712463	340295	8.45	-0.67	-
REF2	-	-	1146942	336327	10.07	-0.60	-
REF3	-	-	1130453	337806	12.92	-0.86	-
C2T3SW8	8	2.44	1019873	413096	6.38	-2.67	-1.43
C2T3SW9	9	2.74	1028770	409673	6.31	-2.55	-1.03
REF1	-	-	712404	340284	8.46	-0.67	-
REF2	-	-	1146921	336333	10.07	-0.60	-
REF3	-	-	1130504	337808	12.92	-0.86	-

The corrected elevation calculated in the last column corrects for the fact that the survey station was a set height above the ground surface. This is the elevation value used for all cross sections. The REF values are the reference points that were taken at the beginning and end of each survey collection period.

Cell 4 Trench 1 North Wall							
Station	Feet Along Fracture	Meters Along Fracture	Horizontal Angle	Vertical Angle	Distance (m)	Vertical Elevation (m)	Corrected Elevation (m)
REF1	-	-	404781	324041	11.88	0.00	-
REF2	-	-	221328	323390	20.68	0.06	-
REF3	-	-	192591	325945	21.31	-0.20	-
C4T1N0	0	0	522559	435324	5.39	-2.77	-1.72
C4T1N1	1	0.30	516686	440655	5.16	-2.77	-1.72
C4T1N2	2	0.61	509963	446393	4.94	-2.76	-1.71
C4T1N3	3	0.91	501311	451799	4.71	-2.73	-1.68
C4T1N4	4	1.22	491967	458575	4.51	-2.74	-1.69
C4T1N5	5	1.52	481095	464748	4.29	-2.70	-1.65
C4T1N6	6	1.83	468934	469905	4.07	-2.64	-1.59
C4T1N7	7	2.13	453656	473190	3.88	-2.57	-1.52
C4T1N8	8	2.44	436873	480167	3.71	-2.55	-1.50
C4T1N9	9	2.74	418691	485204	3.55	-2.50	-1.45
C4T1N10	10	3.05	395854	490068	3.39	-2.45	-1.40
C4T1N11	11	3.35	370148	492317	3.29	-2.39	-1.34
C4T1N12	12	3.66	343192	490400	3.16	-2.28	-1.23
C4T1N13	13	3.96	316548	486778	3.06	-2.17	-1.12
C4T1N14	14	4.27	290611	480757	2.96	-2.04	-0.99
C4T1N15	15	4.57	262454	475385	2.90	-1.94	-0.89
C4T1N16	16	4.88	246931	451955	2.78	-1.62	-0.57
C4T1N17	17	5.18	231152	439754	2.85	-1.52	-0.47
C4T1N16B	16	4.88	244747	471243	2.89	-1.89	-0.84
REF1	-	-	404726	324048	11.88	0.00	-
REF2	-	-	221296	323391	20.68	0.06	-
REF3	-	-	192605	325941	21.31	-0.20	-

The corrected elevation calculated in the last column corrects for the fact that the survey station was a set height above the ground surface. This is the elevation value used for all cross sections. The REF values are the reference points that were taken at the beginning and end of each survey collection period.

Cell 4 Trench 1 South Wall						
Station	Feet Along Fracture	Meters Along Fracture	Horizontal Angle	Vertical Angle	Distance (m)	Vertical Elevation (m)
REF1	-	-	289499	333731	11.21	-0.53
REF2	-	-	39553	329944	16.15	-0.47
REF3	-	-	2195	333055	16.55	-0.73
C4T1SE0	0	0	484502	409387	8.13	-3.27
C4T1SE1	1	0.30	487017	411782	7.92	-3.27
C4T1SE2	2	0.61	489190	414582	7.65	-3.25
C4T1SE3	3	0.91	492462	418240	7.36	-3.25
C4T1SE4	4	1.22	495751	421706	7.12	-3.25
C4T1SE5	5	1.52	499569	423194	6.84	-3.16
C4T1SE6	6	1.83	503831	428134	6.60	-3.19
C4T1SE7	7	2.13	507619	430379	6.31	-3.11
C4T1SE8	8	2.44	512097	431748	6.03	-3.01
C4T1SE9	9	2.74	517898	434254	5.75	-2.93
C4T1SE10	10	3.05	523665	436753	5.51	-2.87
C4T1SE11	11	3.35	530705	440519	5.27	-2.82
C4T1SE12	12	3.66	538322	442244	4.99	-2.71
C4T1SE13	13	3.96	546102	443411	4.72	-2.58
C4T1SE14	14	4.27	555503	447031	4.49	-2.52
C4T1SE15	15	4.57	565772	449508	4.32	-2.47
C4T1SE_A	-	-	561907	441672	4.30	-2.32
C4T1SE_B	-	-	569855	437627	4.19	-2.19
REF1	-	-	289494	333726	11.21	-0.53
REF2	-	-	39551	329943	16.15	-0.47
REF3	-	-	2187	333059	16.55	-0.73

The corrected elevation was not calculated for this trench since sufficient data was not available to complete the calculation. The REF values are the reference points that were taken at the beginning and end of each survey collection period.

Cell 2 Trench 1 Northwest Wall		
Distance along Tape (ft.)	Distance along Tape (m)	Aperture (mm)
0	0	hair line crack
0.1	0.030	1.0
0.5	0.15	2.0
1.0	0.30	3.0
1.5	0.46	3.0
2.0	0.61	4.5
2.5	0.76	12.0
3.0	0.91	7.0
3.5	1.07	8.0
4.0	1.22	11.0
4.5	1.37	12.0
5.0	1.52	12.0
5.5	1.68	14.0
6.0	1.83	13.0
6.5	1.98	13.0
7.0	2.13	13.0
7.5	2.29	12.0
8.0	2.44	12.0
8.5	2.59	17.0
9.0	2.74	15.0
9.5	2.90	10.0
10.0	3.05	10.0
10.5	3.20	8.0
11.0	3.35	9.0
11.5	3.51	12.0
12.0	3.66	14.0
12.5	3.81	10.0
13 (top branch)	3.96	1.0
13 (bottom branch)	3.96	4.0
13.5 (top branch)	4.11	1.0
13.5 (bottom branch)	4.11	3.0
14.0 (top branch)	4.27	1 grain
14.0 (bottom branch)	4.27	1 grain
14.5 (top branch)	4.42	2 grain
14.5 (bottom branch)	4.42	tapered off
14.7 (top branch)	4.48	2 grain
14.7 (bottom branch)	4.48	no trace

Cell 2 Trench 1 Southeast Wall		
Distance along Tape (ft.)	Distance along Tape (m)	Aperture (mm)
0.0	0.00	1.0
0.5	0.15	2.5
1.0	0.30	4.0
1.5	0.46	8.0
2.0	0.61	10.0
2.5	0.76	9.0
3.0	0.91	11.0
3.5	1.07	14.0
4.0	1.22	11.0
4.5	1.37	11.0
5.0	1.52	13.0
5.5	1.68	14.0
6.0	1.83	13.0
6.5	1.98	11.0
7.0	2.13	5.0
7.5	2.29	13.0
8.0	2.44	10.0
8.5	2.59	10.0
9.0	2.74	6.0
9.5 (top branch)	2.90	13.0
9.5 (middle branch)	2.90	8.0
9.5 (bottom branch)	2.90	6.0
10.0	3.05	6.0
10.5	3.20	4.0
11.0	3.35	52.0
11.5	3.51	16.0
12.0	3.66	1.0
12.5	3.81	8.0
13.0	3.96	9.0
13.5	4.11	3.0
14.0	4.27	2.5
14.5	4.42	1.0
15.0	4.57	1.0
15.5	4.72	no trace

Cell 2 Trench 2 North Wall		
Distance along Tape (ft.)	Distance along Tape (m)	Aperture (mm)
0.1	0.030	3
0.5	0.15	6
1.0	0.30	5
1.5	0.46	4
2.0	0.61	7
2.5	0.76	10
3.0	0.91	48
3.5	1.07	20
4.0	1.22	65
4.5	1.37	6
5.0	1.52	22
5.5	1.68	10
6.0	1.83	10
Trench 1 opening from 7.0 to 9.5	-	-
10.0	3.05	20
10.5	3.20	8
11.0	3.35	12
11.5	3.51	7
12.0	3.66	5
12.2	3.72	3

Cell 2 Trench 2 South Wall		
Distance along Tape (ft.)	Distance along Tape (m)	Aperture (mm)
0.1	0.030	1
0.5	0.15	2
1.0	0.30	5
1.5	0.46	7
2.0	0.61	13
2.5 (top branch)	0.76	7
2.5 (bottom branch)	0.76	8
3.0	0.91	14
3.5	1.07	11
4.0	1.22	10
4.5	1.37	10
5.0	1.52	9
5.5	1.68	12
6.0	1.83	17
Opening in Trench 6.2 to 9.1	-	-
9.5	2.90	6
10.0	3.05	14
10.5	3.20	20
11.0	3.35	20
11.5	3.51	22
11.8	3.60	6

Cell 2 Trench 3 Southeast Wall		
Distance along Tape (ft.)	Distance along Tape (m)	Aperture (mm)
0.1	0.030	1
0.5	0.15	1
0.6	0.18	0
1.0	0.30	0
1.0	0.30	4
1.5	0.46	2
2.0	0.61	3
2.5	0.76	3
3.0	0.91	1
3.5	1.07	3
4.0	1.22	4
4.5	1.37	15
Fracture disappears from 0.6 ft to 1.0 ft.		

Cell 2 Trench 3 Southwest Wall		
Distance along Tape (ft.)	Distance along Tape (m)	Aperture (mm)
7.5	2.29	13
8.0 (top branch)	2.44	7
8.0 (bottom branch)	2.44	13
8.5	2.59	15
9.0	2.74	2

Cell 4 Trench 1 North Wall		
Distance along Tape(ft)	Distance along Tape (m)	Aperture (mm)
0.0	0	5
0.5	0.15	4
1.0	0.30	4
1.5	0.46	5
2.0	0.61	4
2.5	0.76	5
3.0	0.91	6
3.5	1.07	5
4.0	1.22	6
4.5	1.37	11
5.0	1.52	15
5.5	1.68	20
6.0	1.83	15
6.5	1.98	4
7.0	2.13	25
7.5	2.29	Washed Out
8.0	2.44	11
8.5	2.59	7
9.0	2.74	15
9.5	2.90	15
10.0	3.05	21
10.5	3.20	15
11.0	3.35	15
11.5	3.51	20
12.0	3.66	34
12.5	3.81	3
13.0	3.96	7
13.5	4.11	30
14.0	4.27	20
14.5	4.42	15

Cell 4 Trench 1 South Wall		
Distance along Tape (ft.)	Distance along Tape (m)	Aperture (mm)
0.0	0	3
0.5	0.15	6
1.0	0.30	5
1.5	0.46	15
2.0	0.61	5
2.5	0.76	6
3.0	0.91	7
3.5	1.07	12
4.0	1.22	14
4.5	1.37	8
5.0	1.52	6
5.5	1.68	11
6.0	1.83	15
6.5	1.98	15
7.0	2.13	12
7.5	2.29	14
8.0	2.44	12
8.5	2.59	13
9.0	2.74	20
9.5	2.90	13
10.0	3.05	14
10.5	3.20	15
11.0	3.35	10
11.5	3.51	8
12.0	3.66	9
12.5 (top branch)	3.81	3
12.5 (bottom branch)	3.81	9
13.0	3.96	4
13.5	4.11	5
14.0	4.27	27
14.5 (top branch)	4.42	3
14.5 (bottom branch)	4.42	2
15.0	4.57	7

REFERENCES

Beaumont, C., Hyndman, R.D., and M.J. Keen. 1970. A new technique for the installation of tiltmeters. Earth and Planetary Science Letters 8 (5), 337-340

Busetti, S., Wenjie, J., and Z. Reches. 2014. Geomechanics of hydraulic fracturing microseismicity: Part 1. Shear, hybrid, and tensile events. AAPG Bulletin 98 (11), 2469-2457

Chen, J. L., and L. C. Murdoch. 1999. Effects of electroosmosis on natural soil: Field test. Journal of Geotechnical and Geoenvironmental Engineering 125 (12), 1090-1098

Crosby, D.G., Yang, Z., and S.S. Rahman. 1998. The successful use of transverse hydraulic fractures from horizontal wellbores. SPE International Conference on Horizontal Well Technology: proceedings: 1-4, 335-344

Daily, W. D., Owen, E., and D. J. LaBrecque. 1990. Cross-Borehole electrical resistivity tomography. Society of Exploration Geophysicists 60, 573-574

Davis-Hoover, W. J., Murdoch, L. C., and S. J. Vesper. 1994. Field application of solid oxygen source for bioremediation. Symposium on Bioremediation, October 1993, Philadelphia. vol: ASTM STP 1235 American Society for Testing Materials

Gidley, J. L., Holditch, S. A., Nierode, D. E., and R. W. Veatch. 1989. *Recent advances in hydraulic fracturing*. Society Petroleum Engineers Monograph 425

Huang, J. and others. 2015. Natural-hydraulic fracture interaction: Microseismic observations and geomechanical predictions. Interpretation (Tulsa) 3 (3), SU17-SU31

Hubbert, M.K. and D.G. Willis. 1972. Mechanics of hydraulic fracturing. Underground Waste Management and Environmental Implications, Memoir – American Association of Petroleum Geologists 18, 239-257

Keck, L. J. and C. L. Schuster. 1978. Shallow formation hydrofracture mapping experiment. Journal of Pressure Vessel Technology 100, 24-27

LaBrecque, D., Sharpe, R., Casale, D. Heath, G. and J. Svobada. 2003. Combined electrical and magnetic resistivity tomography: Synthetic model study and inverse modeling. Journal of Environmental and Engineering Geophysics 8 (4), 251-262

LaBrecque, D. J., Sharpe, R., Wood, T., and G. Heath. 2004. Small-scale electrical resistivity tomography of wet fractured rocks. Groundwater 42 (1), 111-118

LaBrecque, D. J. and X. Yang. 2001. Difference inversion of ERT data: a fast inversion method for 3-D in situ monitoring. Journal of Environmental and Engineering

Geophysics 6 (2), 83-89

Lecampion, B., Jeffrey, R. and E. Detournay. 2005. Resolving the geometry of hydraulic fractures from tilt measurements. Pure and Applied Geophysics 162 (12), 2433-2452

Mahrer, K. 1993. Microseismic logging: A new hydraulic fracture diagnostic method. SPE Formation Evaluation, 41-49

Multi-Phase Technologies, LLC. 2016. AEC Phase I Report: Background and Results of Shallow Hydrofracture Experiment. Submitted to Advanced Energy Consortium

Murdoch, L. C. 1995. Forms of hydraulic fractures created during a field test in overconsolidated glacial drift. Quarterly Journal of Engineering Geology and Hydrogeology, 28, 23-35

Murdoch, L. C. 2002. Mechanical analysis of idealized shallow hydraulic fracture. Journal of Geotechnical and Geoenvironmental Engineering, 488-495

Murdoch, L. C. and J. L. Chen. 1997. Effects of conductive fractures during in situ electroosmosis. Journal of Hazardous Materials 55, 239-262

Murdoch, L. C., Richardson, J. R., Tan, Q., Malin, S. C., and C. Fairbanks. 2006. Forms

and sand transport in shallow hydraulic fractures in residual soil. Canadian Geotechnical Journal 43 (10), 1061-1073

Murdoch, L. C., Siegrist, B., and T. Meiggs. 1997. Advanced hydraulic fracturing methods to create in situ reactive barriers. International containment technology conference and exhibition, February 1997, St. Petersburg, FL. USDOE Office of Environmental Restoration and Waste Management

Murdoch, L. C. and W. W. Slack. 2002. Forms of hydraulic fractures in shallow fine-grained formations. Journal of Geotechnical and Geoenvironmental Engineering, 479-487

Murdoch, L.C. and D. Wilson. 1994. Alternative methods for fluid delivery and recovery; manual. United States Environmental Protection Agency Office of Research and Development. EPA/625/R-94/003, 1-102

Nicholson, R. and D. D. Pollard. 1985. Dilation and linkage of echelon cracks. Journal of Structural Geology 7, 583-590

Northrop, D.A. and N.R. Warpinski. 1978. Stimulation and mineback experiment project – the direct observation of hydraulic and explosive fracturing tests. Second Eastern Gas Shales Symposium 1, 291-302

Oldenborger, G. A., Knoll, M. D., Routh, P. S., and D. J. LaBrecque. Time-lapse ERT

monitoring of an injection/withdrawal experiment in a shallow unconfined aquifer. Geophysics 72 (4), F177-F187

Pollard, D. D. and A. Aydin. 1988. Progress in understanding jointing over the past century. Geological Society of America Bulletin 100, 1181-1204

Pollard, D.D. and G. Holzhausen. 1979. On the mechanical interaction between a fluid-filled fracture and the earth's surface. Tectonophysics 53 (1-2), 27-57

Pollard, D. D. and O. H. Muller. 1976. The effects of gradients in regional stress and magma pressure on the form of sheet intrusions in cross section. Journal of Geophysical Research 81, 975-984

Pollard, D.D., Segall, P. and P.T. Delaney. 1982. Formation and interpretation of dilatant echelon cracks. Geological Society of America Bulletin 93 (12), 1291-1303

Saleh, B. and P.A. Blum. 2005. Monitoring of fracture propagation by quartz tiltmeters. Engineering Geology 79, 33-42

Soil Survey Staff, Natural Resources Conservation Service, United States Department of Agriculture. Web Soil Survey. Available online at https://websoilsurvey.sc.egov.usda.gov/. Accessed 9/28/16.

Soliman, M.Y. and P. Boonen. 1997. Review of fractured horizontal wells technology.

Proceedings: Asia Pacific Oil & Gas Conference and Exhibition, 11-27

Stubben, M. A. and D. J. LaBrecque. 1998. 3-D inversion used to monitor an injection experiment. Proceedings of the Symposium on the Application of Geophysics to Engineering and Environmental Problems, 603-612

Teufel, L. W. and N. R. Warpinski. 1983. In-situ stress variation and hydraulic fracture propagation in layered rock – observations from a mineback experiment. Fifth International Congress on Rock Mechanics 2, F43-F48

Verdon, J. P. and J. M. Kendall. 2011. Detection of multiple fracture sets using observations of shear-wave splitting in microseismic data. Geophysical Prospecting 59, 593-608

Wang, T., Stodt, J.A., Stierman, D.J., and L.C. Murdoch. 1991. Mapping hydraulic fractures using a borehole-to-surface electrical resistivity method. Geoexploration 28 (3-4), 349-369

Warpinski, N.R. and L.W. Teufel. 1987. Influence of geologic discontinuities on hydraulic fracture propagation. Journal of Petroleum Technology 39 (2), 209-220

Wright, C. A. 1998. Tiltmeter fracture mapping: From the surface and now downhole. Hart's Petroleum Engineer International 71 (1), 50-63

Wright, C.A., Davis, E.J., Minner, W.A., Ward, J.F., Weijers, L., Schell, E.J., and S.P. Hunter. 1998. Surface tiltmeter fracture mapping reaches new depths; 10,000 feet and beyond?. Rocky Mountain Regional/Low Permeability Reservoirs Symposium and Exhibition, 135-146

Wright, C. A., Davis, E. J., Wang, G., and L. Weijers. 1999. Downhole tiltmeter fracture mapping: A new tool for direct measurement of hydraulic fracture growth. Rock mechanics for industry: proceedings of the 37th U.S. Symposium, 1061-1068

Wyatt, F. 1980. Investigations of tilt measurements using shallow borehole tiltmeters. Journal of Geophysical Research 85 (b8), 4351-4362

2009. SC-2 Super Conducting Earth Contact Backfill, accessed 7/17/17 http://www.loresco.com/sc2.html

2014. Steel Shot and Steel Grit, accessed 7/18/17 http://www.gmaind.com/recycled-products/recycled-steel-shot-and-steel-grit/